Chemical vapour deposition synthesis of carbons from halogen and silicon sources

By

Mahalieo Kao

Submitted in partial fulfillment of the requirements for the degree of Master of Science in the Faculty of science

Department of Chemistry

University of the Witwatersrand

Private Bag X03

Wits

2050

Supervisor Professor: Neil J. Coville

September 2010

DECLARATION

I declare that “Chemical vapour deposition of carbons from halogen and silicon sources is my own, unaided work submitted for the degree of Master of Science in the University of the Witwatersrand, Johannesburg. It has not been submitted for any degree or examination in any other University, and all sources used or quoted here have been indicated and acknowledged by means of references.

Name: Mahalieo Kao (Ms) Date: 14 September 2010

Signature:……

DEDICATION

TO MY MOTHER MAMASUPHA KAO WITH LOVE

Table of contents

Content.....Page
Abstract..... viii
List of figures..... x
List of tables..... xiii
Abbreviations..... xiv
Acknowledgements..... xv
Chapter 1 1
Introduction..... 1
1.1 Fullerene, C_{60} 1
1.2 Carbon nanotubes..... 3
1.3 Chemical modification of CNTs..... 4
1.3.1 Endohedral/Encapsulation 5
1.3.2 Exohedral/Intercalation Doping..... 6
1.3.3 Substitutional/Inplane Doping 7
1.3.4 Coating with metal atoms 8
1.4 Functionalization..... 9
1.4.1 Covalent functionalization.....10
1.4.2 Non-covalent functionalization..... 13
1.5 Properties of CNTs 14
1.5.1 Friction properties..... 14
1.5.2 Adsorption properties..... 15
1.5.3 Optical properties..... 15
1.5.4 Electrical properties 16
1.5.5 Thermal properties..... 17
1.5.6 Mechanical properties..... 18
1.6 Applications of doped CNTs 18
1.6.1 Field-Effect Transistors 20
1.6.2 Field Emission Sources..... 20
1.6.3 Li-Ion Batteries 21

1.6.4 Gas Sensors 21
1.6.5 Heterogenous Catalysis 21
1.6.6 Polymer Composites with Doped Nanotubes 22
1.6.7 Efficient Metal Surfaces for Anchoring Molecules 22
1. 7 Characterization techniques 22
1.7.1 Scanning electron microscopy (SEM) 23
1.7.2 Transmission electron microscopy (TEM) 23
1.7.3 Raman spectroscopy 23
1.7.4 Photoluminescence spectroscopy 23
1.7.5 X-ray photoelectron spectroscopy (XPS) 24
1.7.6 Scanning tunneling microscopy (STM) 24
1.7.7 Neutron diffraction 24
1.7.8 X-ray diffraction (XRD) 25
1.7.9 Thermogravimetric analysis (TGA) 25
1.8 Carbon Spheres 25
1.8.1 Synthesis of carbon spheres 26
1.9 Halogenation of carbonaceous materials 28
1.9.1 Effects of halogenation 28
1.9.2 Synthesis of carbon materials using halohydrocarbons 31
1.10 The objective of the study 32
1.11 References: 34

Chapter 2 47
Experimental Section 47
Introduction 47
2.1 Experimental apparatus 47
2.2 Experimental materials and procedure 48
2.3 Characterization 49
2.3.1 TEM analysis 50
2.3.2 SEM analysis 50
2.3.3 Raman analysis 50

2.3.4 FT-IR analysis 50
2.3.5 TGA 51
2.3.6 EDS 51
2.4 References: 52

Chapter 3 53
3.1 Introduction 53
3.2 Experimental 55
3.3 Catalytic Pyrolysis 56
3. 3. 1 Catalytic pyrolysis of toluene 56
3.3.2 Catalytic pyrolysis of chlorobenzene 57
Effect of halogen concentration at low gas flow rate 60
Effect of chlorobenzene (ClBz) concentration 60
Effect of bromobenzene(BrBz) concentration 61
Effect of halogen content on yield 61
Effect of halogen on size 61
3.4 Non-catalytic thermal decomposition 64
3.5 Impact of non-carbon containing reagents 67
Effect of chloroform 68
Effect of ammonia 71
Effect of sulphur 71
3.6 Effect of gas composition on sphere size 73
3.7 References: 76

Chapter 4 78
Synthesis of carbons from silicon sources 78
4.1 Introduction 78
4.2 Experimental 83
4.3. Results and discussion 84
4.3.1 Toluene 84
4.3.2 Tertraethylorthosilicate (TEOS) as a Si source 86

Raman analysis 91
4.3.3 Non-catalytic pyrolysis of 60 % TEOS in toluene 92
EDS analysis from 60%TEOS. 95
XRD analysis 95
4.3.4 Thermal decomposition of TEOS 96
IR analysis 97
4.3.5 Thermal decomposition of triethylsilylchloride (TESCl) 99
EDS analysis 102
4.4 Conclusions 103
4.5 References: 105

Chapter 5 107
Conclusions 107

Abstract

In this study carbonaceous materials were produced using the floating catalyst horizontal CVD method by injection of a hydrocarbon solution into the high temperature zone of the reaction chamber. Various hydrocarbon reagents were used. The reagents included toluene, chlorobenzene (ClBz), bromobenzene (BrBz), chloroform, tertraethylorthosilicate (TEOS), and triethylchlorosilane (TESCl). Catalytic and non-catalytic reactions were investigated. Ferrocene was used as a source of catalyst during catalytic reactions. The reactions were carried out under a flowing Ar/H_2 (5 %) (v/v) gas mixture at atmospheric pressure. Carbon materials synthesized in this study were characterized by Raman spectroscopy, TEM analysis, SEM analysis, Infra red spectroscopy, TGA, EDS and XRD analyses.

Catalytic pyrolysis of toluene, ClBz, and BrBz resulted in production of multi-walled carbon nanotubes (MWNTs). It was found that the percentage content of the haloarene in the feed impacts on the morphology of carbonaceous materials produced during catalytic pyrolysis. A change in morphology from spheres to a mixture of spheres and tubes and finally to tubes was observed. The influence of the gas flow rate on the type of carbons prepared from catalytic pyrolysis of ClBz has been studied. At high gas flow rates MWNTs were the sole product but at low flow rates carbon spheres resulted.

Carbon spheres were also prepared from non-catalytic reactions. It was established that non-catalytic pyrolysis of ClBz or chlorinated species and toluene enhance product yields. It was established that the size distribution of spheres can be controlled by using hydrogen as a carrier gas.

The impact of additives such as thiophene and ammonia on the pyrolysis of toluene and ClBz was investigated. They were found to inhibit formation of the graphitic carbon from toluene but not from ClBz.

TEOS and TESCl were used as sources of silicon. CNTs were prepared from a TEOS/toluene feed. It was found that the preparation of CNTs from a feed containing low concentrations of TEOS enables control of the diameter distribution and also results in a remarkable improvement in CNT length as compared to CNTs prepared from toluene. However, it was found that high concentrations of TEOS in toluene are destructive. A drastic deterioration of lengths and yield was observed at high concentrations of TEOS in toluene.

Non-catalytic decomposition of TEOS produced core/shell structures formed from co-deposition of carbon and silica. Subsequent thermal treatment of the carbon/silica core/shell structures in air resulted in formation of hollow core silica structures.

Decomposition of TESCl in the absence of a catalyst produced high yields of carbon spheres with a wide diameter distribution. EDS analysis revealed that the spheres prepared from TESCl are composed of carbon, silicon and chlorine. This suggests production of chlorinated silicon/carbon composites. Thermal treatment in air, at 1000 °C produced core/shell structures.

List of figures

Figures	Page
Fig. 1.1: Schematic representation of endohedral, exohedral, substitutional	4
Fig. 1.2: Preparation of azomethine ylide and 1,3-dipolar cycloaddition to C_{60}	10
Fig. 1.3: pyramidilization angel θp and π-misalignment angles	11
Fig. 1.4: Typical defects in a CNTs, and Stone–Wales defect	12
Fig. 1.5: Noncovalent functionalization	13
Fig. 2.1: Schematic diagram of experimental set-up	48
Fig. 3.1a: TEM image of tube prepared from toluene	56
Fig. 3.1b: Diameter distribution of CNTs from toluene	56
Fig. 3.2a: TEM micrograph of nanotubes synthesis from chlorobenzene	58
Fig. 3.2b: Etching effect of chlorine on the outer walls of Fe-filled tube	58
Fig. 3.2c: Shows wall thickness in relation to diameter of the hollow core in tubes prepared form chlorobenzene	58
Fig. 3.2d: HRTEM image of a tube prepared from ClBZ	59
Fig. 3.3a: An image of tubes prepared from catalytic pyrolysis of toluene at 100 ml/min	62
Fig. 3.3b: Carbon materials produced from the catalytic pyrolysis of ClBz at 100 ml/min	62
Fig. 3.3c: Carbon materials prepared from catalytic pyrolysis of ClBz (5 wt.%)	63
Fig. 3.3d: materials produced from catalytic pyrolysis of ClBz (10 wt.%) at 100 ml/min	63
Fig. 3.3e: Carbon nanotubes prepared from pyrolysis of ClBz (2 wt.%) at 100 ml/min	63
Fig. 3.3f: Spheres produced from catalytic pyrolysis of BrBz only	63
Fig. 3.3g: Materials prepared from the catalytic pyrolysis of BrBz (10 wt.%)	64
Fig. 3.3h: tubes produced from the catalytic pyrolysis of BrBz (2 wt.%)	64
Fig. 3.4a and b: TEM images of spheres prepared from toluene	65
Fig. 3.4c: shows TEM images of spheres from ClBz	65

Fig. 3.4d: SEM image shows purity of carbon spheres from ClBz 65
Fig. 3.5a: Effect of gas flow rate on diameters of carbon spheres prepared from toluene and chlorobenzene 67
Fig. 3.6a, b and c: Spheres prepared from toluene in the presence of Cl 69
Fig. 3.6d: Raman spectra of spheres prepared from toluene and ClBz in the presence of additional Cl atoms from chloroform 70
Fig. 3.7a: Spheres synthesized from toluene under NH_3 gas 72
Fig. 3.7b: Spheres from ClBz under ammonia 72
Fig. 3.8a: Spheres formed from toluene in the presence of sulfur 72
Fig. 3.8b: Spheres formed from ClBz in the presence of sulfur 72
Fig. 3.9a: Shows spheres from ClBz under argon gas 74
Fig. 3.9b: A wide diameter distribution of spheres prepared under argon 74
Fig. 3.9c: Shows spheres from ClBz under H_2 gas 74
Fig. 3.9d: Diameter distribution of spheres prepared under H_2 74
Fig. 3.10: EDS of spheres prepared from non-catalytic pyrolysis of ClBz 75
Fig. 4.1A: Si-C graphene sheets with alternate Si and C sites 80
Fig. 4.1B: Si-C sheet containing pairs of Si=Si and C=C bonds 81
Fig. 4.2a: TEM micrograph of carbon nanotubes prepared from toluene at 900 °C in the absence of a Si source 85
Fig. 4.2b: Average outer diameter distribution for the tubes from toluene 85
Fig. 4.2c: SEM micrographs of CNTs prepared from toluene 86
Fig. 4.3a: TEM micrographs from 5 wt. % TEOS in toluene 87
Fig. 4.3b and c: SEM micrographs from 5 wt. % TEOS in toluene 87
Fig. 4.4a: TEM image of TEOS 10 wt. % in toluene 88
Fig. 4.4b: SEM image of TEOS 10 wt. % in toluene 88
Fig. 4.4c: 15 wt. % TEOS in toluene CNTs 89
Fig. 4.4d: 20 wt. % TEOS in toluene CNTs 89
Fig. 4.5a: Mean outer diameter distribution for 5 wt. % TEOS in toluene 90
Fig. 4.5b: Mean outer diameter distribution for 10 wt. % TEOS in toluene 90
Fig. 4.5c: Mean outer diameter distribution for 15 wt. % TEOS in toluene 90
Fig. 4.5d: Mean outer diameter distribution for 20 wt. % TEOS in toluene 90

Fig. 4.6a: TEM image of 30 wt. % TEOS in toluene 91
Fig. 4.6b: SEM image of 30 wt. % TEOS in toluene 91
Fig. 4.6c: Mean outer diameter distribution for 30 wt. % TEOS in toluene 91
Fig. 4.7a: Raman spectra of materials prepared from TEOS 92
Fig. 4.7b: The I_D/I_G ratios of materials prepared from TEOS 92
Fig. 4.8a: Carbon spheres prepared from 60 wt.% TEOS in toluene 93
Fig. 4.8b: Mean outer diameter distribution for 60 wt.% TEOS in toluene 93
Fig. 4.9: TGA profile of 60 wt. % TEOS in toluene as-synthesized sample 94
Fig. 4.10: TEM micrographs of TGA residue 94
Fig. 4.11: EDS analysis of 60% TEOS in toluene 95
Fig. 4.12a: XRD pattern of sample produced from 60 wt.%TEOS in toluene 96
Fig. 4.12b: XRD pattern of residue 96
Fig. 4.13a and b: TEM micrographs from pure TEOS 97
Fig. 4.13c: TGA profile of materials prepared from pure TEOS 97
Fig. 4.13d: TEM micrograph of TGA residue from TEOS 97
Fig. 4.13e: The IR spectra of as-prepared and residual TEOS 98
Fig. 4.14a: TEM of TESCl Spheres 99
Fig. 4.14b: Diameter distribution of TESCl spheres 99
Fig. 4.14c: Raman analysis of spheres prepared from TESCl 99
Fig. 4.14d: TGA profile of TESCl spheres 101
Fig. 4.14e: FT-IR spectra of the as synthesized TESCl sample and residue 101
Fig. 4.14f: TEM micrograph of the core/shell (C/SiO_2) from TESCl 101
Fig. 4.14g: TEM image showing the golf-ball surface resemblance 101
Fig. 4.15: EDS of spheres prepared from TESCl 102

List of tables

Tables	Page
Table 1.1 Potential applications of chemically modified CNTs	19
Table 2.1: A list of reagents used and their properties	48
Table 3.1 Effect of ClBz on carbon materials	57
Table 3.2: The influence of haloarene content at low gas flow rate	62
Table 3.3: Illustrates influence of gas flow rate on carbon yield	67
Table 3.4: The influence of heteroatom additives	68
Table 3.5: A summary of data obtained from Raman analysis	70
Table 4.1 Effect of TEOS on CNTs	85

ABBREVIATIONS

IPR	isolated pentagon rule
CNTs	carbon nanotubes
SWNTs	single-walled carbon nanotubes
MWNTs	multi-walled carbon nanotubes
DWNTs	double-walled carbon nanotubes
SEM	scanning electron microscopy
TEM	transmission electron microscopy
XPS	X-ray photoelectron spectroscopy
STM	scanning tunneling microscopy
XRD	X-ray diffraction
TGA	thermogravimetric analysis
FT-IR	Fourier transform infrared spectroscopy
ClBz	chlorobenzene
BrBz	bromobenzene
HRTEM	high resolution transmission electron microscopy
SiC	silicon carbide
SiCNTs	silicon carbide nanotubes
GTBMD	tight-binding molecular dynamics
MTS	methyltrichlorosilane
TEOS	tetraethylorthosilicate
TESCl	triethylsilylchloride/ triethylchlorosilane

ACKNOWLEDGEMENTS

I would like to thank my supervisor, Professor Neil J. Coville for his advice and guidance in this research. I am grateful to Centre of Excellence and Lesotho government for funding the project. I also thank the department of chemistry, University of the Witwatersrand for giving me the opportunity to conduct this research in their premises. Special thanks to my co-researchers in CATOMAT. Last but not least the big guy God Almighty.

Chapter 1

Introduction

Diamond and graphite are two of the well-known allotropes of carbon. With three-coordinate sp^2 hybridization, carbon atoms form planar sheets of graphite. On the other hand, the three dimensional network structure of diamond is formed by carbon atoms with four-coordinate sp^3 bonding. In 1985, Kroto et al. [1] discovered a new form of carbon, fullerenes, which are closed cage molecules with three-coordinate sp^2 carbon atoms tiling the spherical or nearly spherical surface. In 1991, Iijima [2] observed nanotubules of graphite deposited on the negative electrode in an arc discharge apparatus during the direct current arcing of graphite for the preparation of fullerenes. These two forms of carbon have played a significant role in the emergence of the areas of nanotechnology and nanoscience. Other carbon materials have been synthesized and discussed over the decades [3-15]. These include carbon spheres (hollow, core/shell, solid), horns, coils etc. As this thesis involves only carbon nanotubes (CNTs) and carbon spheres these will be the only two shaped carbon materials that will be discussed in detail. Due to the importance of fullerenes in the development of the branching in CNTs some discussion of this molecule will also be given.

1.1 Fullerene, C_{60}

C_{60} is the most predominant representative of the fullerene family. In C_{60} no two pentagons share an edge hence it obeys the isolated pentagon rule (IPR) which states that a stable fullerene molecule must have no abutting pentagons [16,17]. The structure of C_{60} is a truncated icosahedron, which resembles a soccer ball containing twelve pentagons and twenty hexagons. It follows from the Euler's polyhedron formula that Euler characteristic $\chi = V - E + F = 2$, (where V- Vertices, E- Edges and F- Faces); hence there are exactly 12 pentagons in a fullerene [18]. It has been indicated that fullerenes obtained

by conventional arc discharge synthesis obey the isolated pentagon rule (IPR) [19]. However non-IPR fullerene isomers have been obtained through appropriate modifications of the arc-discharge methodology to synthesize an already chemically derivatized molecule in which the derivatization stabilizes the pentagon–pentagon junctions [20]. In particular, non-IPR cages are quite common in endohedral metallofullerenes, as encapsulated metal atoms are likely to stabilize the fused pentagon fragments by charge-transfer [21].

More recently, a number of unconventional exohedral fullerene derivatives, including $C_{50}Cl_{10}$,[22, 23] $C_{56}Cl_{10}$,[24] $C_{66}H_4$,[25] $C_{68}C_{l4}$,[23] and non-IPR $C_{60}C_{l8}$ and $C_{60}Cl_{12}$,[26] have been obtained by means of an arc-discharge process in the presence of additives such as CCl_4, and Cl_2. Ioffe et al. reported on the synthesis of a derivatized non-IPR fullerene molecule from a pre-formed IPR fullerene cage via reaction of D_2-C_{76} (IPR) with $SbCl_5$ producing a chlorinated product $C_{76}Cl_{24}$ with a rearranged non-IPR carbon cage [27]. They suggested that chlorination is a simple but efficient tool for structural transformation of carbon cages and that chlorine may be the most convenient addend to effect such transformations, as its moderate binding energy provides a good balance between thermal stability and capability of migrating over the fullerene cage.

C_{60} has been studied extensively for numerous kinds of functionalization reactions. It is known to undergo addition, cycloaddition and polymerization reactions characteristic of unsaturated systems. Hence it seems to behave more like an alkene than an aromatic molecule. The reactivity of C_{60} can be explained by invoking hybridization of carbon atoms on C_{60} which will be explained below.

Shestakov [28] presumed that dimerization of C_{60} molecules occurs when one of the molecules is excited to a triplet state. Shestakov experimentally established that the activation energy of C_{60} dimerization is close to that of the singlet-triplet transition in C_{60}. An excited fullerene molecule is assumed to be biradical and can easily add to neighbouring molecules by formation of double bonds. In fact it has been established that

optically excited C_{60} molecules dimerize and polymerize at room temperature and atmospheric pressure [29].

1.2 Carbon nanotubes

Carbon nanotubes (CNTs) are rolled up layers of graphene sheets forming a hollow cylinder with ends that can be open or closed to give a fullerene-like structure. CNTs can be categorized according to the number of walls found in the material into single-walled carbon nanotubes (SWNTs) and multi-walled carbon nanotubes (MWNTs). SWNTs are made up of a single graphene sheet rolled up to form a tube. The internal diameter of SWNTs can be between 0.4 and 2.5 nm, while their lengths can range from a few microns to several millimeters. MWNTs are made of two or more concentric layers of graphene sheets. The inner diameters of MWNTs can be anything from 1 nm to a few nanometers, while the outer diameters take values from 2 nm up to 100 nm.

SWNTs can be metallic or semi-conducting, depending on their diameters and the arrangement of the hexagonal rings along the tube length. Apart from interesting electronic properties, CNTs exhibit excellent mechanical and thermal properties. These interesting physicochemical properties make CNTs very attractive as reinforcement fillers in nanocomposite materials [30], hydrogen storage [31,32], sensors [33,34] scanning probe, microscopy tips [35,36], and molecular-scale components in macro and nanoscale devices [37-39]. However it is difficult to synthesize CNTs with the surface characteristics required for specific applications. Therefore surface modification and interfacial engineering are essential in making advanced CNTs with good bulk and surface properties. Due to the seamless arrangement of hexagonal rings without any dangling bonds, capped CNTs are rather unreactive. However, like C_{60} fullerene, the fullerene-like tips of CNTs are known to be more reactive than the cylindrical length of the tube [40], hence certain reagents can readily react with the tips. This however does not impact significantly on the chemistry of the nanotube as a whole due to the relatively small portion of the tips in the entire structure. In order to meet the specific requirements

demanded by the particular applications (e.g. bio-compatibility for nanotube sensors or interfacial strength for blending with polymers), chemical modification of CNTs is essential.

1.3 Chemical modification of CNTs

Designing nanotube-based nanoscale materials and devices requires the controllable modification of the physical and chemical properties of CNTs. Chemical modification of CNTs can be realized by a variety of approaches, such as intercalation of electron donors like alkali metal or acceptors like halogens [41,42], substitutional doping [43,44], encapsulating atoms, molecules or clusters in the tube interior space [45–50] (figure 1.1), coating of metal atoms on the tube surface [51], gas adsorption [34,52–54], noncovalent functionalization by organic molecules or wrapping by polymers [55,56], and covalent functionalization on nanotube sidewalls [57,58].

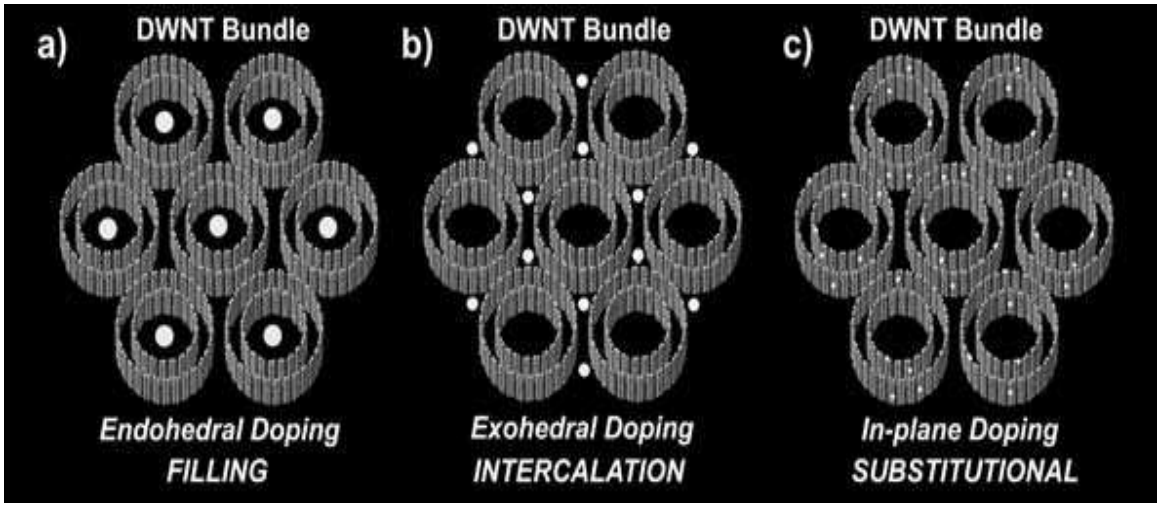

Fig. 1.1. Molecular models representing schematically (a) endohedral doping; (b) exohedral doping or intercalation, and (c) inplane doping (substitutional) in DWNT bundles [114]

1.3.1 Endohedral/Encapsulation

The possibility of encapsulating atoms or molecules inside fullerenes was discovered by Heath et al. [59,1]. Their first endohedral compound was La@C_{60}. The presence of a noble gas dimer inside the C_{60} cage was expected to modify the exohedral reactivity of the cage with respect to that of the free C_{60} cage. Reactivity changes in endohedral fullerenes are attributed to stabilization of the LUMO, increased fullerene strain and compression of the encapsulated noble gas dimer. Heavier noble gas dimer molecules produce profound changes in reactivity when compared to lighter gases [60]. The proposed mechanism for endohedral compound formation is reversible breaking of a carbon-carbon bond of the fullerene surface which opens a “window“ large enough to allow atom or dimer encapsulation [61]. A significant advance in the insertion of atoms or molecules into the C_{60} cage was recently achieved by Murata et al. [62] with chemical opening, insertion and chemical closing of the cage in what is now known as fullerene surgery. Recently, great interest in endohedral metallofullerenes has emerged due to their potential applications in medicine, biology, nanotechnology and most significantly exohedral reactivity of these compounds [63].

Filling CNTs with metals is one field of research which has been gaining a lot of momentum lately due to the exciting properties developed upon filling. Attempts made to form long nanometric filaments were based on the electric-arc method, using composite electrodes impregnated with the filling material [64]. A promising approach exploited the capillary properties of the nanotubes [65]. The procedure to fill nanotubes may be classified in two groups: a) the chemical method, using wet chemistry [66]; and b) the physical method, where capillarity forces induce the filling of a molten material [65, 67, 68]. In the wet chemistry method, the nanotubes were refluxed in a nitric acid bath in order to open their tips. When a metal salt was simultaneously used in the bath, it was possible to obtain oxide or pure metal particles by subsequent annealing [66]. Also, the metal–salt solvent bath has been used on previously opened tubes. In the physical method no solvent was used in the process and opened tubes were directly immersed in the molten material whereby the liquid was driven into the tube by capillary forces [68–70].

The enclosed material could be modified by subsequent treatment (thermal treatment [67] or electron irradiation) [68]. The main advantage of the wet-chemical approach is its flexibility and the level of experimental control that allows a wide variety of materials to be introduced into the nanotubes. Nevertheless the effective quantity of enclosed matter remained low and was in the form of isolated particles. The physical method was found to be more restrictive in the material choice, but the amount of enclosed matter was significantly larger and furthermore, it was in the form of continuous filaments (nanowires) [71]. Size-dependent filling of CNTs have also been observed and it indicated a lowering of cavity-salt interface with decreasing diameters [71]. Incipient wetness impregnation, which is the most common method for catalyst preparation in industry, has also been demonstrated to be a simple filling method [72,73]. Based on capillarity and surface tension, a simple strategy was developed to selectively fill CNTs with Fe, Co, and Ni species using a two-step method consisting of impregnation and selective washing [74].

1.3.2 Exohedral/Intercalation Doping

Weak van der Waals forces associated with the sp^2 hybridization in graphite make insertion of layers of guest species possible and in so doing forming graphite intercalation compounds. In this type of compound the graphite layers remain largely intact. The guest species may be atomic or molecular. When the host (graphite) and the guest interact by charge transfer the in-plane electrical conductivity generally increases. When the guest for covalent bonds with the graphite layers are fluorides or oxides the conductivity decreases as the conjugated sp^2 system collapses. Because of its electronegativity (~ 2.5) carbon acts as an amphoteric element, so in intercalation reactions graphite can provide or accept electrons. The analogy of chemical reactions of graphite and CNTs also extends to intercalation chemistry. The occupation of intertubular gaps in SWNTs bundles has been well investigated and documented by several research groups. However occupation of the interlayer spaces inherent to regular stacking of concentric graphene layers in MWNTs seem to be have been less reported. However effects of intercalation/de-intercalation on the overall morphology of MWNTs have been noted [75,76]. It was

generally established that intercalation of MWNTs resulted in heterogeneous swelling of the tubes, where tubes were characterized by a succession of non-intercalated bottlenecks and intercalated swelling zones [75,76] and upon de-intercalation tubes regained their original diameters.

In the case of MWNTs the intercalation of the dopant can occur as in graphite, in between the graphitic shells leading to an expansion of the interlayer distances. The possibility of insertion into the central canal of the open MWNTs (the tube diameter can vary from 10 to 100 nm) was also examined by some authors [77]. In the case of SWNTs, the intercalated species can be either in between the individual tubes or inside the tubes. By analogy with well-known graphite intercalation compounds and C_{60}, the electronic properties of SWNTs can be engineered by doping either with electron donors or acceptors. The reactivity of SWNTs with dopant (acceptor or donor), i.e. the shift of their Fermi level, is expected to depend upon the electronic properties of host SWNTs.

Early doping experiments focused on common graphite intercalants such as iodine and alkali metals, partly with the hope of finding superconductivity as found in the carbon fullerenes. Instead of superconductivity, though, researchers found irreversible electronic behaviour, which seemed strongly dependent on sample history [78]. The onset of n-type conduction, which might be attributed to alkali metal intercalation, was not reversible in vacuum but immediately disappeared upon exposure to air. Subsequently, it was found that a vacuum treatment alone was sufficient to change the majority carrier type, even in the absence of intentional dopants [52,79-81].

1.3.3 Substitutional/Inplane Doping

The idea of doping CNTs and fullerenes has been attractive since it allows the electronic properties to be controlled by the amount and type of dopant. For instance, the creation of a vacancy by removing one carbon atom in a C_{60} monomer generates a dangling bond with an unpaired electron on each of the three C atoms surrounding the site of the vacancy. In the triplet ground state of the C_{60} dimer with two vacancies, one on each C_{60}

molecule, it is found that two of the three dangling bonds are healed in each C_{60} molecule by the formation of an extended C-C bond also known as a banana bond across the vacancy site leaving just one dangling bond at each vacancy site. Therefore, one may mimic the effect of a C vacancy in a C_{60} molecule by substituting the vacancy with a group15 element in the Periodic Table such as an N or P atom since each of these carries one lone electron in such a substitution. The effects of N substitution in graphite, C_{60} and SWNTs have been extensively investigated recently [82-90]. These investigations reveal that substituting one C atom by a N atom in these systems does not lead to a noticeable disturbance of the graphene lattice. However theory has it that a N/C ratio larger than 20% is necessary to destroy the planarity of the doped graphene sheet [89].

It was demonstrated that SWNTs can be doped with boron (B) [91,92], nitrogen (N) [93], or phosphorous (P) [94,95] atoms. B is an electron acceptor to CNTs while N and P are electron donors. The nature (local vs non-local) of electron doping of N and P are different. First principle calculations show that while the N atom lies on the plane of the nanotube lattice, P is attached to the tube with three sp^2-like bonds to the C neighboring atoms, laying out of the plane of the nanotube [94,96].

Maciel et al. [97] studied substitutionally doped SWNTs with B, N, and P atoms, using resonance Raman spectroscopy. They showed that the small amounts of dopants in the samples are not able to shift the G band frequency. The ω_G frequency shifts only when the measurements are taken at high laser powers. For B and P doping, the red shift due to laser heating is smaller when the amount of doping atoms increases, showing an increase in thermal conductance for the bundled doped SWNTs. This result is not observed for N-doped samples, suggesting differences in the doping induced effects.

1.3.4 Coating with metal atoms

CNTs interactions with metal nanoparticles have gained considerable interest. The metal coated CNTs can be used as sensing materials, catalysts, in the synthesis of metallic

nanowires as well as in nanoelectronic devices. Evaporation of metals on a vertically aligned SWNTs film and metal coating on CNTs [98] have been studied extensively. These techniques are expected to enhance the functionalities of CNTs. For example, SWNTs may work as quantum wires; however one-third of the SWNTs produced are metallic in nature while the remainder is semi-conducting. A semi-conducting SWNT would not be suitable for use as a quantum wire and the metallic SWNT would not be suitable for use as a diode. In contrast, by coating a desired metal species on the SWNTs, control of their electrical properties can be attained. Deposition of metal atoms onto CNTs depends upon the individual metal element properties and degree of adhesion on the nanotube. DFT studies [99] have indicated that the stable site for metal atoms on the CNT is the center of the hexagonal carbon ring. However the size of this site is too small to accommodate large metal atoms like gold. Deposition of many types of metals normally forms discrete particles on nanotubes due to weak interaction between the metals and carbon. However, continuous nanowires of virtually any metal can be obtained by using metals which have strong interaction with carbon such as titanium and nickel and they can form a buffer layer on a CNT [51].

1.4 Functionalization

Some of the impediments for the potential application of CNTs include weak interfacial interaction and poor dispersion capability due to strong van der Waals attractions between the tubes. To improve the properties of the CNTs, low-cost and industrially feasible approaches to their modification have been much pursued vigorously in recent times [100-105]. These approaches can be simply divided into two categories, i.e., (i) covalent [59,102-104] and (ii) noncovalent [103-105] functionalizations of both SWNTs sidewalls (figure 1.5) and MWNTs.

1.4.1 Covalent functionalization

C_{60} reacts readily with nucleophiles and is a reactive 2π component in cycloadditions [106]. Most reactants add to junctions between two six-membered rings of C_{60} (6,6 junctions), where the electron density is higher. Insertion into 5,6 bonds occurs as a

rearrangement that follows a 6,6 junction attack [107,108]. Stable derivatives of C_{60}, which retain the original properties of a pristine fullerene, have been made possible by Prato reaction which entails a 1,3-dipolar cycloaddition of azomethine ylides to C_{60} [109] (figure 1.2). In fact the Prato reaction also describes the functionalization of nanotubes with azomethine ylides in a 1,3-dipolar cycloaddition [110].

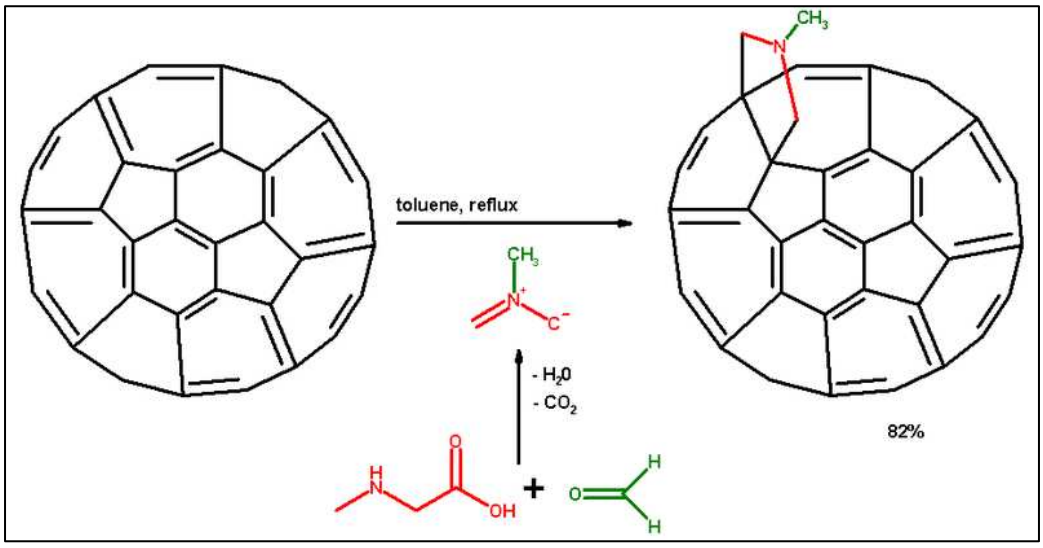

Fig.1.2. Preparation of azomethine ylide and 1,3-dipolar cycloaddition to C_{60} [111]

Covalent functionalization of nanotubes has the remarkable potential to provide a higher degree of tenability of CNT properties compared to methods based on non-covalent functionalization. Sidewall addition chemistry of CNTs differs from that of the fullerenes even though both are curved, conjugated carbon systems. The chemical reactivity in strained carbon systems arises from two factors: a) pyramidalization at the carbon atom and b) π-orbital misalignment between adjacent carbon atoms [112] (figure 1.3). In fullerenes pyramidalization is more intense and relief of pyramidalization strain results in addition reactions to fullerenes being energetically favorable. However, in SWNTs pyramidalization is not as acute as in fullerenes. Therefore π-orbital misalignment has the greater influence on SWNTs reactivity [57]. The π-orbital misalignment is associated with bonds that are neither parallel nor perpendicular to the tube axis, and thus the basis of torsion strain in nanotubes. Relief of this strain influences the extent to which addition reactions occur with nanotubes. The degree of π-orbital misalignment is inversely

proportional to tube diameter [113] hence; small tubes would be expected to be more reactive than larger tubes. In addition to the two factors mentioned above nanotube sidewall functionalization is also made possible by intrinsic defects such as vacancies in the graphitic lattice, sp^3 hybridized defects and pentagon-heptagon pairs, known as a Stone-Wales defect (figure 1.4).

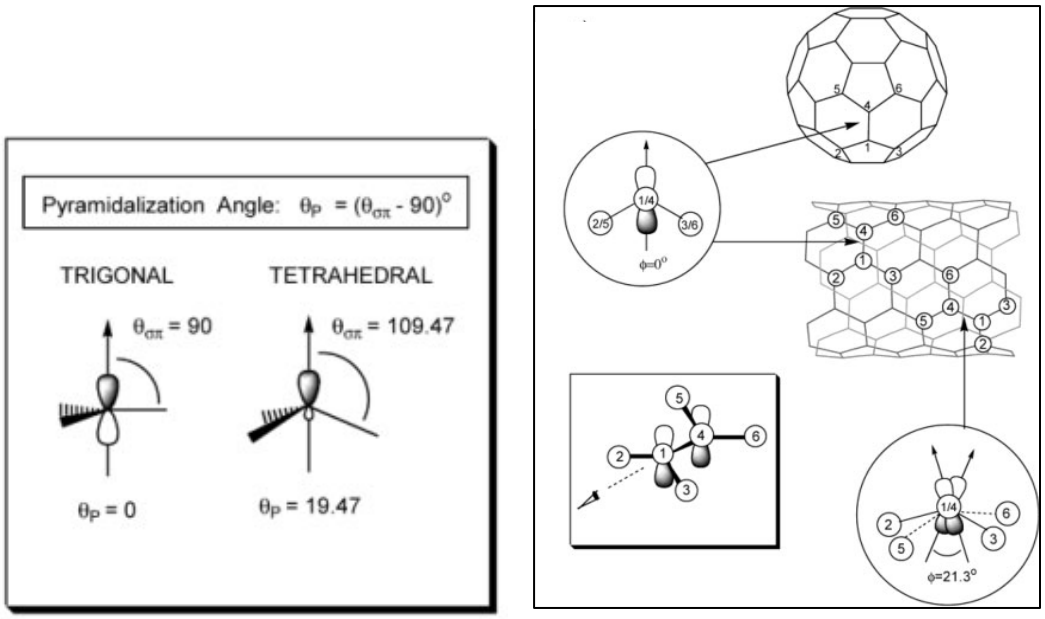

(a) (b)

Fig. 1.3: (a) pyramidilization angel θp (b) π-misalignment angles [57].

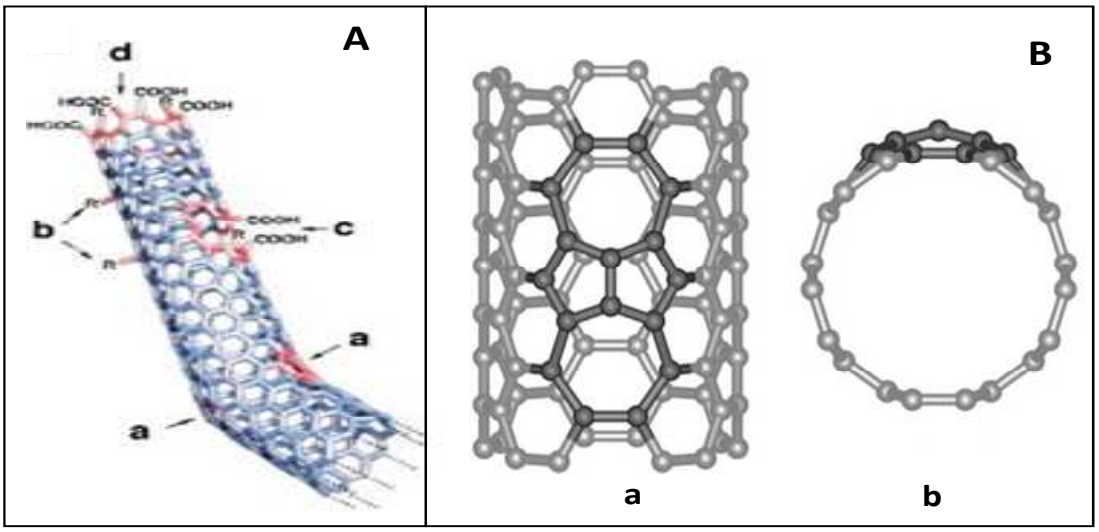

Fig. 1.4: **A**) Typical defects in CNTs: (a) five- or seven-membered rings in the carbon framework, (b) sp^3-hybridized defects (R = OH), (c) carbon framework damaged by oxidative conditions, which leaves a hole lined with COOH groups and (d) open end of the SWNT terminated with COOH groups [115]; **B**) Stone–Wales (or 7-5-5-7) defect on the sidewall of a nanotube [58]: (a) top view and (b) side view

Fluorination [102] of SWNTs has become a popular method for investigating the covalent functionalization because the SWNTs sidewalls are expected to be inert. The fluorine atoms in the fluorinated SWNTs can be substituted by alkyl groups through treatment with alkyl lithium or Grignard reagents. Another convenient method for the covalent functionalization of SWNTs is to convert the SWNT sidewalls to nanotube-bound carboxylic acids upon oxidation [58,101]. SWNTs functionalized with carboxylic acid groups, can be modified further with a range of organic entities by means of amide/ester linkages or carboxylate-ammonium salt ionic interactions. Such functionalized SWNTs can usually be characterized by nuclear magnetic resonance (NMR) and absorption spectroscopies in solution. The covalent functionalization of SWNTs results in a change of carbon hybridization from sp^2 to sp^3, leading to a possible partial loss of conjugation with consequences for electron-acceptor and/or electron-transport properties. Carboxylic acid groups have also been generated on MWNTs by UV/O_3 treatment [117]. The carboxylic groups generated on MWNTs have been used to covalently bind biomaterials such as sugar moieties [118], oligonucleotides [119], and

peptide nucleic acids (PNA) [120] via carbo-diimide coupling of the amino functionalized biomolecules or using heterobifunctional coupling reagents. However covalent functionalization has been shown to disrupt the π-network of a CNT, leading to possible losses in the mechanical and electrical properties.

1.4.2 Non-covalent functionalization

Non-covalent chemistry involves the self assembly of molecules or macromolecules to thermodynamically stable structures. The structures are held together by weak non-covalent interactions. These weak non-covalent interactions include hydrogen bonding, van der Waals forces, hydrophobic/hydrophilic interactions and *π-π* stacking (figure 1.5). SWNT sidewalls have been functionalized non-covalently by, for example, aromatic compounds, surfactants, and polymers, employing *π-π* stacking or hydrophobic interactions for the most part [103-105]. In these approaches, non-covalent modifications of CNTs can do much to preserve their desired properties, while improving their solubility quite remarkably. Aromatic molecules, such as pyrene, porphyrin, and their derivatives, can and do interact with the sidewalls of CNTs by means of *π-π* stacking interactions, thus opening up the way for the non-covalent functionalization of CNTs.

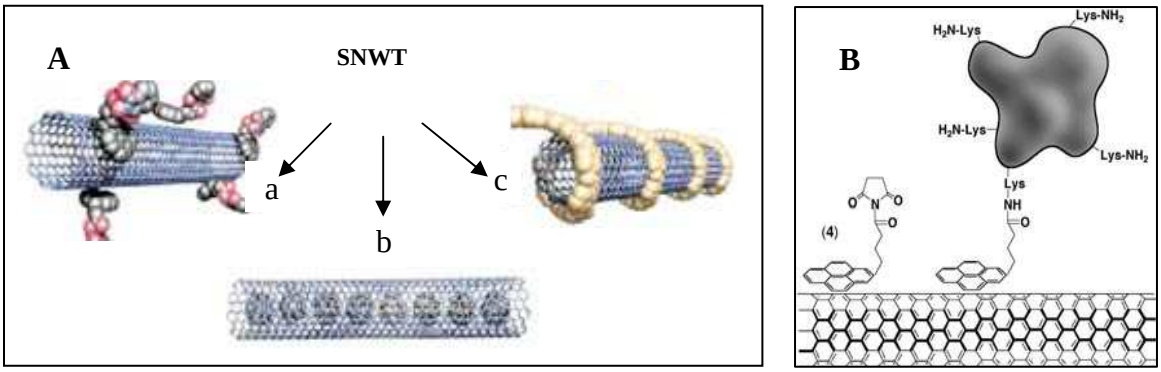

Fig.1.5: **A**) (a) non-covalent exohedral functionalization with surfactants, (b) endohedral functionalization with C_{60} and (c) non-covalent exohedral functionalization with polymers [116]; **B**) Immobilization of proteins on CNTs by 1-pyrenebutanoic acid succinimidylester irreversibly adsorbing onto the sidewall of a SWNT via *π-π* stacking [58].

Recently, several strategies have been reported based on the non-covalent bonding of organic molecules to CNTs. Xue et al. reported non-covalent method of exfoliation and centrifugation cycles with poly (styrene-co-maleic anhydride) carrying pyrene (HPSMAP) and MWNTs, a water soluble complex of HPSMAP–MWNTs was obtained [121]. Non-covalent functionalization of MWNTs by anionic polymer poly (sodium 4-styrenesulfonate) in water by sonication [122] was also reported. In another study MWNTs were functionalized with polyimide (PI) via an in situ polymerization in *N*,*N*-diemethy-formamide. In this study Raman and UV–vis spectroscopies were used to establish the π-π stacking interaction between benzene ring in PI and the graphitic sidewalls of the MWNTs [123]. Li et al. prepared non-covalently functionalized MWNTs by using 2-aminoethanol in the presence of sodium hydroxide under water bath sonication [124]. Yeh et al. [125] also reported non-covalent interaction between gold nanoparticles and MWNTs via an intermediatory ortho-mercaptoaniline.

1.5 Properties of CNTs

1.5.1 Friction properties

The performance of solid lubricants at the nanoscale level largely depends upon the particle size and their shape [126,127]. The seamless structure of CNT helps to inhibit the sticking of the nanoparticles to the rubbing metal or other surfaces they come into contact with. As a result of their morphology tubular particles have the ability to slide and roll during sliding contact, resulting in a low friction and wear. Their high thermal resistance also prolongs their wear life. Surface modification of the tubular or sphere-shaped carbon nanoparticles through chemical treatment, e.g., fluorination, is expected to significantly affect their friction properties in lubricant application [128]. Ultra low friction properties of surface fluorinated CNTs were established on a ball-on-disk tribometer by Vander Wal et al. [129]. In their study friction coefficients for fluorinated nanotubes were found to reach values as low as 0.002-0.07.

1.5.2 Adsorption properties

There has been a lot of interest in the development of hydrogen storage in various systems for the large-scale application of fuel cells [130], automobiles and for automotive uses. CNTs are the promising candidates for hydrogen storage due to a number of favorable points like porous nature, high surface area, hollowness, and light weight, which facilitate the hydrogen adsorption in both outer and inner portions [131]. It was observed that physisorption proved to be an effective and stable way for hydrogen adsorption over chemisorption [132].

According to Gayathri et al. [133] some hydrogen-CNT configurations are more energetically favorable than others. They observed larger adsorption energies for the configuration in which the hydrogen molecular axis is perpendicular to the hexagonal carbon ring than for the one parallel to C–C bond in defect free CNTs. It is claimed that the value of adsorption binding energy has to be around 0.2 to 0.3 eV for possible technological applications such as fuel cells. Pradhan et al. [134] also reported that the defect induced disorder in nanotubes might enhance the physisorption binding energy of H_2 molecules. Nitrogen adsorption studies performed on SWNTs and MWNTs revealed that the former are microporous in nature while the latter are macroporous [135].

1.5.3 Optical properties

Kataura et al. demonstrated that optical absorption spectroscopy is an appropriate tool to study the electronic properties of SWNTs [136]. Several absorption features observed in the visible to near infrared region were assigned to specific optical transitions in the semiconducting or metallic phase. The features usually referred to as S1 (at ~ 0.68 eV) and S2 (at ~1.2 eV) are originated from allowed electronic transitions between the first and second pairs of van Hove singularities of the density of states (DOS) in a semiconducting SWNT, whereas the Ml feature around 1.8 eV is assigned to an allowed electronic transition between the first pair of singularities in a metallic SWNT.

All these three characteristic features on the absorption spectrum can be easily affected by chemical doping on the CNTs. Petit et al. reported the experimental evidence of tuning the Fermi level of SWNTs by exposure to molecules of different redox potentials using optical absorption spectroscopy [137]. They found that the three characteristic features of the absorption spectrum disappear after the SWNT sample is exposed to a solution of naphthalene/lithium, whereas exposure to other n-doping molecules like fluorenone/lithium only remove the S1 peak. For the p-doping by iodine and bromine, the three absorption bands are suppressed. Electronic and optical properties are affected by covalent and non-covalent functionalization [138-141].

1.5.4 Electrical properties

By folding the graphene sheet, three types of SWNTs can be constructed namely, achiral armchair (*n*,*m*) SWNTs (*n* = *m*), achiral zigzag (*n*,0) SWNTs, and chiral (*n*,*m*) SWNTs (*n* > *m* and $m \neq 0$). The structure of a nanotube has a huge impact on its electrical properties. For a given (*n*,*m*) nanotube, if *n* = *m*, the nanotube is metallic; if *n* − *m* is a multiple of 3, then the nanotube is semiconducting with a very small band gap. Thus all armchair (*n* = *m*) nanotubes are metallic, and zigzag are semiconducting [142]. However, this rule has exceptions, because curvature can strongly influence electrical properties in small diameter CNTs. Thus, (5,0) SWNT that should be semiconducting is in fact metallic according to the calculations while zigzag and chiral SWNTs with small diameters that should be metallic have finite gap [143]. In theory, metallic SWNTs have excellent electronic properties: they have a carrier mobility of ~10,000 $cm^2\ V^{-1}\ s^{-1}$, which is better than that of silicon [144], and they can carry an electrical current density of ~4×10^9 A/cm^2, which is three orders of magnitude higher than a typical metal, such as copper or aluminium [145]. MWNTs are expected to behave like carbon fibers, exhibiting 2D-quantum transport features at low temperatures.

For a pristine MWNT physically connected to a metal electrode, only the outermost carbon shell is truly connected in an electrical sense. Inner shells are not ohmically connected but may communicate via tunneling, coulomb drag, diffusive scattering, and a range of other mechanisms. At low temperatures and low bias, these mechanisms can be

minimized and the measured conductance will be exclusively due to the properties of the outermost shell. Under these conditions, MWNTs behave very much like large-diameter SWNTs, with quasi-ballistic conduction, coulomb blockade charging effects, and even Aharonov–Bohm-like interferences from circumferential states [146-148].

1.5.5 Thermal properties

Pop et al. [148] studied the thermal properties of suspended metallic SWNTs over the 300-800 K temperature range. They found that the thermal conductance was ~ 2.4 nW/K, and the thermal conductivity was ~ 3500 $Wm^{-1}K^{-1}$ at room temperature for a SWNT of length 2.6 μm and diameter 1.7 nm. A subtle decrease in thermal conductivity steeper than 1/T was observed at the upper end of the temperature range, claimed to be attributed to second-order three-phonon scattering between two acoustic modes and one optical mode.

The thermal conductivity and thermoelectric power of a single MWNT were measured using a microfabricated suspended device. The thermal conductivity of more than 3000 $Wm^{-1}K^{-1}$ at room temperature was observed. The temperature dependence of the thermal conductivity of nanotubes exhibited the umklapp phonon scattering at 320 K. The measured thermoelectric power showed linear temperature dependence with a value of 80 mV/K at room temperature [149].

1.5.6 Mechanical properties

Mechanical properties of a solid depend on the strength of its interatomic bonds. The strength of carbon bonds in CNTs renders them the strongest and most resilient materials. The strength of a material is not as well defined as the Young's modulus, because it depends not only on the type of material, but also on its history, the atmosphere, the pressure, and the temperature, and the measuring system. It is also intimately linked to structural defects and imperfections that can be present in the solid

The Young's modulus is directly related to the cohesion of the solid and therefore to the chemical bonding of the constituent atoms. Lourie and Wagner [150], reported Young's modulus of 2.8–3.6 TPa, for SWNTs and 1.7–2.4 TPa for MWNTs. Yu et al. [151] measured the tensile strengths of individual MWNTs and found that the tensile strength ranged from 11 to 63 GPa. Analysis of the stress-strain curves for individual MWNTs indicated that the Youngs modulus of the outermost layer varied from 270 to 950 GPa.

1.6 Applications of doped CNTs

The recently developed chemical methods for chemical functionalization of CNTs have opened up a broad range of novel application perspectives. Below we will briefly review some possible applications of doped CNTs in diverse areas such as electronics, biology, composites and catalysis. Balasubramanian and company summarized the potential application of doped carbon nanotubes in table 1.1 below [58].

Table 1.1 Potential applications of chemically modified carbon nanotubes [58]

Potential Application	**Function of the covalently bonded moiety**
Nanostructured electronic devices,e.g., nanodiodes	Local modification of the electronic band structure
(Bio-) chemical sensors	Selective recognition of analyte molecules
Catalyst supports	Anchoring of molecules or metal nanoparticles
Mechanically reinforced composites	Chemical coupling with a matrix
Chemically sensitive tips for scanning probe microscopy	Selective chemical interaction with surfaces
Field emission	Reduction of the work function for electrons at the tube ends
Nanofiltration	Control of the passage of molecules or ions through steric effects or Coulombic interactions
Artificial muscles	Mechanical stabilization of nanotube films through covalent cross-linking
Controlled drug release	Biocompatibility; recognition of biological fingerprints
Pharmacology	Enzyme inhibition or blocking of ionic channels in the cell membrane
Directed cell growth on surfaces	Specific interactions with cell surfaces

1.6.1 Field-Effect Transistors

Fabrication of transistor devices requires exclusively semi-conducting nanotubes. The present synthesis methods do not allow a reliable control over the electrical properties of the produced nanotubes. Separation of the two types of nanotubes have been achieved by chemical modification procedures such as alternating current dielectrophoresis of surfactant-stabilized SWNTs [152], which takes advantage of the differing concentrations of freely movable charge carriers in nanotubes: Metallic nanotubes possess a high density of such carriers, which gives them a large electronic polarizability. Hence, when a suitable alternating electric field is applied, they are attracted to the regions of highest field strength, whereas the semiconducting tubes are repelled. Separation was also achieved by selective destruction/functionalization of the metallic nanotubes in a tube ensemble. This was done by applying an increasing electrical voltage across the tube ensemble until the metallic tubes are burnt off as a consequence of Joule heating arising from the high current densities [153]. The procedure is performed by simultaneous application of a gate voltage to deplete the semi-conducting nanotubes of charge carriers, so that exclusively the metallic nanotubes remain conductive.

1.6.2 Field Emission Sources

Charlier et al. [154] demonstrated experimentally and theoretically that B-doped MWNTs exhibit enhanced field emission (turn-on voltages at ca. 1.4 V/μm) when compared to pure carbon MWNTs (turn-on voltages at ca. 3 V/μm). This phenomenon is thought to be due to the presence of B atoms at the nanotube tips, which results in an increased density of states close to the Fermi level. Theoretical tight-binding and ab-initio calculations demonstrate that the work function of B-doped SWNT was much lower (1.7 eV) than that observed in pure-carbon MWNTs. Individual N-doped MWNTs have also shown excellent field emission properties at 800 K; experimental work functions of 5 eV and emission currents of ca. 100 nA have been obtained at ±10 V [155].

1.6.3 Li-Ion Batteries

Endo and coworkers [156] demonstrated that B-doped vapor-grown carbon fibers (VGCFs) and carbon nanofibers are by far superior compared with any other carbon source present in the graphitic anode inside Li-ion batteries. This effect could be due to the fact that the population of Li ions has a stronger affinity in the B-doped sites, thus resulting in higher storage efficiency. N-doped CNTs and nanofibers have also shown efficient reversible Li storage (480 mAh/g); much higher when compared to commercial carbon materials used for Li^+ batteries (330 mAh/g) [157].

1.6.4 Gas Sensors

It has been demonstrated by various groups [34,52] that pure carbon SWNTs and MWNTs can be used to detect toxic gases and other species [34]. However, a necessary prerequisite is that the molecules to be detected must have a distinct electron donating or accepting ability, which is fulfilled, for example, by ammonia (NH_3) as a donor and nitrogen dioxide (NO_2) as an acceptor. However, for the detection of molecules that are only weakly adsorbed (e.g., carbon monoxide and hydrogen), the change in resistance is often too small. Therefore sensitive hydrogen sensors operating at room temperature can be obtained via the deposition of palladium nanoparticles by direct evaporation [158].

1.6.5 Heterogenous Catalysis

For a long time, active carbon has found widespread application as a support material in heterogeneous catalysis. Compared to this form of carbon, CNTs offer the advantage of a more defined morphology and chemical composition as well as the possibility to attach catalysts onto their surface through covalent bonds. The applicability of SWNTs as carriers for catalytically active molecular functional units has recently been demonstrated through the covalent coupling of an organic vanadyl complex [159].

1.6.6 Polymer Composites with Doped Nanotubes

In order to fabricate nanotube composites exhibiting high performance, the formation of stable tube-surface/polymer interfaces is crucial. The surfaces of highly crystalline MWNTs tend to be similar to graphite, and chemically "inert". Therefore, surface-modification treatments are required to attain efficient tube–matrix interactions [160]. Creation of nanotubes containing defects or heteroatoms in the hexagonal network such as N or B, could circumvent this problem. It has also been demonstrated that it is possible to grow polystyrene (PS) on the surface of N-doped MWNTs using atomic transfer radical polymerization (ATRP) [161].

1.6.7 Efficient Metal Surfaces for Anchoring Molecules

Recently, it has been possible to create active nitrogen-rich sites for the efficient covalent anchoring of proteins [162], Au [163], Ag [164], Fe and Pt clusters [165] to the surfaces of N-doped MWNTs. It has been demonstrated that the doped tubes are much more efficient for anchoring molecules when compared to pure carbon nanotubes.

1. 7 Characterization techniques

In order to investigate the morphological and structural characterizations of nanotubes, techniques such as scanning tunneling microscopy (STM), transmission electron microscopy (TEM) and scanning electron microscopy (SEM) could be used. X-ray photoelectron spectroscopy helps determine the chemical structure of nanotubes while X-ray diffraction (XRD), infrared (IR) and Raman spectroscopies are mostly global characterization techniques. Changes in the Raman spectrum of a nanotube sample can indicate if functionalization has occurred. Solid state ^{13}C NMR spectroscopy is a definitive method of demonstrating covalent attachment of particular functional groups. Functionalized nanotubes can be characterized by the above mentioned techniques, as well as atomic force microscopy (AFM) and UV-vis spectroscopy. A brief account of some of the techniques is presented below.

1.7.1 Scanning electron microscopy (SEM)

SEM provides topographical information of nanomaterials. It shows whether carbon nanotubes are aligned or randomly arranged. It can provide information about length of CNTs especially if they are well aligned.

1.7.2 Transmission electron microscopy (TEM)

TEM enables the quality of the CNT structure, the presence of amorphous matter in and around the tube as well metal encapsulation by the tube to be determined. Data about the dimensions of CNTs such as, diameter distribution, lengths, number of walls and intershell spacing can be obtained from TEM.

1.7.3 Raman spectroscopy

Raman spectroscopy is a fast and non-destructive technique for characterization of carbon nanotubes. All allotropic forms of carbon are active in Raman spectroscopy [166]: fullerenes, carbon nanotubes, amorphous carbon, polycrystalline carbon, etc. The position, width, and relative intensity of bands are modified according to the carbon forms [167]. The most characteristic features have been summarized by Belin et al. [168] as follows: (i) a low-frequency peak < 200 cm^{-1} characteristic of the SWNT assigned to a A_{1g} "breathing" mode of the tubes (RBM: radial breathing mode), (ii) a large structure (1340 cm^{-1}) assigned to residual ill-organized graphite, the so-called D-line (D: disorder), (iii) a high-frequency peak (between 1500 and 1600 cm^{-1}) called G band also characteristic of nanotubes, corresponding to a splitting of the E_{2g} stretching mode of graphite, (iv) a second order mode between 2450 and 2650 cm^{-1} assigned to the first overtone of the D mode and often called G mode and (v) a combination mode of the D and G modes between 2775 and 2950 cm^{-1}.

1.7.4 Photoluminescence spectroscopy

The energy of the Van Hove singularities maxima is mainly dependent on the nanotube diameter [169]. Thus, different (*n*,*m*) SWNTs in a sample will show various

superpositions of distinct transitions which will appear with different wavelengths [170]. As a consequence, the nature (semiconducting or not), the geometries and the diameters could be accessible using the photoluminescence technique. Moreover, the luminescence spectra seem to be very sensitive to the presence of chemical defects and to the purity of the samples [171].

1.7.5 X-ray photoelectron spectroscopy (XPS)

XPS technique provides information about the chemical structure of carbon nanotubes. But the most widely used data refer to the structure modification of the CNT walls due to the chemical interaction with organic compounds or gases adsorption. The information obtained focuses on the following aspects of CNTs; (i) the C1s peak energy position, (ii) the full width at half maximum and (iii) its energy loss fine structures in relation to graphite, for which the C1s is usually observed at 284.6 eV [168].

1.7.6 Scanning tunneling microscopy (STM)

STM images give directly the three-dimensional morphology of tubes and are consistent with the structure inferred from scanning electron microscopy [172]. Moreover, STM can resolve simultaneously both the atomic structure and the electronic density of state (DOS).

1.7.7 Neutron diffraction

Neutron diffraction is a form of elastic scattering where the neutrons exiting the experiment have more or less the same energy as the incident neutrons. The technique is similar to X-ray diffraction but a different type of radiation gives complementary information. A sample to be examined is placed in a beam of neutrons and the intensity pattern around the sample gives information of the structure of the material Neutron diffraction is widely used for determination of structural features such as bond length and possible distortion of hexagonal network [173]. The neutron diffraction pattern of the

CNTs exhibits lines with general (*hkl*) indices, and the (*hkl*) peaks are broader than those of graphite.

1.7.8 X-ray diffraction (XRD)

X-ray diffraction analysis is a powerful method by which X-rays of a known wavelength are passed through a sample to be identified in order to identify the crystal structure. The wave nature of the X-rays are diffracted by the lattice of the crystal to give a unique pattern of 'reflections' at differing angles and of different intensity, just as light can be diffracted by a grating of suitably spaced lines. The intensity of diffracted X-rays is measured as a function of the diffraction angle 2θ and the sample orientation. This characterization method is not sample destructive and is used to obtain some information on the interlayer spacing, the structural strain and the impurities. The main feature of an XRD pattern of CNTs is a peak at ~ 26.5° on the 2θ scale. Depending on the crystallinity of the specimen this peak can broaden or weaken.

1.7.9 Thermogravimetric analysis (TGA)

Thermogravimetric analysis is performed on samples to determine changes in weight in relation to change in temperature. Such analysis relies on a high degree of precision in three measurements: weight, temperature, and temperature change. A derivative weight loss curve can be used to tell the point at which weight loss is most apparent. TGA is commonly employed in research and testing to determine thermal characteristics of CNTs, to determine decomposition temperatures, absorbed moisture content of materials, the level of inorganic and organic components in materials, and solvent residues.

1.8 Carbon Spheres

Carbon is unique in that it can bond in different ways to create structures with quite dissimilar properties. The successful growth of diamond thin films [174], the fullerene molecule C_{60} [1] and its related family of C_n [175] and carbon nanotubes are an indication

of the versatility of shapes that carbon can take. The variety of structures produced by carbon is determined by its versatile hybridization; sp, sp^2 and sp^3. Among several allotropes of carbon, graphite is the basis of most structured forms of carbon such as carbon nanotubes, nanorods, fullerenes and carbon spheroids. Incorporation of pentagonal and heptagonal carbon rings into the graphitic lattice is responsible for the spherical carbon structures [176]. So far four classifications of spherical carbon have been proposed; i) Inagaki [177,178] classified the spherical carbon structures into three cluster types according to the arrangement of carbon layers being concentric, radial and random; ii) Later Serp et al. [181] categorized the spherical carbon bodies according to their size; fullerene (< 2 nm), carbon onions (2-20 nm) carbon spheres (50-1000 nm) and carbon beads (1 μm); iii) spheres can also be described as solid, core-shell or hollow [179] and iv) it is possible to classify spheres in terms of strategies used in their synthesis [180].

1.8.1 Synthesis of carbon spheres

Carbon sphere synthesis methods can be divided into two categories: one is the catalytic method, which could further be divided into two sub-divisions; supported and unsupported catalyst synthetic methods. The other category involves non-catalytic methods such as arc evaporation, lazer vaporization and electrochemical methods. In general catalytic synthesis involves the decomposition of a carbon source typically diluted with an inert (Ar,He) and a reactive (H_2) gas flow. In catalytic synthesis the yield and nature of the carbonaceous product is determined by the catalytic metal, the hydrocarbon source and the temperature [181]. In general carbon spheres can be synthesized by methods that are normally used to fabricate CNTs [182-189]. Wang et al. [190] developed a mixed-valent oxide catalytic carbonization (MVOCC) process for the production of carbon spheres. By varying temperature this produced either spheres or CNTs when methane was used as a carbon source. The dependency of the nature of the carbonaceous material on temperature was evident from their work.

Also Viera et al. [191] reported formation of carbon microspheres when using a hot tungsten filament CVD method at temperatures as high as 1650 ºC from methane. On the other hand Xu et al. [192] demonstrated the important role of a catalyst-substrate/support interaction during the synthesis of shaped carbon materials, where CVD methods using cobalt as a catalyst gave different carbon structures based on the type of support used. When they used Kaolin as a support, spheres were obtained; when a ceramic support was used a mixture of both CNTs and carbon spheres was obtained, whereas in the absence of a support, the carbonaceous materials formed were exclusively CNTs under the same experimental conditions. They suggested that, substrates which induce catalyst sintering usually result in carbon species containing unstable hexagonal or heptagonal rings or reactive dangling bonds which lead to bond switching and migration processes to attain the more stable spherical carbon structures. It is believed that the arrangement of the metal atom at the face where carbon is deposited ultimately regulates the nature of the precipitated carbon. The heterogeneity of the supported metal in terms of particle size, exposed crystal face and defects which in turn result in a range of interaction energetics can be expected to result in a diversity of deposited carbon morphologies as has been demonstrated in [193].

The use of transition metals as catalysts leads to the formation of catalyst-encapsulated carbon spheres, leading to the issue of catalyst removal from the product. For some practical applications, pure carbon spheres without any impurity are required. Some research groups have reported the synthesis of carbon spheres by non-catalytic methods. Qian et al. [194] prepared carbon spheres from toluene without any catalyst; the size of the spheres could be controlled by changing gas flow rate as well as the composition of the carrier gas. Jin et al. [195] reported the large-scale synthesis and characterization of carbon spheres (diameters from 50 nm to 1 μm) by direct pyrolysis of hydrocarbons (containing 2–8 carbon atoms). Pol et al. [196] produced carbon spheres by dissociating various hydrocarbons (containing 5–14 carbon atoms in liquid form) under autogenic pressure at 700 °C. Without using a catalyst, Govindaraj et al. examined the pyrolysis of methane under hydrogen atmosphere and obtained carbon spheres at 1140 °C [197].

1.9 Halogenation of carbonaceous materials

Pristine nanotubes are unfortunately insoluble in many liquids such as water, polymer resins, and most solvents. Thus they are difficult to evenly disperse in a liquid matrix made of epoxides and other polymers. This complicates efforts to utilize the nanotubes' outstanding physical properties in the manufacture of composite materials, as well as in other practical applications which require preparation of uniform mixtures of CNTs with many different organic, inorganic, and polymeric materials. The unique electronic and structural properties of pristine CNTs have endowed CNT-based electrochemical sensors with excellent analytical properties even without any surface functionalization of CNTs. The widespread development of novel electrochemical nanotube devices will however require rational surface functionalization of CNTs because the CNTs themselves do not bear many (bio) electrochemically functional moieties that could be employed as electrocatalysts for electrochemical sensing or as bio-recognition elements for electrochemical biosensing and biofuel cells. Chemical doping is expected to substantially increase the density of free charge carriers and thereby enhance the electrical and thermal conductivity of carbon materials as well as improve their solubility.

In the earlier part of the review the above issues were described in general terms. A more specific approach to these issues can be achieved by halogenation of carbon materials. Although it is unlikely that halogen atoms can be added as a dopant to a carbon material the halogens can be present on the inside or the outside of a structure. As will be seen from the literature review below, all studies have so far focused on the reactions that occur on the external faces of carbon materials.

1.9.1 Effects of halogenation

It has been stated earlier in the review that C_{60} as well as any other fullerenes can undergo addition reactions with many electrophiles and nucleophiles [198,199]. Halogens

have been found to react with C_{60} to give a range of $C_{60}X_n$ (n > 0) molecules. Below are given some examples of the properties of $C_{60}X_n$ (X = F, Cl, Br, I).

The physicochemical properties of halogenated fullerenes depend on the extent of halogenation. It was established by cyclic voltammetry that the electron affinity of $C_{60}F_{36}$ is smaller than that of $C_{60}F_{46}$ by *ca.* 0.56 eV [200]. This demonstrated that the electron affinity and, consequently, the electronic structure of $C_{60}F_x$ vary as a function of the number of fluorine atoms attached to the C_{60} molecule.

Amarantov et al. [201] observed a drastic change in the photoluminescence and absorption properties of C_{60} fluorides from $C_{60}F_{18}$ to $C_{60}F_{48}$. They noted a blue shift of the luminescence spectra with increasing fluorine content. The absorption spectra obtained for $C_{60}F_{18}$ conserved the three main features of the pristine C_{60} whereas only a single peak was seen in the UV region for $C_{60}F_{48}$. They established that the increasing number of fluorine atoms attached to the C_{60} molecule shifted the absorption spectra to higher energy. It was suggested that the spectrum shifted to the higher energy region due to the reduction of the initial π-electron subsystem of pure C_{60} and the creation of new δ-orbitals with CF bonds.

The electronic structure of the chlorinated fullerene $C_{60}Cl_{30}$ has been studied by photoemission and X-ray emission spectroscopy. Interpretation of the experimental spectra has been based on the calculations of a $C_{60}Cl_{30}$ molecule of D_{3d} symmetry in the density functional approximation. Participation of the Cl 3d atomic orbital in formation of the C–Cl bonds of the molecule has been established from comparison of the experimental and theoretical data. It was suggested that this was an explanation for the high thermal stability of the D_{3d} isomer of the $C_{60}Cl_{30}$ [202].

Priyadarsini et al. studied the UV-vis absorption spectra of chlorinated fullerenes ($C_{60}Cl_6$, $C_{60}Cl_{12}$) in cyclohexane and established that they exhibited bands with λ_{max} at 210 and 255 nm. Their studies indicated that the sharpness and molar absorptivity of chlorinated fullerenes decreases with increase in the number of chlorine atoms [203].

The interfacial properties of the spread Langmuir films of $C_{60}Br_{24}$ and stearic acid have been studied at an air–water interface by measuring their surface pressure–area isotherms. Monolayer studies on $C_{60}Br_{24}$ suggested a strong aggregation at air–water interface. The mixed films were found to be immiscible and non-ideal with the exception of X = 0:5 (where X is the molar ratio) which showed the greatest stability. The interaction between $C_{60}Br_{24}$ and stearic acid resulted in the lowering of the surface pressure by stearic acid and hence the decrease in compressibility with the increasing $C_{60}Br_{24}$ molar ratio, which indicated the domination of $C_{60}Br_{24}$ characteristics in the mixed monolayers [204].

Although carbon nanotubes are generally known to be inert towards fluorination at room temperature, Yudanov and co-workers achieved fluorination of MWNTs at room temperature even though only the outside shell was modified [205]. Fluorination of SWNTs has been carried out in a similar manner to fluorination of graphite [206]. On the other hand Nakajima et al. [207] demonstrated chemical fluorination of CNTs at temperatures from 250 °C to 400 °C. Even though fluorination of CNTs between 250 °C and 400 °C does not cause detrimental damage to the structure, it reduces the conductivity of the CNTs due to partial destruction of the graphitic lattice [207]. Various physicochemical properties of fluorinated CNTs including high-resolution electron energy loss [207], thermal recovery behavior [208] and solvation in alcoholic solvents have been investigated.

Unger et al. by electrochemical methods improved the solubility of MWNTs in water and/or ethanol by covalently incorporating chlorine and bromine onto the outer walls of MWNTs [209]. Also the controlled non-destructive fluorination of SWNT sidewalls at temperatures up 325 °C was reported in 1998 by Mickelson et al. [206]. According to Mickelson this reaction yielded “fluorocarbon SWNTs of approximately C_2F stoichiometry”. In further work Mickelson et al. [210] demonstrated that F-SWNTs dissolved well in alcohol solvents to give long-lived metastable solutions. Thus a solution-phase chemistry of F-SWNTs was established, where the unfluorinated SWNTs could be precipitated out of solution with anhydrous hydrazine.

On the other hand Ray et al. chlorinated nitrogen-doped carbon nanotubes (N-CNTs) in an inductively coupled plasma reactor using chlorine gas and found that field emission properties of N-CNTs were enhanced upon chlorination [211]. Based on electronic studies done in another study, Ray et al. [212,213] concluded that the overall field emission improvement of chlorinated N-CNTs is due to an etching effect on chlorine plasma treatment with the formation of C-Cl bonds after reducing the carbon content. An overall increase in density of free charge carriers was noted.

Rao et al. [214] doped SWNTs with bromine and iodine at room temperature. They found via Raman spectroscopy studies, that the high frequency tangential vibration modes of carbon atoms in SWNTs shifted substantially to higher frequencies upon doping with halogens. Bromine doping showed substantial changes but only a small change was seen for iodine doping. I_2 and Br_2 are expected to pull electrons from the carbon π-states to the dopant molecule creating holes.

1.9.2 Synthesis of carbon materials using halohydrocarbons

Synthesis of CNTs via a dechlorination route is said to be a cost effective process, which avoids rigorous conditions such as high temperature, high pressure or complicated instrumentation and it is easily applicable on a large scale. As such it has aroused the interest of several research groups. The most common dechlorination path is via metal reduction. For example metallic potassium was reacted with hexachlorobenzene [215] and ethylene tetrachloride [216] at 350 °C and 200 °C respectively to produce MWNTs. Catalytic solid-state metathesis reactions between polymers containing chlorine, such as PVC and Li_2C_2 have also been used to prepare MWNTs [217]. Also synthesis of MWNTs through an anhydrous $AlCl_3$ assisted C_2Cl_4 dechlorination process at temperatures as low as 160 °C have been reported [218]. Using magnesium metal which is a less violent metal than the alkaline metals, Ni et al. [219] reported the synthesis of hollow carbon spheres at mild temperatures of around 200 °C, from C_2Cl_6 in the presence of $AlCl_3$.

Chien et al. also reported on the synthesis of hollow spheres from CCl_4 at 600-900 °C under argon in the presence of molybdenum powders. They proposed that Mo acts as a template for the initial hollow carbon sphere formation and as the reaction proceeds the Mo core is etched away by the chlorine atoms produced by the dechlorination of CCl_4 to form the amorphous hollow carbon spheres [220]. From their previous studies where 1-chlorobutane and hexachlorobenzene were used, Chien et al. [193] noticed that the Mo core was preserved, so they suggested that the reason for the observed difference was due to the different Cl:C ratios found in the chlorinated reactants. Thus, the more chlorine atoms there are on the reactants the higher the tendency of etching.

1.10 The objective of the study

Synthesis of carbon materials by chemical vapour deposition suggests a condition dependent process. This study investigates the synthesis of carbons by floating catalyst horizontal CVD via injection of precursor solutions.

It is well known that non-carbon containing precursors impact on the properties of the carbon materials. Thermal pyrolysis of halogen and silicon containing precursors is a major focus of this study. Thermal pyrolysis of chlorobenzene as a source of halogen will be investigated. In order to learn more about the thermal pyrolysis of chlorobenzene, it will be subjected to various non-carbon containing reagents, which are well known sources of poisons (thiophene), radical initiators (chloroform) and radical abstractors (ammonia). Also the impact of reaction conditions such as gas flow rate and gas composition (inert or reactive gas) on morphology, yield, size and dimensions of the will be studied.

Preparation of carbon materials from silicon sources will be undertaken in order to establish the possibility as well as forms in which silicon may be encorporated into the produced carbons. The influence of different Si-Y bonds on the overall production of

carbons will be investigated by studying the thermal pyrolysis of tertraethylorthosilicate against thermal decomposition of triethylchlorosilane (Si-O vs Si-Cl bond).

Properties of carbons prepared from halogen and silicon sources will be investigated by various techniques. Raman analysis will be employed to investigate the graphitization of the carbons. Thermogravimetric analysis (TGA) will be preformed to investigate thermal properties such as thermal stability and degradation temperature. Also the constituents of the carbons like moisture, inorganic and organic content will be established via TGA. Infra-red spectroscopy will provide information on the functional groups generated on the carbon materials produced. EDS analysis will provide information on the overall elemental composition and relative abundances of the elements.

The morphology as well as dimensions of carbon materials prepared here will be determined by transmission electron and scanning electron microscopies.

1.11 References:

1. H. W. Kroto, J. R. Heath, S. C. O'Brien, R .F. Curl, R. E. Smalley, *Nature* **318** (1985) 162
2. S. Iijima, *Nature* **354** (1991) 56
3. Y. M. Shyu, F. Chau-Nan Hong, *Diam. Relat. Mater.* **101** (2001) 241
4. M. Zhang, D. W. He, L. Ji, B. Q. Wei, D. H. Wu, X. Y. Zhang, *Nanostruct. Mater.* **10** (1998) 291
5. T. Cabioc'h, E. Thune, M. Jaouen, *Chem. Phys. Lett*. **320** (2000) 202
6. T. Cabioc'h, E. Thune, M. Jaouen, *Phys. Rev. B* **65** (2002) 132103
7. N. Sano, H. Wang, M. Chhowalla, I. Alexandrou, G. A. J. Amaratunga, *Nature* **414** (2001) 506
8. X. H. Chen, F. M. Deng, J. X. Wang, H. S. Yang, G. T. Wu, X. B. Zhang, *Chem. Phys. Lett*. **336** (2001) 201
9. X. Bing-She, *New Carbon Mater.* **23** (2008) 289
10. D. Ugarte, *Nature* **359** (1992) 707
11. W. A. de Heer, D. Ugarte, *Chem. Phys. Lett.* **207** (1993) 480
12. T. Stockli, J-M. Bonard, A. Chatelain, Z. L. Wang, P. Stadelmann, *Phys. Rev. B* **57** (1998) 15599
13. J. Du, Z. Liu, Z. Li, B. Han, Z. Sun, Y. Huang, *Mater. Chem. Phys*. **93** (2005) 178
14. Z. L. Wang, J. S. Yin, *Chem. Phys. Lett.* **289** (1998) 189
15. R. K. Rana, A. Gadanken, *J. Phys. Chem. B* **106** (2002) 9769
16. H. W. Kroto, *Nature* **329** (1987) 529
17. X. Liu, T. G. Schmalz, D. J. Klein, *Chem. Phys. Lett.* **188** (1992) 550
18. http//en.wikipedia.org/wiki/Eular_characteristic 01-02-09, 14.00 hrs
19. T. G. Schmalz, W. A. Seitz, D. J. Klein, G. E. Hite, *J. Am. Chem. Soc*. **110** (1988) 1113
20. S-Y. Xie, F. Gao, X. Lu, R.-B. Huang, C.-R.Wang, X. Zhang, M. Liu, S.-L. Deng, L.-S. Zheng, *Science* **304** (2004) 699

21. C. M. Beavers, T. Zuo, J. C. Duchamp, K. Harich, H. C. Dorn, M. M. Olmstead, A. L. Balch, *J. Am. Chem. Soc.***128** (2006) 11352
22. Z.-F. Chen, *Angew. Chem. Int. Ed.* **43** (2004) 4690
23. X. Han, S.-J. Zhou, Y.-Z. Tan, X. Wu, F. Gao, Z.-J. Liao, R.-B. Huang, Y.-Q. Feng, X. Lu, S.-Y. Xie, L.-S. Zheng, *Angew. Chem.* **120** (2008) 5420; *Angew. Chem. Int. Ed.* **47** (2008) 5340
24. Y.-Z. Tan, X. Han, X. Wu, Y.-Y. Meng, F. Zhu, Z.-Z. Qian, Z.-J. Liao, M.-H. Chen, X. Lu, S.-Y. Xie, R.-B. Huang, L.-S. Zheng, *J. Am. Chem. Soc.* **130** (2008) 15240
25. C.-R. Wang, Z.-Q. Shi, L.-J. Wan, X. Lu, L. Dunsch, C.-Y. Shu, Y.-L. Tang, H. Shinohara, *J. Am. Chem. Soc.* **128** (2006) 6605
26. X. Han, S.-J. Zhou, Y.-Z. Tan, X. Wu, F. Gao, Z.-J. Liao, R.-B. Huang, Y.-Q. Feng, X. Lu, S.-Y. Xie, L.-S. Zheng, *Nat. Mater.* **7** (2008) 790
27. I. N. Ioffe, A. A. Goryunkov, N. B. Tamm, Lev. N. Sidorov, E. Kemnitz, S. I. Troyanov, *Angew. Chem. Int. Ed.* **48** (2009) 5904
28. A. F. Shestakov, *Russian J. Gen. Chem.* **78** (2008) 811
29. A. M. Rao, Z. Ping, W. Kai-An, G. T. Hager, J .M. Holden, W. Ying, W. T. Lee, Bi Xiang-Xin, P. C. Eklund, M .A. Cornett,. M. A. Duncan, I .J. Amster, *Science* **259** (1993) 955
30. M. M. J. Treacy, T. W. Ebbesen, J. M. Gibson, *Nature* **381** (1996) 678
31. C. Liu, Y. Y. Fan, M. Liu, H. T. Cong, H. M. Cheng, M. S. Dresselhaus, *Science* **286** (1999) 1127
32. H. M. Cheng, Q. H. Yong, C. Liu, *Carbon* **39** (2001) 1447
33. S. Wong, E. Joselevich, A. Wooley, C. Cheung, C. Lieber, *Nature* **394** (1998) 52
34. J. Kong, N. R. Franklin, C. Zhou, M. G. Chapline, S. Peng, K. Cho, H. Dai, *Science* **287** (2000) 622
35. H. Dai, N. Franklin, J. Han, *Appl. Phys. Lett.* **73** (1998) 1508
36. J. H. Hafner, Chin-Li Cheung, T. H. Oosterkamp, C. M. Lieber, *J. Phys. Chem. B* **105** (2001) 743

37. E. Frackowiak, K. Metenier, V. Bertagna, F. Beguin, *Appl. Phys. Lett*. **77** (2000) 2421
38. R. Martel, T. Schmidt, H. R. Shea, T. Hertel, P. H. Avouris, *Appl. Phys. Lett.* **73** (1998) 2447
39. S. Tans, A. Verschueren, C. Dekker, *Nature* **393** (1998) 49
40. P. M. Ajayan, T. W. Ebbesen, T. I. Chihashi, S. Iijima, K. Tanigaki, H. Hiura, *Nature* **362** (1995) 522
41. A. M. Rao, P. C. Eklund, S. Bandow, A. Thess, R. E. Smalley, *Nature* **388** (1997) 257
42. R. S. Lee, H. J. Kim, J. E. Fischer, A. Thess, R.E. Smalley, *Nature* **388** (1997) 255
43. D. L. Carroll, Ph. Redlich, X. Blase, J. C. Charlier, S. Curran, P. M. Ajayan, S. Roth, M. Ruhle, *Phys. Rev. Lett*. **81** (1998) 2332
44. R. Czerw, M. Terrones, J. C. Charlier, X. Blase, B. Foley, P. Kamalakaran, N. Grobert, H. Terrones, D. Tekleab, P. M. Ajayan, W. Blau, M. Rühle, D. L. Carroll, *Nano. Lett.* **1** (2001) 457
45. M. Monthioux, *Carbon* **40** (2002) 1809
46. J. Sloan, A. I. Kirkland, J. L. Hutchison, M. L. H. Green, *Chem. Comm*. (2002) 1319
47. C. G. Piecourt, Y. L. Bouar, A. Loiseau, H. Pascard, *Nature* **372** (1994) 761
48. B. W. Smith, M. Monthioux, D. E. Luzzi, *Nature* **396** (1998) 323
49. H. Kataura, Y. Maniwa, M. Abe, A. Fujiwara, T. Kodama, K. Kikuchi, H. Imahori, Y. Misaki, S. Suzuki, Y. Achiba, *Appl. Phys.* **74** (2002) 349
50. T. Takenobu, T. Takano, M. Shiraishi, Y. Murakami, M. Ata, H. Kataura, Y.J. Achiba, Y. Iwasa, *Nat. Mater*. **2** (2003) 683
51. Y. Zhang, H. Dai, *Appl. Phys. Lett*. **77** (2000) 3015
52. P. G. Collins, K. Bradley, M. Ishigami, A. Zettl, *Science* **287** (2000) 1801
53. G. U. Sumanasekera, C. K. W. Adu, S. Fang, P. C. Eklund, *Phys. Rev. Lett.* **85** (2000) 1096
54. A. Kleinhammes, S. H. Mao, X. J. Yang, X. P. Tang, H. Shimoda, J. P. Lu, O. Zhou, Y. Wu, *Phys. Rev. B* **68** (2003) 075418

55. G. U. Sumanasekera, B. K. Pradhan, H. E. Romero, K. W. Adu, P. C. Eklund, *Phys. Rev. Lett.* **89** (2002) 166801
56. M. J. O'Connell, P. Boul, L. M. Ericson, C. Huffman, Y. Wang, E. Haroz, C. Kuper, J. Tour, K. D. Ausman, R. E. Smalley, *Chem. Phys. Lett.* **342** (2001) 265
57. S. Niyogi, A. Hamon, H. Hu, B. Zhao, P. Bhowmik, R. Sen, M. E. Itkis, R. C. Haddon, *Acc. Chem. Res*. **35** (2002) 1105
58. K. Balasubramanian, M. Burghard, *Small* **1** (2005) 180
59. J. R. Heath, S. C. Obrien, Q. Zhang, Y. Liu, R. F. Curl, H. W. Kroto, F. K. Tittel, R. E. Smalley, *J. Am. Chem. Soc*. **107 (**1985) 7779
60. S. Osuna, M. Swart, M. Solá, *Chem. Eur. J.* **00** (2009) 0
61. R. L. Murry, G. E. Scuseria, *Science* **263** (1994) 791
62. M. Murata, Y. Murata, K. Komatsu, *Chem. Comm*. (2008) 6083
63. N. Martín, *Chem. Comm*. (2006) 2093
64. C. Guerret-Pi´ecourt, Y. Le Bouar, A. Loiseau, H. Pascard, *Nature* **372** (1994) 761
65. E. Dujardin, T. W. Ebbesen, H. Hiura, K. Tanigaki, *Science* **265** (1994) 1850
66. S. C. Tsang, Y. K. Chen, P. J. F. Harris, M. L. H. Green, *Nature* **372** (1994) 159
67. Y. K. Chen, M. L. H. Green, S. C. Tsang, *Chem. Comm.* (1996) 2489
68. D. Ugarte, A. Châtelain, W. A. de Heer, *Science* **274** (1996) 1897
69. A. Chu, J. Cook, R. Heesom, J. L. Hutchison, M. L. H. Green, J. Sloan, *Chem. Mater* **8** (1996) 2751
70. Y. K. Chen, A. Chu, J. Cook, M. L. H. Green, P. J. F. Harris, R. Heesom, M. Humpries, J. Sloan, S. C. Tsang, J. F. C. Turner, *J. Mater. Chem.* **7** (1997) 545
71. D. Ugarte, T. Stöckli, J. M. Bonard, A. Châtelain, W. A. de Heer, *Appl. Phys. A* **67** (1998) 101
72. C. Pham-Huu, N. Keller, C. Estournes M. J. Ledoux, *Chem. Comm*. (2002) 1882
73. J. P. Tessonnier, L. Pesant, G. Ehret, *Appl. Catal. A* **288** (2005) 203
74. F. Qiang, G. Weinberg, S. Dang-sheng, *New Carbon Mater.* **23** (2008) 17

75. G. Maurin, Ch. Bousquet, F. Henn, P. Bernier, R. Almairac, B. Simon, *Chem. Phys. Lett.* **312** (1999) 14
76. V. Z. Mordkovica, M. Baxendale, S. Yoshimua, R. P. H. Chang, *Carbon* **43** (1996) 1301
77. V. A. Nalimova, D. E. Sklovsky, G. N. Bondarenko, H. Alvergnat- Gaucher, S. Bonnamy, F. Béguin, *Synthetic Metals* **88** (1997) 89
78. M. Bockrath, J. Hone, A. Zettl *Phys. Rev. B* **61** (2000) 10606
79. K. Bradley, S. H. Jhi, P. G. Collins, *Phys. Rev. Lett.* **85** (2000) 4361
80. R. Martel, V. Derycke, C. Lavoie, *Phys. Rev. Lett*. **87** (2001) 6805
81. V. Derycke, R. Martel, J. Appenzeller, P. Avouris, *Appl. Phys. Lett*. **80** (2002) 2773
82. P. O. Lehtinen, A. S. Foster, Y. Ma, A. V. Krasheninnikov, R. M. Nieminen, *Phys. Rev. Lett.* **93** (2004) 187202
83. P. Esquinazi, D. Spemann, R. Hohne, A. Setzer, K. H. Han, T. Butz, *Phys. Rev. Lett.* **91** (2003) 227201
84. J. A. Chan, B. Montanari, J. D. Gale, S. M. Bennington, J. W. Taylor, N. M. Harrison, *Phys. Rev. B* **70** (2004) 041403
85. S. Talapatra, P. G. Ganesan, T. Kim, R. Vajtai, M. Huang, M. Shima, G. Ramanath, D. Srivastava, S. C. Deevi, P. M. Ajayan, *Phys. Rev. Lett.* **95** (2005) 097201
86. W. Andreoni, F. Gygi, M. Parrinello, *Chem. Phys. Lett.* **190** (1992) 159
87. G. Csanyi, T. A. Arias, *Chem. Phys. Lett.* **360** (2002) 552
88. A. H. Nevidomskyy, G. Csanyi, M. C. Payne, *Phys. Rev. Lett*. **91** (2003) 105502
89. L. H. Chan, K. H. Hong, D. Q. Xiao, T. C. Lin, S. H. Lai, W. J. Hsieh, H. C. Shih, *Phys. Rev. B* **70** (2004) 125408
90. A. N. Andriotis, R. M. Sheetz, E. Richter, M. Menon, *Europhys. Lett*. **72** (2005) 658
91. K. McGuire, N. Gothard, P. L. Gai, M. S. Dresselhaus, G. Sumanasekera, A. M. Rao, *Carbon* **43** (2005) 219

92. P. L. Gai, O. Stephan, K. McGuire, A. M. Rao, M. S. Dresselhaus, G. Dresselhaus, C. Colliex, *J. Mater. Chem.***14** (2004) 669
93. F. Villapando-Paez, A. Zamudio, A. L. Elias, H. Son, E. B. Barros, S. G. Chow, Y. A. Kim, H. Muramatsu, T. Hayashi, J.Kong, H. Terrones, G. Dresselhaus, M. Endo, M. Terrones, M. S. Dresselhaus, *Chem. Phys. Lett.* **424** (2006) 345
94. E. Cruz-Silva, D. A. Cullen, L. Gu, J. M. Romo-Herrera, E. Muoz-Sandoval, F. Lopez-Uras, B. G. Sumpter, V. Meunier, J.-C. Charlier, D. J. Smith, H. Terrones, M. Terrones, *ACS Nano.* **2** (2008) 441
95. I. O. Maciel, N. Anderson, M. A. Pimenta, A. Hartschuh, H. Qian, M. Terrones, H. Terrones, J. Campos-Delgado, A. M. Rao, L. Novotny, A. Jorio, *Nat. Mater.* **7** (2008) 878
96. B. G. Sumpter, J. Huang, V. Meunier, J. M. Romo-Herrera, E. Cruz-Silva, H. terrones, M. Terrones, *Int. J. Quantum Chem.* **109** (2009) 97
97. I. O. Maciel, J. Campos-Delgado, M. A. Pimenta, M. Terrones, H. Terrones, A. M. Rao, A. Jorio, *Phys. Status Solidi. B* (2009) 1
98. Y. Zhang, N. W. Franklin, R. J. Chen, H. J. Dai, *Chem. Phys. Lett.* **331** (2000) 35
99. S. Inoue, Y. Matsumura, *Chem. Phys. Lett* **464** (2008) 160
100. D. M. Guldi, G. M. A Rahman, F. Zerbetto, M. Prato, *Acc. Chem. Res.* **38** (2005) 871
101. M. Prato, K. Kostarelos, A. Bianco, *Acc. Chem. Res.* **41** (2008) 60
102. V. N. Khabashesku, W. E. Billups, J. L Margrave, *Acc. Chem. Res.* **35** (2002) 1087
103. R. J. Chen, Y. Zhang, D. Wang, H. Dai, *J. Am. Chem. Soc.* **123** (2001) 3838
104. O.-K. Kim, J. Je, J. W. Baldwin, S. Kooi, P. E. Pehrsson, L. J. Buckley, *J. Am. Chem. Soc.***125** (2003) 4426
105. A. Star, Y. Liu, K. Grant, L. Ridvan, J. F. Stoddart, D. W. Steuerman, M. R. Diehl, A .Boukai,. J. R. Heath, *Macromolecules* **36** (2003) 553
106. F. Wudl, *Acc. Chem. Res.* **25** (1992) 157

107. M, Prato, V. Lucchini, M. Maggini, E. Stimpfl, G. Scorrano, M. Eiermann, T. Suzuki, F . Wudl, *J. Am. Chem. Soc.* **115** (1993) 8479

108. M. Prato, Q. Li, , F.Wudl, V. Lucchini, *J. Am. Chem. Soc.* **115** (1993) 1148

109. M. Maggini, G. Scorrano, M. Prato, *J. Am. Chem. Soc.* **115** (1993) 9798

110. V. Georgakilas, K. Kordatos, M. Prato, D. M. Guldi, M. Holzinger, A. Hirsch, *J. Am. Chem. Soc*. **124** (2002) 760

111. http// upload.wikimedia.org/commons/pratoreaction.png

112. C. Haddon, *Acc. Chem. Res* **21** (1998) 243

113. Z. Chen, W. Thiel, A. Hilsh, *ChemPhysChem* **4** (2003) 93

114. M. Terrones, A. G. S. Filho, A. M. Rao, *Topics Appl. Physics* **111** (2008) 531

115. E. Katz, I. Willner, *ChemPhysChem* **5** (2004) 1084

116. A. Hirsch, *Angew. Chem.* **114** (2002) 1933

117. M.-L. Sham, J.-K. Kim, *Carbon* **44** (2006) 768

118. F. Pompeo, D. E. Resasco, *Nano. Lett.* **2** (2002) 369

119. C. V. Nguyen, L. Delzeit, A. M. Cassel, J. Li, J. Han, M. Meyyappan, *Nano. Lett.* **2** (2002) 1079

120. K. A. Williams, P. T. M. Veenhuizen, B. G. de la Torre, R. Eritjia, C. Dekker, *Nature* **420** (2002) 761

121. C.-H. Xue, R.-J. Zhou, M.-M. Shi, Y. Gao, G. Wu, X.-B. Zhang, H-Z. Chen, M. Wang, *Nanotech.* **19** (2008) 215604

122. S. Zhan, Y. Li, *J. Dispersion Science and Technology* **29** (2008) 240

123. Z. Yang, X. Chen, C. Chen, W. Li, H. Zhang, L. Xu, B. Yi, *Polymer Composites* (2007) 36

124. X. Li, S. Y. Wong, W. C. Tjiu, B. P. Lyons, S. A. Oh, C. B. He, *Carbon* **46** (2008) 818

125. J.-M. Yeh, K.-Y. Huang, S.-Y. Lin, Y.-Y. Wu, C.-C., Huang, S.-J. Liou, *J. Nanotech*. (2009), (article ID 217469, doi:10.1155/2009/217469)

126. L. Rapoport, Y. Bilik, Y. Feldman, M. Hoyofer, S. R. Cohen, R. Tenne, *Nature* **387** (1997) 791

127. M. Chowalla, G. A. J. Amaratunga, *Nature* **407** (2000) 164

128. V. N. Khabashesku, W. E. Billups, J. L. Margrave, *Acc. Chem. Res.* **35** (2002) 1087

129. R. L. Vander Wal, K. Miyoshi, K. W. Street, A. J. Tomasek, H. Peng, Y. Liu, J. L. Margravem, V. N. Khabashesku, *Wear* **259** (2005) 738

130. S. B. Sinnott, R. Andrews, *Critical Reviews in Solid State and Materials Science* **26** (2001) 145

131. J. A. Alonso, J. S. Arellano, L. M. Molina, A. Rubio, M. J. López, *IEEE Trans. Nanotech*. **3** (2004) 304

132. O. Gulseren, T. Yildirim, S. Ciraci, *Phys. Rev. Lett.* **87**, (2001) 116802

133. V. Gayathri, R. Geetha, *Adsorption* **13** (2007) 53

134. B. K. Pradhan, A. R. Harutyunyan, D. Stojkovic, J. C. Grossman, P. Zhang, M. W. Cole, V. Crespi, H. Goto, J. Fujiwara, P. C. Eklund, *J. Mater. Res.* **17** (2002) 2209

135. M. Eswaramoorthy, R. Sen, C. N. R. Rao, *Chem. Phys. Lett*. **304** (1999) 207

136. H. Kataura, Y. Kumazawa, Y. Maniwa, I. Umezu, S. Suzuki, Y. Ohtsuka, Y. Achiba, *Synth. Met.* **103** (1999) 2555

137. P. Petit, C. Mathis, C. Journet, P. Bernier, *Chem. Phys. Lett.* **305** (1999) 370

138. J. L. Bahr, J. Yang, D. V. Kosynkin, M. J. Bronikowski, R. E. Smalley, J. M. Tour, *J. Am. Chem. Soc*. **123** (2001) 6536

139. J. L. Steven, A.Y. Huang, H. Peng, I. W. Chiang, V. N. Khabashesku, J. L. Margrave, *Nano. Lett*. **3** (2003) 331

140. K. Kamaras, M. E. Itkis, H. Hu, B. Zhao, R. C. Haddon, *Science* **301** (2003) 1501

141. H. Hu, B. Zhao, M. A. Hamon, K. Kamaras, M. E. Itkis, R. C. Haddon, *J. Am. Chem. Soc*. **125** (2003) 14893

142. X. Lu, Z. Chen, *Chem. Reviews* **105** (2005) 3643

143. S. Hong, S. M. Yung, *Nat. Nanotech.* **2** (2007) 207

144. X. Zhou, J.-Y. Park, S. Huang, J. Liu, P. McEuen, *Phys. Rev. Lett*. **95** (2005) 146805

145. H. Dai, A. Javey, E. Pop, D. Mann, Y. Lu, *Brief Reports and Reviews* **1** (2006) 1

146. A. Bachtold, C. Strunk, J. P. Salvetat, *Nature* **397** (1999) 673

147. A. Bachtold, M. de Jonge, K. Grove-Rasmussen, *Phys. Rev. Lett*. **87** (2001) 6801

148. E. Pop, D. Mann, Q. Wang, K. Goodson, H. Dai, *Nano. Lett.* **6** (2006) 96

149. P. Kim, L. Shi, A. Majumdar, P. L. McEuen, *Phys. Rev. Lett*. **87** (2001) 215502

150. O. Lourie, H. D. Wagner, *J. Mater. Res*. **13** (1998) 2418

151. M.-F. Yu, O. Lourie, M J. Dyer, K. Moloni, T. F. Kelly, R. S. Ruoff, *Science* **287** (2000) 637

152. R. Krupke, F. Hennrich, H. van Lçhneysen, M. M. Kappes, *Science*, **301** (2003) 344

153. P. G. Collins, M. S. Arnold, P. Avouris, *Science* **292** (2001) 706

154. J.-C. Charlier, M. Terrones, M. Baxendale, V. Meunier, T. Zacharia, N. L. Rupesinghe, W. K. Hsu, N. Grobert, H. Terrones, G. A. J. Amaratunga, *Nano. Lett*. **2** (2002) 1191

155. M. Doytcheva, M. Kaiser, M. Reyes-Reyes, M. Terrones, N. de Jonge, *Chem. Phys. Lett.* **396** (2004) 126

156. M. Endo, Y. A. Kim, T. Hayashi, K. Nishimura, T. Matusita, K. Miyashita, M. S. Dresselhaus, *Carbon* **39** (2001) 1287

157. D. Y. Zhang, G. Y. Zhang, S. Liu, E. G. Wang, Q. Wang, H. Li, X. J. Huang, *Appl. Phys. Lett.* **79** (2001) 3500

158. J. Kong, M. G. Chapline, H. Dai, *Adv. Mater.* **13** (2001)1384

159. C. Baleizo, B. Gigante, H. Garcia, A. Corma, *J. Catal.* **221** (2004) 77

160. P. Calvert, *Nature* **399** (1999) 210

161. B. Fragneaud, K. Masenelli-Varlot, A. Gonz´alez-Montiel, M. Terrones, J. Y. Cavaill´e, *Chem. Phys. Lett.* **419** (2005) 567

162. K. Jiang, L. S. Schadler, R. W. Siegel, X. J. Zhang, H. F. Zhang, M. Terrones, *J. Mater. Chem.* **14** (2004) 37

163. K. Jiang, A. Eitan, L. S. Schadler, P. M. Ajayan, R. W. Siegel, N. Grobert, M. Mayne, M. Reyes-Reyes, H. Terrones, M. Terrones, *Nano. Lett.* **3** (2003) 275

164. A. Zamudio, A. L. Elìas, J. A. Rodríguez-Manzo, F. Lòpez-Uŕıas, G. Rodríguez-Gattorno, F. Lupo, M. Rühle, D. J. Smith, H. Terrones, D. Díaz, M. Terrones, *Small* **2** (2005) 346

165. X. Lepŕo, Y. Vega-Cant´u, F. J. Rodríguez-Macìas, Y. Bando, D. Golberg, M. Terrones, *Nano. Lett.* **7** (2007) 2220

166. S. Arepalli, P. Nikolaev, O. Gorelik, V. Hadjiev,W. Holmes, B. Files, L. Yowell, *Carbon* **42** (2004) 1783

167. A. Ferrari, J. Robertson, *Phys. Rev. B* **61** (2000) 14095

168. T. Belin, F. Epron, *Mater. Sci. Eng. B* **119** (2005) 105

169. M. J. O'Connell, S. M. Bachilo, C. B. Huffman, V. C. Moore, M. S. Strano, E. H. Haroz, K. L. Rialon, P. J. Boul, W. H. Noon, C. Kittrell, J. Ma, R. H. Hauge, R. B. Weisman, R. E. Smalley, *Science* **297** (2003) 503

170. Y. Miyauchi, S. Chiashi, Y. Murakami, Y. Hayashida, S. Maruyama, *Chem. Phys. Lett.* **387** (2004) 198

171. J. S. Lauret, C. Voisin, G. Cassabois, P. Roussignol, C. Delalande, A. Filoramo, L. Capes, E. Valentin, O. Jost, *Physica E* **21** (2004) 1057

172. K. Sattler, *Carbon* **33** (1995) 915

173. A. Burian, J. Koloczk, J. Dore, A.C. Hannon, J.B. Nagy, A. Fonseca, *Diam. Relat. Mater.* **13** (2004) 1261

174. J. C. Angus, C. C. Hayman, *Science* **241** (1988) 913

175. H. W. Kroto, K. Mckay, *Nature* **331** (1988) 328

176. P. Serp, R. Feurer, P. Kalck, Y. Kihn, J. L. Faria, J. L. Figueiredo, *Carbon* **39** (2001) 621

177. M. Inagaki, *Solid State Ion* **86** (1996) 833

178. M. Inagaki, *Carbon* **35** (1997) 711

179. Y. Xia, B. Gates, Y Yin, Y Lu, *Adv. Mater.* **12** (2000) 693

180. A. A. Deshmukh, S. D. Mhlanga, N. J. Coville unpublished work 2009

181. C. Park, P. M. Patterson, M. A. Keane, *Curr. Top. Colloid. Interface Sci.* **5** (2002) 93

182. Y. N. Xia, B. Gates, Y. D. Yin, Y. Lu, *Adv. Mater.* **12** (2000) 693

183. M. Sharon, K. Mukhopadhyay, K. Yase, S. Iijima, Y. Ando, X. Zhao, *Carbon* **36** (1998) 507

184. Z. Y. Zhong, H. Y. Chen, S. B. Tang, J. Ding, J. Y. Lin, K. L. Tan. *Chem. Phys. Lett.* **330** (2000) 41

185. Q. Wang, H. Li, L. Q. Chen, X. J. Huang, *Carbon* **39** (2001) 2211

186. X. Y. Liu, B. C. Huang, N. J. Coville, *Carbon* **40** (2002) 2791

187. D. Pradhan, M. Sharon, *Sci. Eng. B* **96** (2002) 24

188. J. S. Qiu, Y. F. Li, Y. P. Wang, C. H. Liang, T. H. Wang, D. B. Wang, *Carbon* **41** (2003) 767

189. Z. L. Wang, Z. C. Kang, *J. Phys. Chem.* **100** (1996) 5163

190. Z .L. Wang, Z. C. Kang, *J. Phys. Chem.* **100** (1996) 17725

191. S. M. C. Vieira, C. A. Rego, P. R. Birkett, *Diam. Rel. Mater.* **17** (2008) 100

192. Z.-X Xu, J.-D Lin, V. A. L. Roy, Y. Ou, D.-W Liao, *Mater. Sci. and Eng. B* **123** (2005) 102

193. C.-H. Chien, P.-S. Sheng, C.-H. Wang, C.-H. Huang, H.-K. Lin, C.-Y. Lee, H.-T. Chiu, *Mater. Lett.* **61** (2007) 3593

194. H. S. Qian, F. M. Han, B. Zhang, Y. C. Guo, J. Yue, B. X. Peng, *Carbon* **42** (2004) 761

195. Y. Z. Jin, C. Gao, W. K. Hsu, Y. Q. Zhu, A. Huczko, M. Bystrzejewski, M. Roe, C. Y. Lee, S. Acquah, H. Kroto, D. R. M. Walton, *Carbon* **43** (2005) 1944

196. V. G. Pol, S.V. Pol, J. M. C. Moreno, A. Gedanken, *Carbon* **44** (2006) 3285

197. A. Govindaraj, R. Sen, B. V. Nagaraju, C. N. R. Rao, *Philos. Mag. Lett.* **76** (1997) 363

198. A. Skiebe, A. Hirsch, *J. Chem. Soc. Chem. Comm*. (1994) 335

199. Q. Zhu, D. E. Cox, J. E. Fischer, K. Kniaz, A. R. Mc Ghie, *Nature* **355** (1992) 712

200. N. Liu, Y.Morio, F. Okino, H. Touhara, *Synthetic Metals* **86** (1997) 2289

201. S. V. Amarantov V. N. Bezmelnitsyna, O. V. Boltalinab, M. Danailovc, P. V. Dudina, A. V. Ryzkova, V. G. Stankevitcha, *Nuclear Instruments & Methods in Physics Research A* **470** (2001) 318

202. Yu. V. Lavskaya, T. A. Duda, S. I. Troyanov, I. P. Asanov, L. G. Bulusheva, A.V. Okotrub, *J. Molecular Structure* **921** (2009) 264

203. K. I. Priyadarsini, H. Mohan, P. R. Birkett, J. P. Mittal, *J. Phys. Chem.* **100** (1996) 501

204. S. S. Gayathri, A. Patnaik, *Chem. Phys. Lett*. **433** (2007) 317

205. F. Yadanov, A. V. Okotrub, Y. V. Shubin, L. I. Yudanov, L. G. Bulusheva, A. L. Chuvilin, J.-M. Bonard, *Chem. Mater.* **14** (2002) 1472

206. E. T. Mickelson, C. B. Huffman, A. G. Rinzler, R. E. Smalley, R. H. Hauge, J.-L. Margrave, *Chem. Phys. Lett*. **296** (1998) 188

207. T. Hayishi, M. Terrones, C. Scheu, Y. A. Kim, M. Rühle, T. Nakajima, M. Endo, *Nano. Lett*. **2** (2002) 491

208. W. Zhao, C. Song, B. Zheng, J. Liu, T. Viswanatha, *J. Phys. Chem. B* **106** (2002) 293

209. E. Unger, *Curr. Appl. Phys.* **2** (2002) 107

210. E. T. Mickelson, I. Chiang, J. Zimmerman, P. Boul, J. Lozan, J. Liu, R. E. Smalley, R. Hauge, J. Margrave, *J. Phys. Chem. B* **103** (1999) 4318

211. S. C. Ray, C. W. Pao, U. Palnitkar, H. M. Tsai. W. F. Pong, I. N. Lin, P. Papakonstantinou, A. Ganguly, L. C. Chen, K.H. Chen, *J. Appl. Phys.* **104** (2008) 063710

212. S. C. Ray, C. W. Pao, H. M. Tsai, J. W. Chiou, W. F. Pong, C. W. Chen, M.-H. Tsai, P. Papakonstantinou, L. C. Chen, K. H. Chen, *Appl. Phys. Lett*. **91** (2007) 202102

213. S. C. Ray, C. W. Pao, H. M. Tsai, J. W. Chiou, W. F. Pong, C. W. Chen, M.-H. Tsai, P. Papakonstantinou, L. C. Chen, K. H. Chen, W. G. Graham, *Appl. Phys. Lett.* **90** (2007) 192107

214. M. Rao, P. C. Eklund, S. Bandow, A. Thess, R. E. Smalley, *Nature* **388** (1997) 257

215. Y. Jiang, Y. Wu, S.Y. Zhang, C. Y. Xu, W. C. Yu, Y. Xie, *J. Am. Chem. Soc*. **122** (2000) 12383

216. X. J. Wang, J. Lu, Y. Xie, G. A. Du, Q. X. Guo, S. Y. Zhang, *J. Phys. Chem. B* **106** (2002) 933

217. J. L. Loughlin C.-H. Kiang, C. H. Wallace, T. K. Reynolds, L. Rao, R. B. Kaner, *J. Phys. Chem. B* **105** (2001)1921

218. J. Shen, Z. Huang, J. Li, L. Gao, H. Zhou, Y. Qian, *Carbon* **43** (2005) 2817

219. Y. Ni, M. Shao, Y. Tong, G. Qian, X. Wei, *J. Solid State Chem.* **178** (2005) 908

220. C.-H. Chien, P.-S. Sheng, C.-H. Wang, C.-H. Huang, H.-K. Lin, C.-Y. Lee, H.-T. Chiu, *Mater. Lett.* **62** (2008) 1176

Chapter 2

Experimental Section

Introduction

Three main generic synthesis methods have been used for the preparation of carbonaceous materials namely; laser ablation [1] arc-discharge [2], and chemical vapor deposition (CVD) methods [3]. All three methods can produce SWNTs and MWNTs. Of the various means for nanotube synthesis, CVD shows the most promise for industrial-scale synthesis, because of its low price/unit ratio cost, the possibility of continuous production and the greater control over the growth conditions. In general carbon spheres can also be synthesized by methods that are normally used to fabricate carbon nanotubes [4-11]. Two of the most promising CVD methods for making commercial quantities of CNTs are the floating catalyst [12] and injection methods [13]. In this study only these two CVD methods have been used to make carbonaceous materials.

2.1 Experimental apparatus

Carbonaceous materials were deposited using a double stage furnace system in which a quartz tube reactor about 120 cm in length was inserted horizontally into an electric furnace with the outlet of the tube connected to a gas bubbler as shown in figure 2.1. The temperatures of the two chambers were controlled by two separate thermocouples each placed in the middle of an individual furnace. The 1st small chamber was kept at 300 ºC, while the 2nd main chamber was kept at 900 ºC. An inert gas (argon) was purged through the tube to replace air present inside, as the furnace was heated to the desired set pyrolysis temperature. In a typical experiment, 15-20 ml of the precursor solution in a syringe was loaded onto a SAGE syringe pump and injected into the 1st chamber of the furnace via a water cooled quartz tubule similar to that described by Liu et al [14].

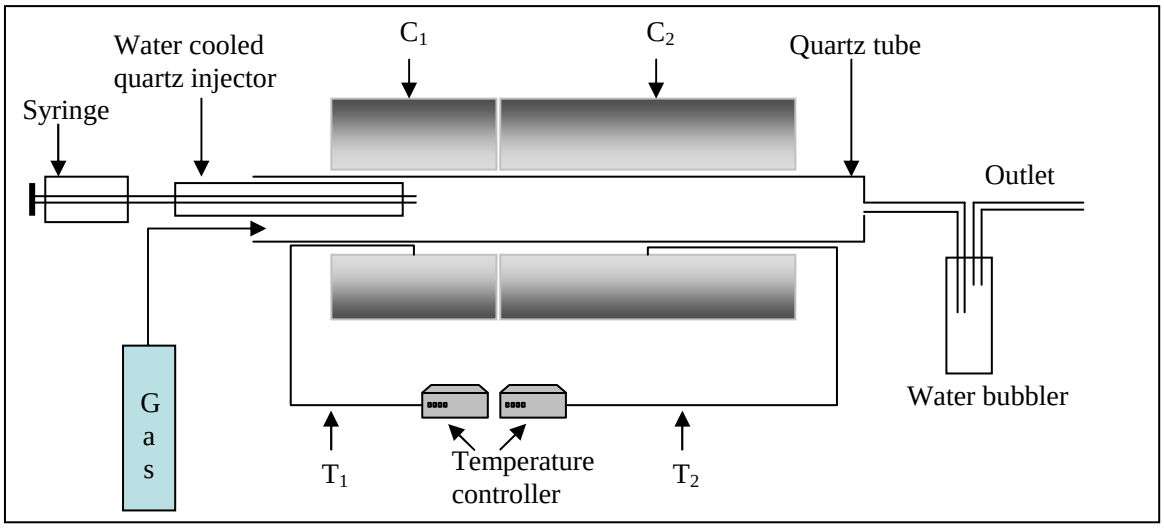

Fig. 2.1: Schematic diagram of experimental set-up (C_1-vaporization chamber, C_2-pyrolysis chamber; T_1,T_2-Thermocouples)

2.2 Experimental materials and procedure

All reagents listed in table 2.1 were commercially available from Strem chemicals and were used without further purification.

Table 2.1: A list of reagents used and their properties.

Reagent	Boiling point (°C)	Density (g/ml)	Purity (%)	Grade
Toluene (C_7H_8)	110	0.860	99.5	ACS
Chlorobenzene (C_6H_5Cl)	132	1.106	99.5	ACS
Bromobenzene (C_6H_5Br)	156	1.495	99.5	ACS
Chloroform ($CHCl_3$)	61	1.482	99.0	ACS
Thiophene (C_4H_8S)	119	1.000	97.0	Purum
Ferrocene ($C_{10}H_{10}Fe$)	186	1.490		

The composition of the carrier gas is known to play an important role during the synthesis of carbonaceous materials. As such, different carrier gases available from AFROX were used to establish the impact on the thermal decomposition of the primary precursors. The compositions of the carrier gases used were as follows; (i) 5% hydrogen balance argon, (ii) 4.1% ammonia balance helium, (iii) argon (99.999%) and (iv) hydrogen (99.999%).

Carbon nanotubes were prepared by the pyrolysis of the 0.1 g/ml ferrocene solutions at atmospheric pressure. A 20 ml solution of ferrocene in either toluene or chlorobenzene was injected into the 1st chamber at a rate of 0.16 ml/min. The vapors generated from the solutions were carried into the 2nd chamber by a flow of argon (400 ml/min) and hydrogen (120 ml/min).

Carbon spheres were prepared by injecting 20 ml of toluene or chlorobenzene at 1.2 ml/min in the absence of ferrocene (catalyst). The 2nd reaction chamber was kept at the desired pyrolysis temperature (700-900 °C) for 20 min, as various gases (100-800 ml/min) mentioned above carried the precursor vapors into the furnace. The gases were allowed to flow through the system as it cooled down until the temperature was well below 200 ºC in the main chamber. The carbonaceous materials deposited on the walls of the quartz reactor were scraped out, weighed and analyzed.

2.3 Characterization

Carbon materials were characterized by transmission electron microscopy (TEM), scanning electro microscopy (SEM), Raman spectroscopy and Fourier transform infrared spectroscopy (FT-IR).

2.3.1 TEM analysis

Low magnification transmission electron microscopy (TEM) analysis was performed with a FEI TECHNAI G^2 SPIRIT electron microscope. Samples for TEM analysis were prepared by sonication of carbonaceous materials in ethanol for ~ 15 min and a few droplets of the resulting suspension were placed onto a holey SPI copper grid. High magnification transmission electron microscopy (HMTEM) was performed with a Philips CM200 microscope.

2.3.2 SEM analysis

Scanning electron microscopy (SEM) results were obtained from a Jeol JSM 840 microscope. Analysis was done with the sample placed at a working distance of 15 mm from the probe current. Three days prior to analysis, the samples were mounted onto an aluminium stub, using colloidal graphite and finally coated with carbon and gold/ palladium.

2.3.3 Raman analysis

Raman spectra were obtained with a Senterra micro Raman spectrometer. Excitation was provided by the 532 nm green laser. The laser was operated at a power of 10 mW to minimize local heating. Spectral resolution of 3-5 cm^{-1} was used. The laser light was focused onto the sample using the 20x objective of an Olympus microscope with aperture of 50*1000 μm. The spectrometer was calibrated using the 520.5 cm^{-1} line of silicon.

2.3.4 FT-IR analysis

Fourier transform infrared spectra were obtained using a Bruker Tensor 27 diamond tip spectrometer. About 64 transmittance scans per sample were gathered in the range 600-4000 cm^{-1} wavenumbers.

2.3.5 TGA

Thermal gravimetric analysis data was collected with a Perkin Elmer TGA 7 analyser. Samples of sizes 10-15 mg of carbonaceous materials were loaded into platinum pans and heated to 950 °C at a heating rate of 5 °C/min, in a flowing air stream at 20 ml/min.

2.3.6 EDS

Elemental composition was obtained for the as-synthesized carbonaceous materials was analysed by an X-ray detector attached to FEI TECHNAI G^2 SPIRIT electron microscope. Samples for TEM analysis were prepared by sonication of carbonaceous materials in ethanol for ~ 15 min and a few droplets of the resulting suspension were placed onto a holey SPI copper grid.

2.4 References:

1. J. Liu, A. G. Rinzler, H. Dai, J. H. Hafner, R. K. Bradley, P. J. Boul, A. Lu, T. Iverson, K. Shelimov, C. B. Huffman, F. Rodriguez-Macias. Y. Shon, R. T. Lee, D. T. Colbert, R. E. Smalley, *Science* **101** (1998) 1253
2. T. W. Ebbesen, P. M. Ajayan, *Nature* **358** (1992) 220
3. S. Amelinckx, X. B. Zhang, D. Bernaerts, X. F. Zhang, V. Ivanov, J. B. Nagy, *Science* **265** (1994) 635
4. Y. N. Xia, B. Gates, Y. D. Yin, Y. Lu. *Adv. Mater.* **12** (2000) 693
5. M. Sharon, K. Mukhopadhyay, K. Yase, S. Iijima, Y. Ando, X. Zhao, *Carbon* **36** (1998) 507
6. Z. Y. Zhong, H. Y. Chen, S. B. Tang, J. Ding, J. Y. Lin, K. L. Tan, *Chem. Phys. Lett.* **330** (2000) 41
7. Q. Wang, H. Li, L. Q. Chen, X. J. Huang, *Carbon* **39** (2001) 2211
8. X. Y. Liu, B. C. Huang, N. J. Coville, *Carbon* **40** (2002) 2791
9. D. Pradhan, M. Sharon, *Sci. Eng. B* **96** (2002) 24
10. J. S. Qiu, Y. F. Li, Y. P. Wang, C. H. Liang, T. H. Wang, D. B. Wang, *Carbon* **41** (2003) 767
11. Z. L. Wang, Z. C. Kang, *J. Phys. Chem*. **100** (1996) 5163
12. B. C. Satishkumar, A. Govindaraj, R. Sen, C. N. R. Rao, *Chem. Phys. Lett*. **293** (1998) 47
13. R. Andrews, D. Jacques, A. M. Rao, F. Derbyshire, D. Qian, X. Fan, E. C. Dickey, J. Chen, *Chem. Phys. Lett*. **303** (1999) 467
14. X. Y. Liu, B. C. Huang, N. J. Coville, *Fullerenes, Nanotubes and Carbon Nanostructures* **10** (2002) 339

Chapter 3

Chemical vapour deposition synthesis of carbon nanotubes and spheres from halogen-substituted arenes[1]

3.1 Introduction

It is known that addition of non-carbon containing reagents impact on the products, yield and chemical properties of carbon containing reagents in the synthesis of shaped carbon materials. The addition of sulphur and nitrogen containing reagents for example has been studied by many researchers over the years. Sulphur is present as an impurity in various industrial feedstocks and is generally regarded as a catalyst poison. There is still controversy even to date on the role of sulphur as an impurity during the synthesis of carbon nanotubes. Several research groups have reported from their work that thiophene as a source of sulphur plays a key role in controlling the formation of SWNTs [1,2] and DWNTs [3,4] over MWNTs. Mechanisms proposed to explain the findings were based on the possibility of sulphur interacting with the catalyst to either block active sites [5,6], lower the catalyst melting point [7,8] or directly interact with the growing tube [9], to inhibit graphitic carbon growth. On the contrary other research groups in their studies found that the presence of sulphur resulted in the synthesis of MWNTs [10] instead of SWNTs or DWNTs or that the fibres/carbon nanotubes were larger in diameter [1,11,12]. Based on their findings they believed that sulphur enhanced growth of graphitic carbon.

1. M. M. Kao, N. J. Coville, *Carbon* xxx **2010** xxx

Zhang et al. [13] studied the effects of ammonia as a reducing gas on the preparation of carbon nanotubes from xylene and catalyst made from an iron nitrate solution, by varying the percentage concentration of ammonia gas in argon. They found that ammonia had an optimum concentration of 20%; above which or below which, NH_3 did not support graphitic carbon growth. They believed that ammonia served to activate and clean the catalyst surface. Hence, at low concentrations catalyst activation is compromised. The authors suggested that ammonia, in addition to the above mentioned duties, favours catalyst agglomeration. Thus at high concentrations, catalyst agglomeration is predominant and structured carbon formation is diminished.

The effects of several factors such as catalyst, reagents, reaction temperature, gas flow rate and the nature of the carrier gas play a significant role during the synthesis of carbon materials. For example, early investigations have shown that hydrogen can accelerate and suppress production of carbonaceous materials from carbon containing reagents [14]. The explanation for the retarding effect is a thermodynamic one i.e. hydrogen drives the reverse reaction for decomposition.

This study describes the effect of halogens, in particular chlorine, on the formation of carbonaceous materials. Early work with chlorine by others has shown the influence on the morphology and yield of carbonaceous materials produced. A gradual change in morphology of the carbon structures as well as enhanced product yields has been observed with increasing amounts of chlorine [15]. Also, the nature of carbon materials generated from chlorinated species was found to be strongly temperature dependent [16]. A shift from pseudo-fibrous product at 773 K to predominantly nanosphere formation at 923 K was observed from pyrolysis of trichloroethylene [17]. The effects of chlorine on the physicochemical properties of shaped carbon materials have been reviewed in chapter 1.

Gui et al. reported the synthesis of carbon nanotubes from a dichlorobenzene/ferrocene solution [18]. They found that the resulting tubes were thin-walled and partially filled with iron. They claimed that thin-walls were formed as a result of restrained growth due

to an HCl etching effect on the walls. They also investigated the effect of varying H_2 gas flow rate on the synthesis of thin-walled tubes. One of the outstanding observations was that as H_2 gas flow reached 400 ml/min and beyond abundant amorphous carbon resulted. However H_2 has been shown to be beneficial in initiating decomposition of the carbon containing precursors [19] and exerting additional structure on the growth of carbon [20]. This study therefore serves to determine the effects of the above mentioned factors on the growth of CNTs in the presence of chlorine and to characterize the carbon products.

3.2 Experimental

All reagents were commercially available from Sigma and used without further purification (See chapter 2). In order to understand the effects of chlorine on the catalyst activity and selectivity during synthesis of carbonaceous materials, different volume percentages of chlorobenzene and toluene were used as a solvent mixture. The concentration of ferrocene for all solutions was 0.1 g/ml. The experiments were carried out under Ar/H_2 (5%) gas mixture at atmospheric pressure with the main chamber held at 900 ºC for 20 min as the precursor solutions were injected in at the rate of 1.2 ml/min.

To investigate the effects of chlorine on the morphology, size and yield, non-catalytic thermal decomposition of toluene (C_7H_8) was carried out as a control against thermal decomposition of chlorobenzene (ClBz). Also chloroform ($CHCl_3$) was added to both toluene and chlorobenzene to investigate the effect of alkylhalides on the pyrolysis of substituted arenes.

In some experiments a small amount of sulphur additive (thiophene) was added to the primary precursors to investigate the impact of sulphur in the absence of a catalyst. The composition as well as the flow rate of the carrier gas is known to play an important role during the synthesis of carbonaceous materials. As such, different carrier gases and different flow rates were used to establish if they impacted on the thermal decomposition of the primary precursors. H_2 (5%) in argon, NH_3 (4.1%) in helium, argon and hydrogen

gases were used. Also gas flow rates 200 - 800 ml/min of H_2 (5%) in argon were investigated.

3.3 Catalytic Pyrolysis

3. 3. 1 Catalytic pyrolysis of toluene

Thermal pyrolysis of toluene in the presence of the catalyst under dilute conditions i.e high gas flow rate and low injection rate was first investigated. A solution of 0.06 g/ml ferrocene in toluene was injected into the furnace at a rate of 0.16 ml/min and carried by argon and hydrogen gases flowing at 400 and 120 ml/min respectively. The other experimental conditions are summarized in table 3.1. Pyrolysis of toluene resulted in deposition of carbon nanotubes and amorphous carbon (Fig. 3.1a). Most of the tube cores are free of iron. The carbon nanotubes prepared from toluene under dilute conditions have diameters in the range 10-60 nm with ~ 57 % of the tubes being 10 nm thick (Fig. 3.1b).

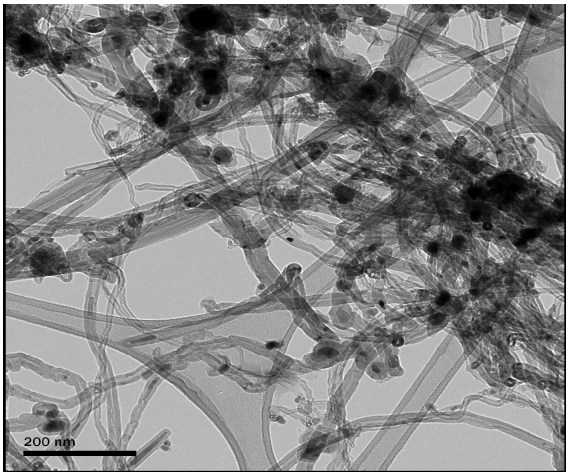

Fig. 3.1a: TEM image of tubes prepared toluene.

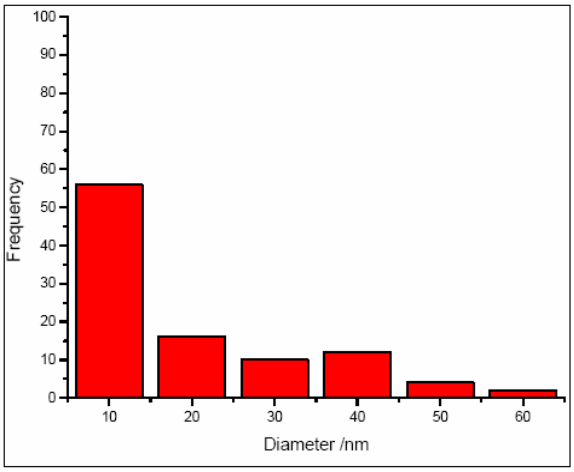

[1] Fig. 3.1b: Diameter distribution of CNTs from toluene.

[1] For Fig. 3.1b the standard deviation is ± 13

Table 3.1: Effect of chlorine

Carbon source	Notes	Mean diameter / nm
Toluene	empty tubes (95%), ά-C (5%)	10
Chlorobenzene	Fe-filled tubes (75%), ά-C	40

Temperature = 860 ˚C, Injection rate = 0.16 ml/min, Ar:H_2 (400:120 ml/min), Ferrocene conc. (0.06 g/ml), ά-C = amorphous carbon

3.3.2 Catalytic pyrolysis of chlorobenzene

Chlorobenzene (ClBz) was also pyrolysed under the same conditions as toluene to investigate the influence of the chlorine substituent on the carbon materials deposited. Pyrolysis of ClBz under the conditions stated in table 3.1 resulted in the deposition of MWNTs (Fig 3.2). Tubes deposited from ClBz have an uneven wall thickness. The white arrow heads show regions where the walls seem to have been eroded. A closer look at the tube shown in figure 3.2b indicates that some outer layers of the MWNT have been etched and also that the tube has its core filled with iron. It is evident from the TEM images that chlorine has a carbon etching effect on CNTs and enhances iron packing inside the tube. The observed etching is thought to be due to the corrosive effect of HCl. The other effect observed is the increased hollow core diameter (Fig. 3.2c) with the ratio of wall diameter to overall tube diameter being ~ 1:7.

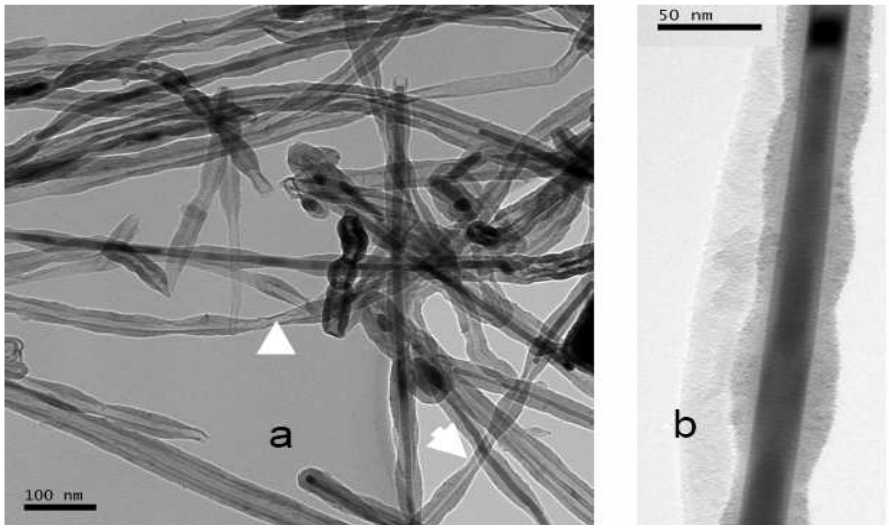

Fig. 3.2a: TEM micrograph of nanotubes synthesized from ClBz, (b) shows the etching effect of chlorine on the outer walls of Fe-filled tube.

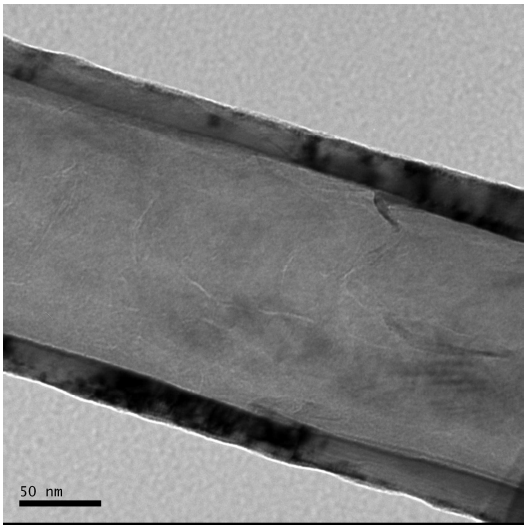

Fig. 3.2c: Wall thickness in relation to diameter of the hollow core in tubes prepared from ClBz.

A high resolution TEM image (Fig. 3.2d) shows that the tube walls consist of well ordered graphene sheets. The uppermost right end of the wall contains 21 graphene sheets just before the white arrow. All points marked by white arrows and a black arrow head, show discontinuities in the graphene sheets. These indicate that termination of growth

occurred at these points. A part of the wall labeled with the letter X consists of only 17 graphene sheets. The outermost fringes are larger than the average inner fringes. Fringes have an average spacing of 0.34 nm which is a value close to that of graphite (0.334 nm). There are points along the wall e.g. the one labeled with a letter Y where the graphene sheet is seen to bend out of plane. This is due to strain, relaxation or defects within the graphene sheets.

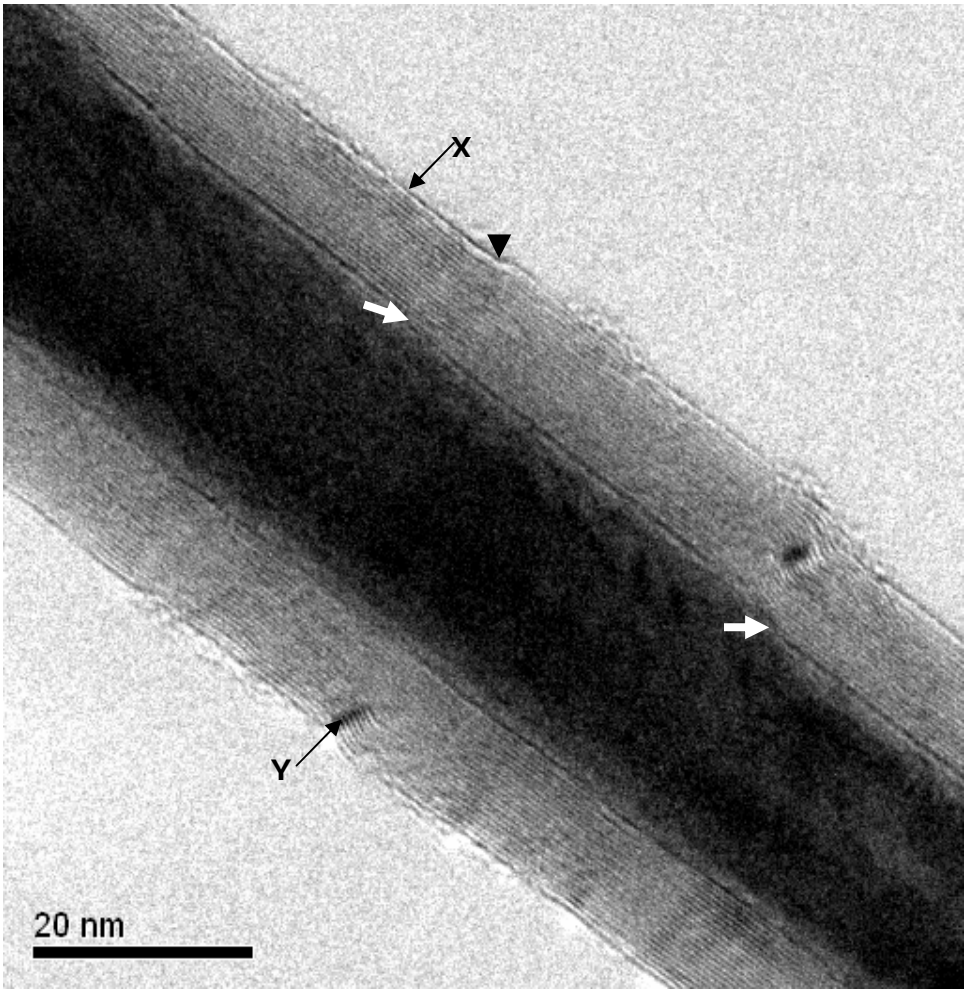

Fig. 3.2d: HRTEM image of a tube prepared from ClBz, showing details of the fringes. Thick arrows show graphene sheet termination points. The letter Y marks a defective point. X shows a portion of the wall with a smaller number of graphene sheets.

Effect of halogen concentration at low gas flow rate

The results summarized in table 3.2 indicate the crucial role that the halogen concentration plays on the morphology of the carbon materials produced at a low gas flow rate of 100 ml/min. We have seen previously that when ClBz was catalytically pyrolysed under a mixture of Ar and H_2 flowing at 400 and 120 ml/min respectively the products obtained were strictly tubes. On the contrary, table 3.2 shows that catalytic pyrolysis of monohaloarenes at low flow rates of the carrier gas result in a drastic change in morphology of products; spheres are now predominantly produced. This change in morphology is an indication that catalyst deactivation in the presence of halogens in the feed is dependent on the time the halogen spends in the reaction chamber. The longer the halides are present in the reaction chamber the higher the degree of catalyst deactivation. We assume that catalyst deactivation is due to interaction of the halogen radicals with the catalyst. It is also possible that HX surface poisoning can occur. During ClBz pyrolysis HCl production was confirmed by bubbling the outlet gas through a solution of sodium hydroxide (pH 11) and recording the pH of the solution by a benchtop pH meter. Upon completion of the reaction, the pH of the solution dropped from pH 11 to pH 1.6.

Effect of chlorobenzene (ClBz) concentration

The TEM image of materials prepared from the highest concentration of ClBz (Fig. 3.3b) shows that spheres are produced at the expense of tubes. The tubes that are formed are solid and are fiber-like (Fig. 3.3b). When the ClBz content was reduced to 10 wt.%, by dilution with toluene, partially iron-filled hollow cored tubes were produced. Surface etching is observable on these tubes (Fig. 3.3c). However production of amorphous carbon is also observed. We suggest that the absence of unstructured carbon at high haloarene concentrations indicates catalyst deactivation from the onset. Thus, carbon formation at this concentration is almost entirely independent of the catalyst. On the other hand co-deposition of tubes, amorphous carbon and spheres for the 10 wt.% and 5 wt.% ClBz feed (Fig. 3.3c and d) indicates gradual catalyst deactivation with time. At a low ClBz content of 2 wt.% catalyst deactivation is no longer observed and products are

hollow cored iron free tubes (Fig. 3.3e) similar to those obtained from the pyrolysis of toluene (Fig. 3.3a).

Effect of bromobenzene(BrBz) concentration

TEM images of materials prepared from bromobenzene (BrBz) shows that products are similar to those prepared from ClBz. Catalytic pyrolysis of BrBz results in the production of spheres only (Fig. 3.3f). At 10 wt.% BrBz in toluene co-deposiotion of solid fiber-like tubes, spheres and amorphous carbon occurred (Fig.3.3g), while iron-filled hollow core tubes are produced at 2 wt.% BrBz (Fig.3.3h).

Effect of halogen content on yield

The mass of solid carbon deposited from ClBz and BrBz are very similar. The general observed trend (table 3.2) is that the amount of solid carbon deposited increases with an increasing amount of haloarene content. TEM analysis reveals that solid carbon produced from BrBz pyrolysis contains similar amounts of amorphous carbon to that deposited from ClBz. Table 3.2 shows that about 15 % amorphous carbon is deposited when a feed containing 10 wt.% BrBz is pyrolysed.

Effect of halogen on size

The size of the products is also dependent on the haloarene content in the feed. Larger average diameters for both tubes and spheres are the result of high concentrations of ClBz and BrBz (table 3.2). This observation is in agreement with the observed increase in the yield with increasing X content. This phenomenon suggests that halogens enhance carbon deposition.

Table 3.2: The influence of haloarene content at low gas flow rate

Halogen source	Haloarene wt. %	Notes	Mean diameter / nm	Yield %
Toluene	0	tubes (75%), ά-C (25%)	50t	1.27
ClBz	100	Spheres (98%), tubes (2%)	300s, 160t	9.13
	10	Spheres (70%), tubes (10%), ά-C (20%)	200s, 70t	6.21
	5	Spheres (50%), tubes (30%), ά-C (20%)	200s, 40t	2.89
	2	tubes (90%), ά-C (10%)	20t	1.63
BrBz	100	Spheres	300s	9.79
	10	Spheres (50), tubes (35), ά-C (15)	200s, 100t	6.28
	2	tubes (85), ά-C (15)	30t	2.10

T- 900 °C, Gas-Ar/H_2 (5%), Flow rate- 100 ml/min, Injection rate- 1.2 ml/min, Ferrocene conc.- 0.1 g/ml, Balance solvent wt % -toluene, Volume of solution injected = 20 ml. s = spheres, t = tubes ά-C = amorphous carbon.

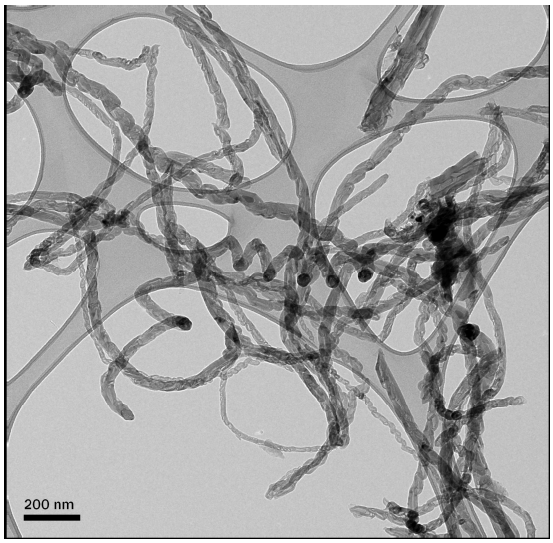

Fig. 3.3a: An image of tubes prepared from the catalytic pyrolysis of toluene at 100 ml/min.

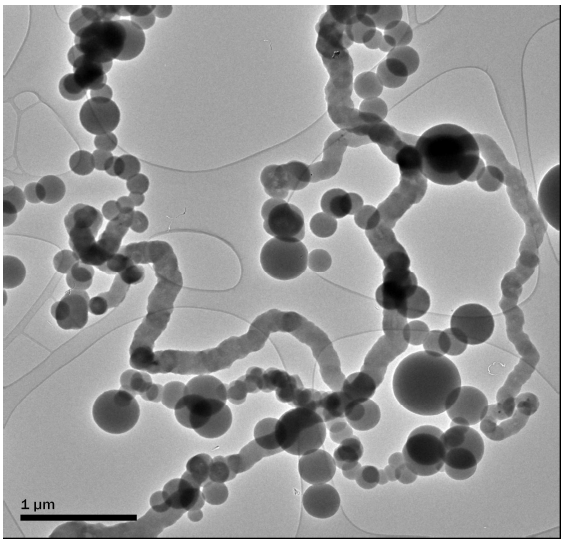

Fig. 3.3b: Carbon materials produced from the catalytic pyrolysis of ClBz at 100 ml/min.

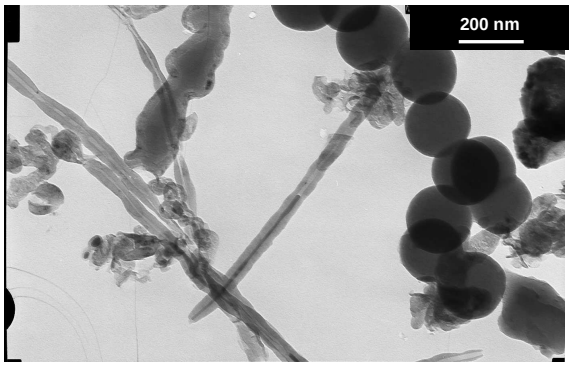

Fig. 3.3c: Carbon materials prepared from the catalytic pyrolysis of ClBz (10 wt.%) at 100 ml/min.

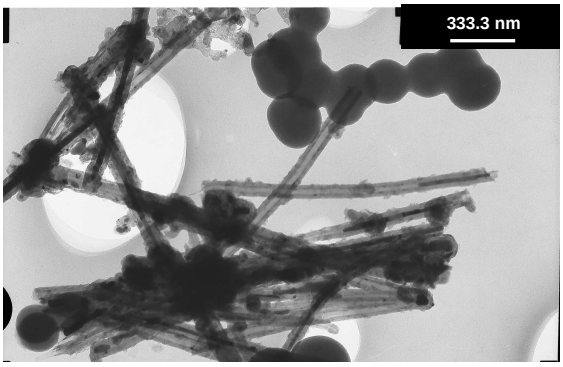

Fig. 3.3d: Materials produced from the catalytic pyrolysis of ClBz (5 wt.%) at 100 ml/min.

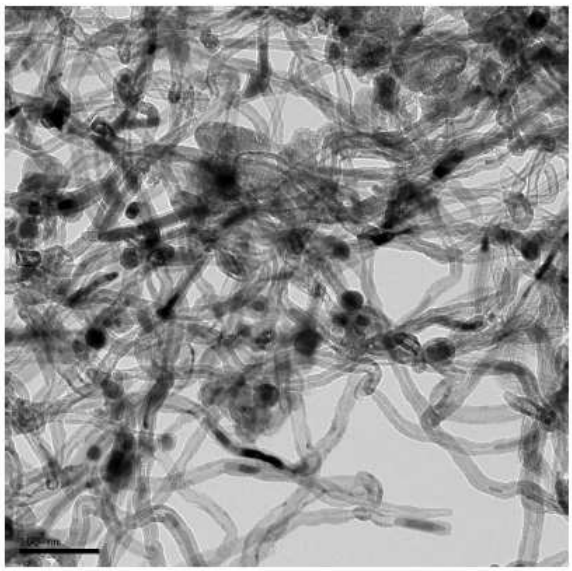

Fig. 3.3e: Carbon nanotubes prepared from pyrolysis of ClBz (2 wt.%) at 100 ml/min.

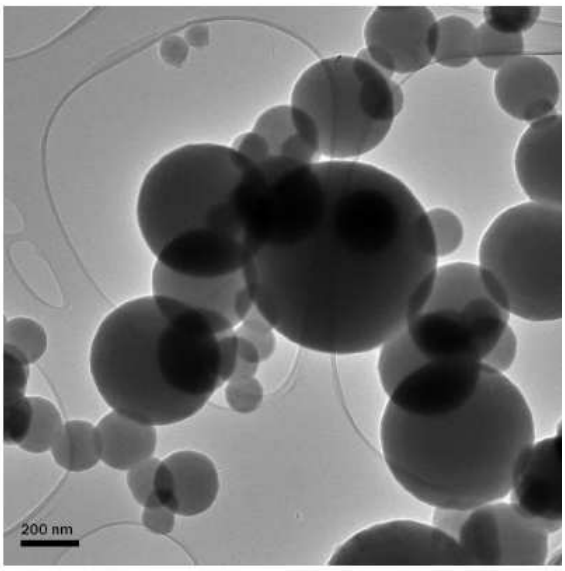

Fig. 3.3f: Spheres produced from catalytic pyrolysis of BrBz (100 wt.%).

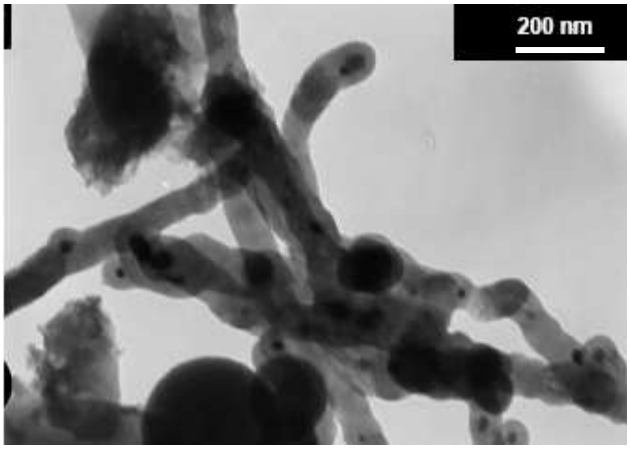

Fig. 3.3g: Carbon materials prepared from the catalytic pyrolysis of BrBz (10 wt.%) at 100 ml/min.

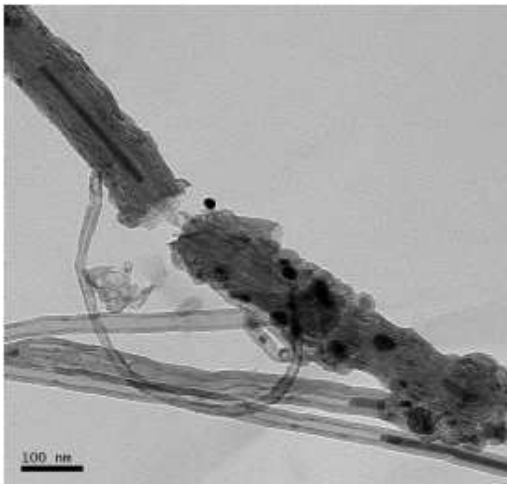

Fig. 3.3h: Tubes produced from the catalytic pyrolysis of BrBz (2 wt.%) at 100ml/min.

3.4 Non-catalytic thermal decomposition

Cullis and Priday [21] suggested that thermal decomposition of benzene derivatives which contain only monoatomic substituents must initially involve either the rupture of bonds directly attached to the benzene nucleus or the opening of the aromatic ring. It has however been established by Szwarc [22] that the primary step during decomposition of toluene is the removal of the methyl substituents leaving the benzene ring intact. However details of other competing primary processes have not been confirmed and agreed upon.

Non-catalytic pyrolysis of toluene was carried out under Ar/H_2 (5%) (v/v) at 900 °C. TEM images of the product (Fig. 3.4a) indicated that chain-like carbon spheres and amorphous carbon were produced. A more detailed view of the merged spheres is shown by figure 3.4b. Merging carbon spheres is an indication of carbon shell accretion. Carbon shell accretion was explained by Wang and Kang [23] to be due to high chemical activity on the surface of carbon spheres. Non-catalytic pyrolysis of chlorobenzene resulted in the synthesis of perfectly spherical carbon spheres (Fig. 3.4c). SEM micrograph of spheres prepared from non-catalytic pyrolysis of ClBz shows that the spheres are free of

amorphous carbon (Fig. 3.4d). We assume that chlorine radicals generated from the chlorinated reactants interact and donate electrons to the unsaturated π-bonding carbon orbital thus rendering the surface chemically inert and hence preventing accretion of spheres in the presence of chlorinated species.

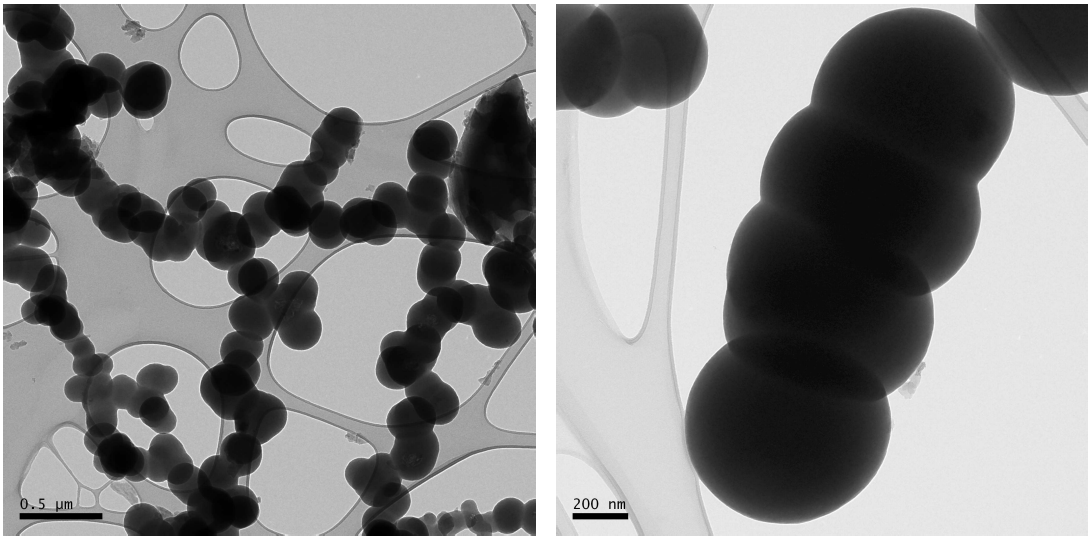

Fig. 3.4a: TEM images of spheres prepared from toluene forming a chain, (b) image showing accretion of spheres.

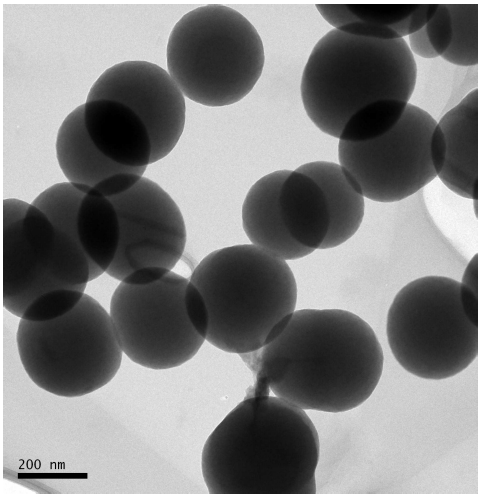

Fig. 3.4c: TEM images of spheres from ClBz with minimal accretion.

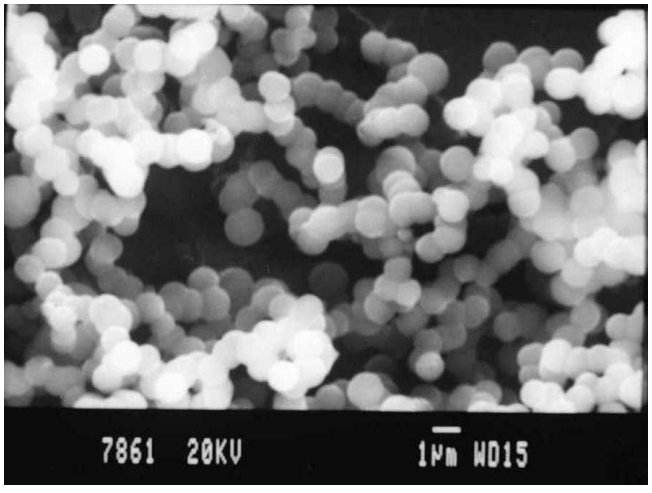

Fig. 3.4d: SEM image shows purity of carbon spheres from ClBz with minimal accretion.

It is immediately evident from table 3.3 that the yield of carbon deposited from ClBz exceeds that from toluene. These results are in agreement with the recent results obtained by Keane et al [24] where they observed an elevated carbon product yield due to the presence of chlorine in the feed for reactions of ClBz when compared with benzene. They suggested that the high carbon yields were attributed to a Cl/catalyst interaction which induces electronic perturbations through a reduction in d-electron density of the surface metal that serves to strengthen the interaction with the incoming reactant, weakening the C-C bonds in the adsorbed species and hence favouring decomposition. However the fact that in our studies a similar effect of enhanced yield from chlorinated species is observed in the absence of the metal catalyst is a clear indication that the phenomenon of enhanced yields from chlorinated species can not necessarily be attributed to Cl/metal interactions. We therefore speculate that elevated yields are attributed to chlorine radicals generated from the chlorinated species. It is suspected that electron transfer from the generated radicals into the π-orbitals of carbon atoms of the intermediate hydrocarbon species induces elongation and weakening of the C-C δ-bond within these species. Hence, result in lowering of the C-C bond dissociation energy promoting decomposition of the hydrocarbon species.

Spheres from ClBz have a wide diameter distribution from 100 nm to 1 μm and on average have larger diameters than spheres prepared from toluene. The increase in average diameter and the widening of the diameter distribution suggests that carbon deposition from chlorinated species occurs over a long period of time indicating prolonged chemical activity. We therefore assume that the deposition of carbon in the presence of chlorinated species entails a chain reaction mechanism.

The influence of gas flow rate on carbon product and mean diameter of the carbon spheres prepared from toluene and ClBz was studied by varying the carrier gas flow rate from 200 ml/min to 800 ml/min. Table 3.3 shows that the carbon product yield decreases with increasing gas flow rate for products obtained from both toluene and ClBz. Also figure 3.5 shows that the mean diameter of carbon spheres produced from toluene decrease with increasing gas flow rate. The observed reduction in carbon product yield

and mean carbon sphere diameter, suggest that increasing the carrier gas flow rate reduces the residence time for precursors in the reaction chamber. However, the average diameter of carbon spheres prepared from ClBz appears to be relatively less sensitive to gas flow rates. This highlights the impact of chlorinated species on non-catalytic thermal decomposition of hydrocarbons.

Table 3.3: Illustrates influence of gas flow rate on carbon yield.

Ar/H_2 (ml/min)	Chlorobenzene Yc% = C_{in}/C_{out}	Toluene Yc% = C_{in}/C_{out}
200	2.77	0.64
400	1.75	0.29
800	1.28	negligible

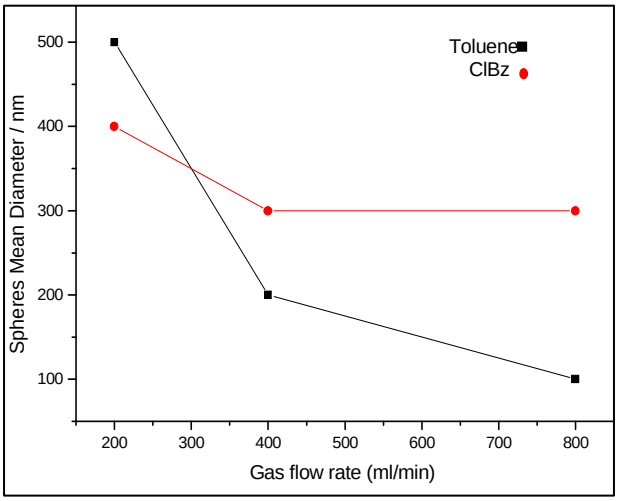

Fig.3.5: Effect of gas flow rate on diameters.

3.5 Impact of non-carbon containing reagents

The issue of non-carbon containing reagents has been discussed earlier. It has been suggested that addition of non-carbon containing reagents impacts on the products, yield and chemical properties of carbon containing reagents in the synthesis of shaped carbon materials. Non-carbon containing reagents can promote or suppress carbon deposition during pyrolysis of the prospective precursors. Table 3.4 shows the impact of chlorine, sulphur and nitrogen containing reagents on the solid carbon yield from toluene and ClBz.

Effect of chloroform

When chloroform (trichloromethane) was added to toluene (flow rate 200 ml/min) the yield increased twofold. A large diameter distribution was now seen for toluene after the introduction of chlorinated species. Further, introduction of chlorinated species in toluene resulted in spheres which were well defined (Fig. 3.6a) with a well dispersed distribution. There is the possibility that there exists an optimum concentration of chlorine atoms which eliminates accretion since we observed that addition of trichloromethane to ClBz resulted in tightly accreted spheres with a very narrow diameter distribution (200-400 nm; Fig. 3.6b) The fine details on the surface of spheres corresponding to the unclosed graphitic flakes on the surface of two merging spheres are shown in figure 3.6c. Therefore carbon atoms at the edge of the curling graphitic flakes must have dangling bonds with sp^3 orbitals. The expectation is that these sites are chemically active.

Table 3.4: Shows the influence of heteroatom additives

Solvent	Additive	Notes	Mean diameter / nm	Diameter range / nm	Yield / g
Toluene	--------	spheres, ά-C	500	(400-800)	0.098
Toluene	chloroform	spheres	200	(50-900)	0.246
	thiophene	spheres, ά-C	800	(600-1100)	0.033
	*ammonia	spheres, ά-C	500	(300-600)	0.012
ClBz	--------	spheres	300	(100-1600)	0.411
ClBz	chloroform	spheres	200	(200-400)	4.928
	thiophene	spheres	600	(500-800)	0.436
	*ammonia	spheres	600	(400-800)	0.258

T = 900 °C, injection rate = 1.2 ml/min, gas = Ar/H_2 (5%) at 100ml/min, * Gas = He/NH_3 (4.1%)

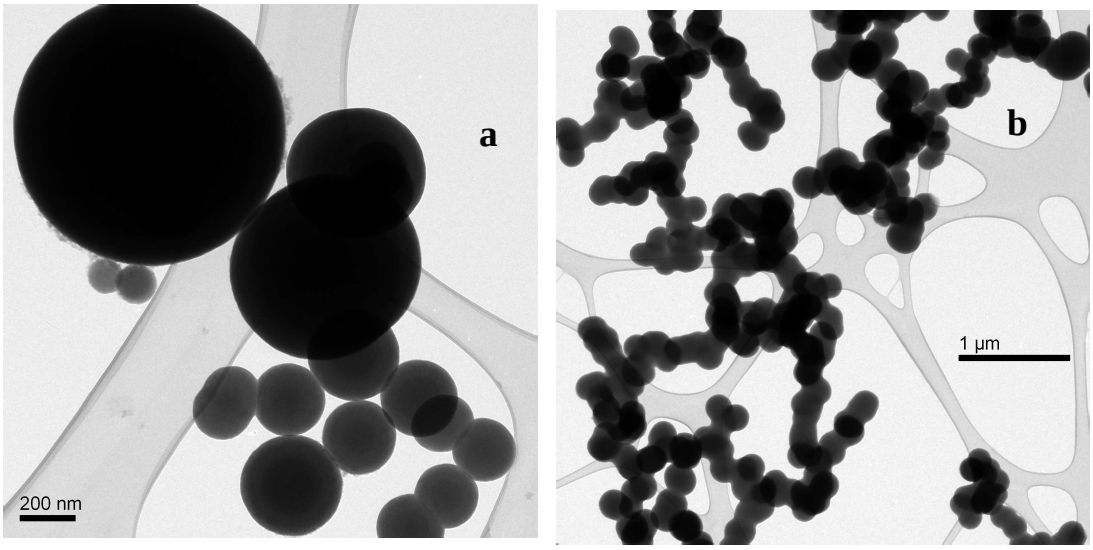

Fig. 3.6a: Spheres prepared from toluene in the presence of Cl, (b) Accreted spheres prepared from ClBz in the presence of extra Cl atoms from chloroform.

Fig. 3.6: (c) External shells of two spheres joining to form a bridge resulting in the accretion of the spheres.

Raman analysis permits an evaluation of the graphitic nature of carbons. The G band at ~1580 cm^{-1} corresponds to an E_{2g} mode of graphite and the D band at around 1350 cm^{-1} is associated with vibrations of sp^3 hybridized carbon atoms of disordered graphite. The relative intensity ratio of I_D and I_G is regarded as a measure of the graphitic ordering; the greater the ratio of I_D and I_G, the higher the degree of disorder [25]. On the basis of the Raman analysis, the carbon produced from the decomposition of toluene possesses a moderate degree of order (table 3.5).

The I_D/I_G ratios of the products produced from chlorinated precursors indicates that carbon generated from these precursors is far less graphitic than that from toluene. According to the Raman analysis, carbon resulting from the chlorinated precursors would be expected to have a substantial amount of amorphous matter but both TEM and SEM

micrographs do not confirm this. Therefore it can be suggested, based on Raman and SEM data, that carbon on the surface layer of spheres is not strictly sp^2 hybridized due to pyramidilization strain. There could be a certain level of sp^3 hybridization and defects can react with Cl to give C-Cl bond formation on the surface. In fact spheres would naturally contain pentagon-heptagon pairs (Stone-Wales defects). Nieto et al. [17] reported a surface Cl content of 0.4-0.9 atom % on spheres formed from catalytic decomposition of trichloroethylene over Ni/SiO_2. Also Brichka et al. [26] reported 0.25 atom % Cl incorporation into MWNTs synthesized from CH_2Cl_2 via a template method. We established 0.25 ppm Cl incorporation onto spheres synthesized from ClBz as determined from ICP measurements.

Table 3.5. A summary of data obtained from Raman analysis.

Precursors	A_1	A_2	I_D/I_G ratio
C_7H_8	18704.6	7918.6	2.4
C_7H_8/ $CHCl_3$	37214.7	11159.7	3.3
ClBz	7327.2	2702.1	2.7
ClBz/ $CHCl_3$	11220.4	4299	2.6

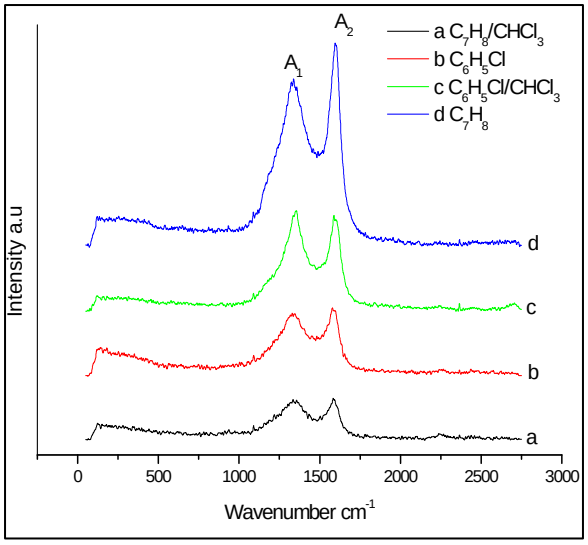

Fig.3 6d: Raman spectra of spheres prepared from toluene and ClBz in the presence of additional Cl atoms from chloroform.

Effect of ammonia

A mixture of He/NH_3 (4.1%) (v/v) was passed through the reaction quartz tube to drive out air. Toluene contained in a 20 ml plastic syringe was then injected into the hot zone of the reactor at an injection rate of 1.2 ml/min. The He/NH_3 (4.1%) (v/v) gas mixture was kept flowing at a constant rate of 100 ml/min as the toluene pyrolysis occurred and the reaction was cooled down under this gas mixture. A similar experiment was performed for ClBz.

Based on the amount of amorphous carbon detected in figure 3.7(a) and the poor yields obtained from pyrolysis of toluene in ammonia gas (table 3.4), it can be suggested that the benzyl intermediates resulting from toluene decomposition interacts with ammonia in the carrier gas such that formation of nitrogen substituted hydrocarbons predominates. This inhibits formation of the graphitic carbon. In the case of ClBz the impact of ammonia on the yield is quite minimal and there is no observable difference in the type of spheres produced when compared to those synthesized under an Ar/H_2 gas mixture. This could be because ammonia reacts with chlorine and is eliminated as ammonium chloride and hence does not impact on decomposition of ClBz.

Effect of sulphur

A mixture of thiophene and toluene was prepared by adding 4 ml of thiophene to 11.2 ml of toluene such that the S:C ratio is ~ 1:20. The solution was then injected into the hot zone of the reaction chamber under a Ar/H_2 (5%) (v/v) gas mixture. Similarly a mixture of ClBz and thiophene with an S:C ratio of ~ 1:20 was prepared and pyrolysed.

Similar results to the ones obtained when reagents were subjected to ammonia addition were obtained for the decomposition of toluene and ClBz in the presence of a sulphur derivative, thiophene. Poor yields and amorphous carbon formation were observed from toluene (figure 3.8a). However yields from ClBz were unaffected by sulphur but a certain increase in degree of accretion was observed. We suggest that the susceptibility to

inhibitors must largely be dependent on their decomposition mechanisms. The fact that ammonia gas and the sulphur impurity have a retarding influence on toluene but ClBz seems resistant to both, suggests two completely different decomposition mechanisms for these substituted arenes.

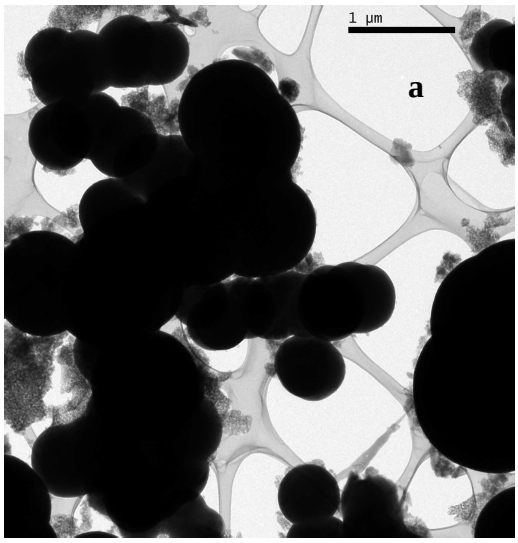

Fig.3.7a: Spheres with amorphous carbon synthesized from toluene under NH_3 gas.

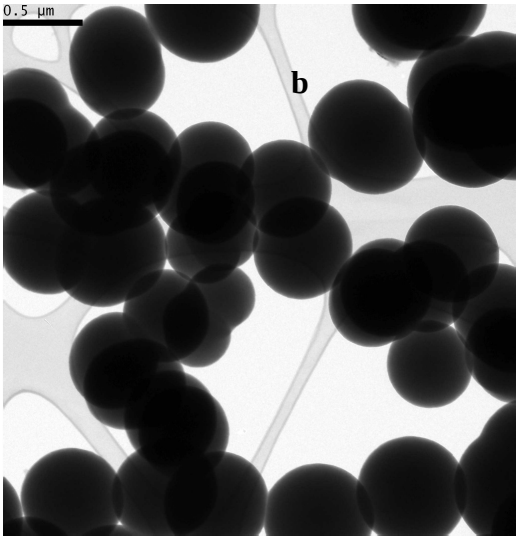

Fig. 3.7b: Spheres with no amorphous carbon (from ClBz under ammonia).

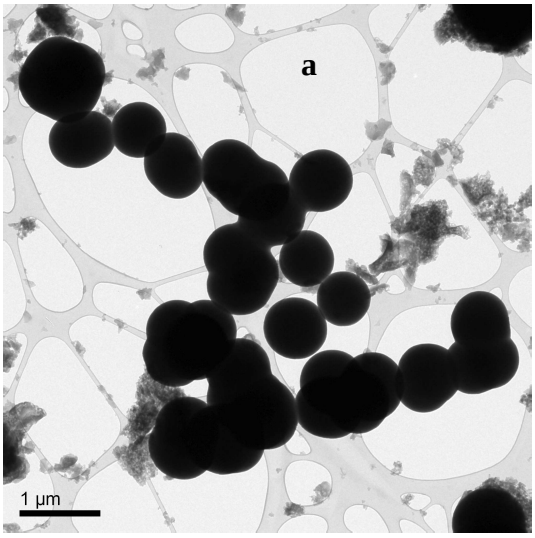

Fig.3.8a: Spheres with amorphous carbon formed from toluene in the presence of sulfur.

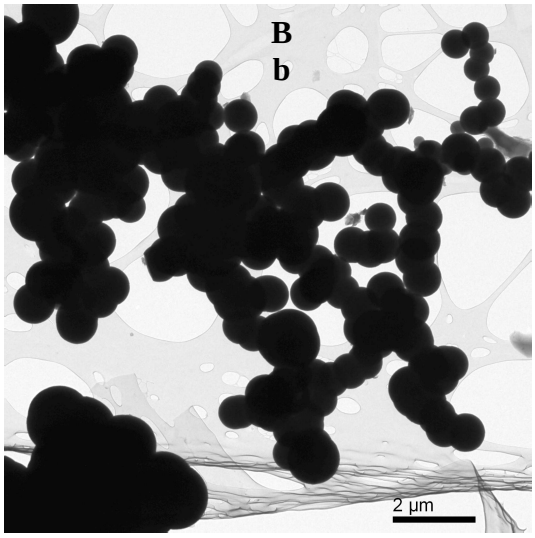

Fig. 3.8b: Spheres with no amorphous carbon formed from ClBz in the presence of sulfur.

3.6 Effect of gas composition on sphere size

Our findings have shown that non-catalytic pyrolysis of ClBz results in a large diameter distribution of the carbon spheres formed in the reaction. Since the dimensions of carbon materials influence their properties, fabrication of materials of controlled diameters is important. Therefore the influence of carrier gas composition on carbon sphere diameter was studied by preparing spheres from ClBz in hydrogen gas and in argon. When spheres were prepared under argon a large diameter distribution ranging from 300-1100 nm was observed (Fig. 3.9a and b). However, when spheres were prepared under hydrogen gas the diameter distribution was reduced to between 200 nm and 600 nm. Figure 3.9d shows that in the presence of hydrogen gas ~ 90 % of the spheres are between 200 and 300 nm in size.

It was also observed that carrier gas composition had an impact on the solid carbon yield. A substantial decrease in yield was observed when H_2 was used for the carrier gas as opposed to when argon was used. According to Keane [24] decomposition and hydrodechlorination reactions of ClBz are mutually exclusive but there is a time based transition between the two. We therefore suggest that hydrodechlorination of ClBz becomes the dominating process in the presence of H_2 gas, hence deferred decomposition is inevitable, and thus poor carbon deposition results. Under argon, decomposition is not compromised by hydrodechlorination. The retarding effect of H_2 gas on the decomposition of ClBz is more enhanced at a low injection rate of 0.16 ml/min where no carbonaceous materials were formed as compared to high injection rate of 1.2 ml/min where carbon spheres were formed.

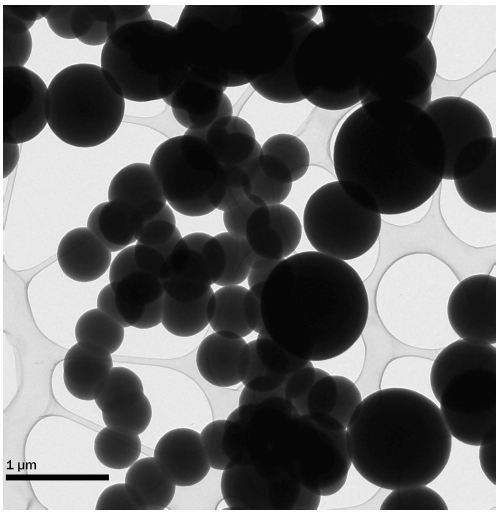

Fig.3. 9a: Different sizes of spheres from ClBz under argon gas at 200 ml/min.

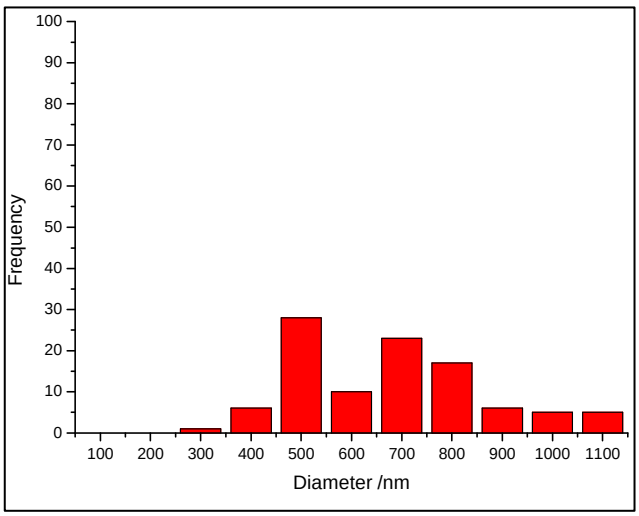

Fig. 3.9b: A wide diameter distribution of spheres prepared under argon.

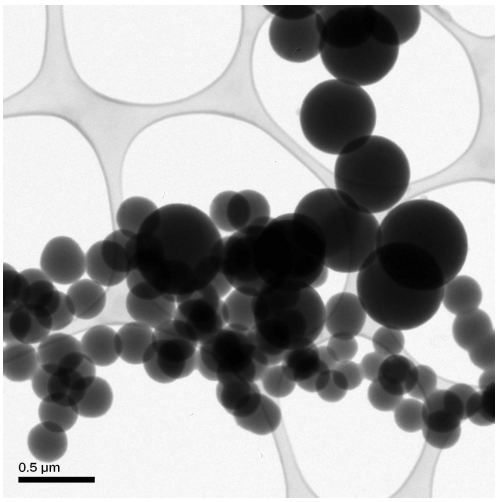

Fig.3.9c: Different sizes of spheres from ClBz under H_2 gas at 200 ml/min.

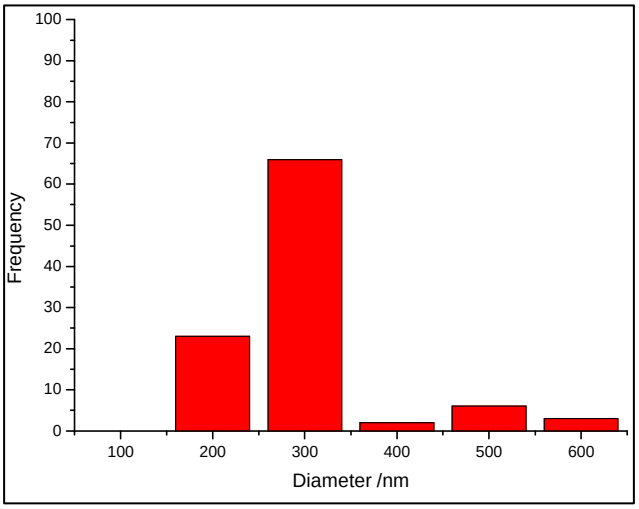

Fig. 3.9d: A small diameter distribution of spheres prepared under hydrogen gas.

A typical elemental analysis by EDS of spheres prepared from ClBz is shown in figure 3.10. EDS reveals that the carbon content of the spheres is approximately 99 %. The chlorine content is very small ranging from 0-0.04 %. This observation is consistent with the ICP-OES analysis in terms of Cl data. Oxygen is also observed. Its presence is due to

the reaction of surface carbons with oxygen. Silicon is an impurity from the quartz tube system while copper is detected from the SPI Cu grid used to load the sample during analysis.

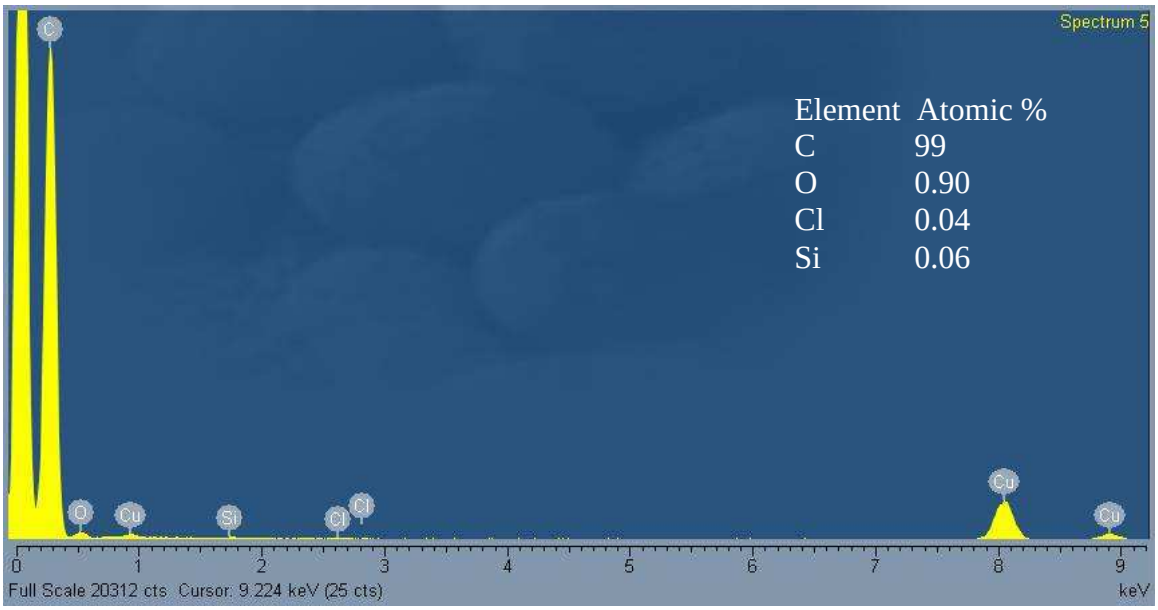

Fig.3.10: EDS of spheres prepared from non-catalytic pyrolysis of chlorobenzene.

3.7 References:

1. H. M. Cheng, F. Li, G. Su, H. Y. Pan, L. L. He, X. Sun, M. S. Dresselhaus, *Appl. Phys. Lett.* **72** (1998) 3282
2. H. M. Cheng, F. Li, X. Sun, S. D. Brown, M. A. Pimenta, A. Marucci, G. Dresselhaus, M. S. Dresselhaus, *Chem. Phys. Lett.* **289** (1998) 602
3. L. Ci, B. Wei, J. Liang, C. Xu, D. Wu, *Carbon* **39** (2001) 329
4. H. Zhu, C. Xu, B. Wei, D. Wu, *Carbon* **40** (2002) 2023
5. M. S. Kim, N. M. Rodríguez, R. Baker, *Catalysis.* **143** (1993) 449
6. L. Ci, H. Zhu, B. Wei, J. Liang, C. Xu, D. Wu, *Carbon* 37 (1999) 1652
7. I. Martin-Gullon ,J. Vera, J. A. Conesa, J. L. Gonzalez, C. Merino, *Carbon* **44** (2006) 1572
8. G. G. Tibbetts, M. P. Balogh, *Carbon* **37** (1999) 241
9. J. C. Hutchinson, N. A. Kiselev, E. P. Krinichnaya, A. V. Krestini, R. O. Loutfy, A. P. Morowsky, V. E. Muradyan, E. D. Obraztsova, J. Sloan, S. V. Terekhov, D. N. Zakharov, *Carbon* **39** (2001) 761
10. M. S. Mohlala, X. Y. Liu, M. J. Witcomb, N. J. Coville, *Appl. Organometal. Chem.* **21** (2007) 275
11. Z. Zhou, L. Ci, X. Chen, D. Tang, X. Yan, D. Liu, Y. Liang, W. Zhou, G. Wang, S. Xie, *Carbon* **41** (2003) 337
12. Y. Saito, T. Nakahira, S. Uemura, *J. Phys. Chem. B* **107** (2003) 931
13. H. Zhang, Y. Chen, S-S. Kim, Y-S. Lim, *Metals & Mater. Inter.* **14** (2008) 269
14. K. L. Yang, R. T. Yang, *Carbon* **24** (1986) 687
15. A. Nieto-Márquez, J. L. Velverde, M. A. Keane, *Appl. Catal. A Gen.* **332** (2007) 237
16. C-H. Chien, P-S. Sheng, C-H. Wang, C-H. Huang, H-K. Lin, C-Y. Lee, H-T. Chiu, *Mater. Lett.* **62** (2008) 1176
17. A. Nieto-Márquez, J. L. Velverde, M. A. Keane, *Appl. Catal. A Gen.* **352** (2007) 159

18. X. C. Gui, K. Wang, W. X. Wang, J. Wei, X. F. Zhang, R. Lv, Y. Jia, Q. Shu, F. Kang, D. Wu, *Mater. Chem. Phys.* **xxx** (2008) xxx
19. P. E. Nolan, D. C. Lynch, A. H. Cutler, *Carbon* **32** (1994) 477
20. W. T. Owens, N. M. Rodríquez, R. T. K. Baker, *J. Phys. Chem* **96** (1992) 5048
21. C. F. Cullis, K. Priday, *Proc. Roy. Soc. London. A* **224** (1954) 308
22. M. Szwarc, *J. Chem. Phys.* **16** (1948) 126
23. Z. C. Kang, Z. L. Wang, *J. Phys. Chem.* **100** (1996) 5163
24. M. A. Keane, G. Jacobs, P. M. Patterson, *J. Colloid. Interface Sci*. **302** (2006) 576
25. K. Niwase, T. Homae, K.G. Nakamura, K. Kondo, *Chem. Phys. Lett.* **362** (2002) 47
26. S. Ya. Brichka, G. P. Prikhod'ko, Yu. I. Sementsov, A. V. Brichka, G. I. Dovbeshko, O. P. Paschuk, *Carbon* **42** (2004) 2581

Chapter 4

Synthesis of carbons from silicon sources

4.1 Introduction

Since their discovery by Iijima in 1991 [1], the peculiar electronic and physical properties of carbon nanotubes, have triggered a lot of interest in making materials with novel properties. Many devices possessing these novel properties leading to different applications and having a chemical composition beyond that of pure carbon nanotubes have been proposed and realized [2, 3].

Generally two major research directions have emerged in the carbon nanomaterials area: (i) the study of properties of the already existing nanomaterials and (ii) the design of new materials that present specific properties. Following the second research direction many research groups have tried to either synthesize nanotubes based on elements other than carbon or to theoretically model tubes [4,5]. Silicon by virtue of being a group 14 element has attracted much attention as a replacement for carbon in carbon nanotube synthesis. It is however well known today that carbon and silicon present different bonding characteristics, despite the fact that they are both in the fourth column of the Periodic Table and have the same number of valence electrons. Actually silicon differs from carbon in that amongst other factors, it has a larger atomic radius and hence larger orbital size; a smaller energy difference between the s and p orbitals [Si ($E_{3p} - E_{3s}$ = 5.66 eV) Vs C ($E_{2p} - E_{2s}$ = 10.60 eV] [6], and hence lower hybridization energies. As a result silicon prefers to be sp^3 hybridized as opposed to sp^2 hybridized. Therefore fullerene-like or cage formations based fully on silicon are difficult if not impossible to obtain [7]. Until today silicon nanotubes are but hypothetical materials [8].

Even though complete replacement of carbon by silicon in cage materials has not yet been experimentally successful, partial substitution, which results in the coexistence of

carbon and silicon atoms, is in principle possible resulting in silicon carbide cage materials. A 1:1 replacement to give silicon carbide (SiC), a non-oxide ceramic compound is widely studied as a material with high thermal conductivity, hardness and high temperature stability [29].

SiC materials have therefore been developed for their potential properties that enable them to survive in high temperature and harsh environment applications. SiC has a potential in the construction of devices that possess increased tolerance to radiation damage hence becoming a desirable material for defense and aerospace applications. SiC remarkable resistance to oxidation has led to significant interest in its use as a heterogeneous catalyst support. SiC is known to occur naturally as an extremely rare mineral, moissanite, found in minute quantities in corundum deposits and kimberlites. Hence silicon carbide is mostly a synthetic material.

Heterofullerenes containing 50% Si were obtained in 1999 [9], and in 2001 the first synthesis of silicon carbide nanotubes (SiCNTs) was reported [4]. It has been shown that doping of carbon nanotubes induces fundamental modifications to a tube structure when compared to their undoped counterparts [10]. Three types of carbon nanotube doping procedures have been proposed and experimentally proven: (i) adsorption of atoms at the nanotube surface, (ii) incorporation of atoms into the nanotube walls and (iii) substitutional doping. Most research groups that have performed silicon doping of carbon nanotubes (CNTs) have employed the first approach using CNTs as templates [3,5].

Theoretical investigations on SiCNTs have been performed in order to understand the nature of SiCNTs and determine their properties [2]. Silicon, as an isovalent substitutional impurity in carbon nanotubes, is expected to result in doping which will generate electrically inactive materials [11]. However ab initio studies by Froudakis et al. [2] indicated that Si atoms introduce perturbations to the π-system resulting in electrical activity. From the same ab initio studies Froudakis et al.[2] determined that SiCNTs are stable. Nevertheless they predicted that SiCNTs lose their stability when the ratio of silicon over carbon increases with the cross over point for replacing C with Si without the

tube collapsing to a cluster or nanowire being 50% Si substitution. They also suggested that a 50% substitution would result in stable nanotubes with an ionic character. The electronic density of states of SiCNTs determined by the same research group show that the substitution of a few C atoms by Si inserts levels into the HOMO-LUMO gap, while in the "Si rich" SiCNTs the gap increases again due to the structure regaining symmetry. It has also been established that as the number of Si atoms incorporated increases, the diameter of the tube also increases [2].

From a structural point of view, the lone orbital on Si in the graphite-like lattice can act as a binding center to attach different atoms or molecules for nanotube functionalization [12]. In another study [13] tight-binding molecular dynamics (GTBMD) and ab initio methods were used to investigate properties of SiCNTs with Si:C ratios of 1:1. Two types of rolled graphene sheet structures of SiCNTs, shown in figures 4.1 (A) and (B), were studied: type 1 involved alternate Si and C sites, whereas type 2 contained pairs of Si=Si and C=C bonds. Type 1 had severe wavelike distortions as compared to type 2. However it was found that type 1 structures are more stable than type 2 structures by 0.43 eV per Si-C pair.

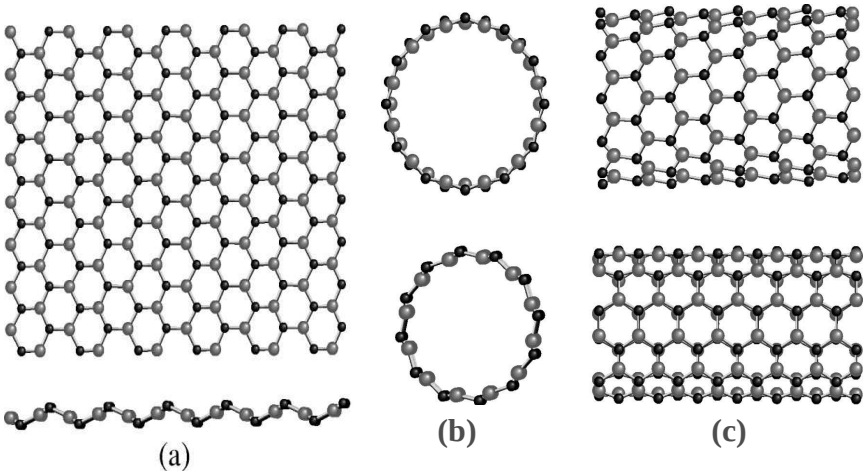

Fig. 4.1A: (a) Type-1 graphene sheets of SiC with a Si to C ratio of 1:1 obtained by tight-binding molecular dynamics (GTBMD) relaxation studies. The surface reconstruction results in a wavelike appearance. The top and bottom panels in each of these figures show top and side views of the structures, respectively. In both structures Si atoms, coloured grey, are all in a single plane, while C atoms coloured black are displaced above and

below this plane. (b) End views of single wall SiCNTs of zigzag (top) and armchair (bottom) configurations. (c) Side views of the structures [13].

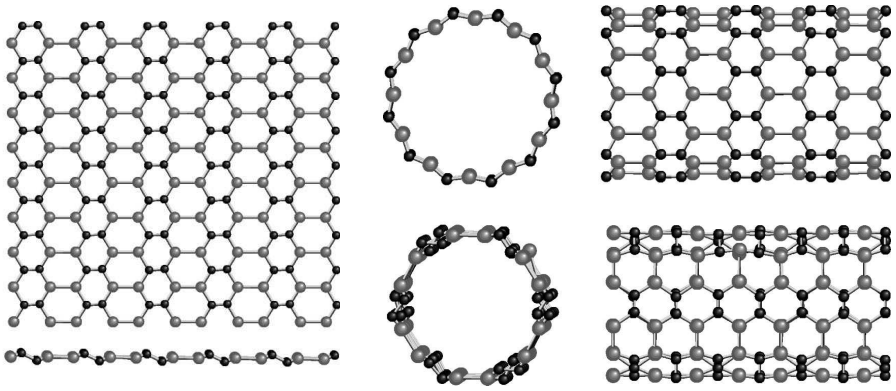

(a) **(b)** **(c)**

Fig.4.1B: Type-2; (a) graphene sheets of SiC with a Si to C ratio of 1:1 obtained by tight-binding molecular dynamics (GTBMD) relaxation studies. (b) End views of single wall SiCNTs of zigzag (top) and armchair (bottom) configurations. (c) Side views of the structures respectively [13].

Several papers have been published reporting the synthesis of carbon nanomaterials via co-pyrolysis of pitch and heteroatom precursors [14-16]. Formation of substituted carbon materials by co-pyrolysis is reported to be highly effective for boron because it can form planar bonds through sp^2 hybrid orbitals, unlike silicon with sp^3 hybrid orbitals.

Among the different methods for nanomaterials synthesis, chemical vapor deposition (CVD) seems to be the most promising in terms of large scale industrial applications, due to the relatively low cost of the method and the ease with which it is possible to upscale both the preparation and purification methods [29]. Chemical vapour deposition is a suitable and widely used method to produce silicon carbides in various shapes (thin films, powders, whiskers and nanorods.) [17].

The first successful synthesis of SiCNTs, by Pham-Huu and co-workers in 2001, was done by shape memory synthesis, which is based on the gas-solid reaction between a

vapour of a Si source and carbon nanotubes or nanofibers [3]. Another research group has synthesized SiCNTs by the reaction between Si (produced by disproportionation of SiO) and CNTs as templates [5], while others have prepared SiCNTs by CVD using commercial nanoporous alumina filter disks as templates [18]. Most preparations of SiCNTs reported to date have involved the use of a template or a support.

SiC materials either in thin films or in bulk form may be produced using a CVD method. Several research groups have prepared SiC materials using gaseous precursors as feed in CVD. The feed may consist of different gas sources for silicon and carbon or a single source for both elements [19]. For the preparation of SiC materials from two or more sources most studies have used various mixtures of silanes and hydrocarbons [20,21] whereas the preparation from a single source feed has employed carbosilanes [22-24]. The use of more than one source of feed enables the Si:C ratio to be varied as desired unlike with the single source where the Si:C ratio is fixed. Several studies, through manipulation of the Si:C ratio, have successfully reported SiC/Si or SiC/C composites [25-28]. For example Xie et al. [29] prepared silicon carbide nanotubes by CVD using methyltrichlorosilane (MTS) as a source of both Si and C, while in another study a SiC/C composite was deposited from MTS and ethene by CVD [30]. Silanes and chlorosilanes have largely been associated with the introduction of hydrogen and chloride impurities which impact on the deposited products. Some studies have employed tetraethylorthosilicate (TEOS) as an alternative silicon source since it is known to produce relatively pure CVD oxides [31].

TEOS has been widely used in the preparation of mesoporous materials. In a conventional method mesoporous materials are prepared by hydrolyzing the inorganic precursor (silicon alkoxide) in an acidic, basic or neutral medium in the presence of an organic structure directing agent (surfactant). TEOS has also become popular as a single source precursor for SiO_2 in thin film optics and anti-reflection coatings [31]. It has been used in studies as either a source of carbon or silicon. For instance, Shi et al. [32] reported on the synthesis of double-walled carbon nanotubes by CVD where they employed TEOS as a source of carbon. Also Pol et al. [33] reported on a single step

method to deposit Si nanoparticles on the surface of in-situ formed carbon spheres in a closed swagelok cell at 700 °C using TEOS as a Si and C source. Synthesis of SiCNTs by CVD suggests a condition dependent process.

Here we report on the deposition of SiO_2 coatings on the surface of in-situ formed carbon spheres by thermal pyrolysis of TEOS via horizontal CVD as well as the preparation of silica hollow shells from subsequent thermal treatment of the SiO_2 covered carbon spheres.

4.2 Experimental

Tetraethylorthosilicate (TEOS), triethylsilylchloride (TESCl), toluene and ferrocene were purchased from Strem chemicals and used as received. Synthesis was carried out in the temperature range of 700 - 1100 °C, in an Ar/H_2 (5 %) (v/v) gas mixture from AFROX at atmospheric pressure. The gas flow rate was kept constant at 100 ml/min. A constant wt. % of ferrocene (5 %) was added to a solvent mixture of toluene and TEOS with different weight ratios of both solvent constituents. The catalyst solutions were placed in a 20 ml syringe and injected into the heated quartz tube by means of a SAGE syringe pump at a constant injection rate of 1 ml/min. The solutions were injected into the reactor via a specially designed quartz tubule (2 mm i.d., 200 mm in length) similar to that described in (chapter 2). The carbon materials were deposited using a single chamber horizontal furnace based on similar principles as that described in chapter 2 (figure 2.1).

The carbonaceous materials deposited were scraped from the walls of the quartz tube and weighed. The as-synthesized samples were dispersed in ethanol and placed onto a copper grid for TEM analysis. Carbon products were characterized by scanning electron microscopy (SEM) (Jeol JSM-840), transmission electron microscopy (TEM) (Jeol JEM-100S), XRD (Philips PW187020/00), Raman spectroscopy (J-Y T64000) and thermal analysis (TGA) (Perkin Elmer TGA 7). TGA was conducted in air by heating samples from 25 °C to 950 °C at a heating rate of 5 °C/min. The diameter measurements of the

carbon materials were performed using the ImageJ program on the TEM digital micrographs. The yield was calculated from the wt. % of the products obtained relative to the mass of the solvent injected into the system.

A series of experiments were performed in which the wt. % of TEOS was varied in the reaction mixture containing ferrocene, toluene and TEOS. The TEOS wt. was varied from 0 – 30 % in the presence of the catalyst. Data are shown in table 4.1.

4.3. Results and discussion

4.3.1 Toluene

Deposition of carbon materials from toluene and ferrocene with no silicon source produced nanotubes and amorphous carbon with the relative abundances as depicted in table 4.1. Carbon nanotubes as seen in the TEM micrograph (figure 4.2a), vary in diameter. The thickness of the outer walls indicated that the tubes are multi-walled. Figure 4.2 (b) provides information on the outer diameter distribution showing a range of diameters varying from 20 to 100 nm with the majority of the tubes having average diameters around 50 nm. Information on the amount of amorphous carbon was obtained from the SEM micrograph (Fig. 4.2c), as well as the length of the tubes which on average were *ca.* 50 μm long.

Table 4.1**:** Effect of TEOS on CNTs

TEOS Wt.%	% Yield	Notes	Mean diameter[a] / nm	Length[b] / μm (CNTs)
0	5.82	Tubes (80%), ά-C (20%)	50t	48
5	12.3	Tubes (85%), ά-C (15%)	30t	300
10	7.16	Tubes (85%), ά-C (15%)	20t	28
15	2.24	Tubes (80%), ά-C (20%)	20t	____
20	1.58	Tubes (75%), ά-C (25%)	20t	____
30	1.54	Spheres(55%),Tubes (15%), ά-C (35%)	250s	____
*60	1.00	Spheres (60%),ά-C(5%),Si-coats(35%)	250s	____
*100	2.22	Spheres (90%) ά-C (10%)	_____	____

Temperature = 900 °C; Ar/H_2 (5%) (v/v) flow rate = 100 ml/min; ferrocene = 5% wt.; ά-C = amorphous carbon; injection rate = 1 ml/min, *wt.% TEOS deposited in the absence of a catalyst. [a] t = tubes & s = spheres.

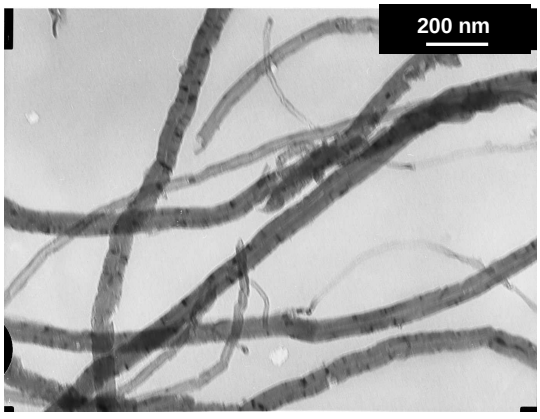

Figure 4.2a: TEM micrograph of carbon nanotubes prepared from toluene at 900 °C in the absence of a Si source

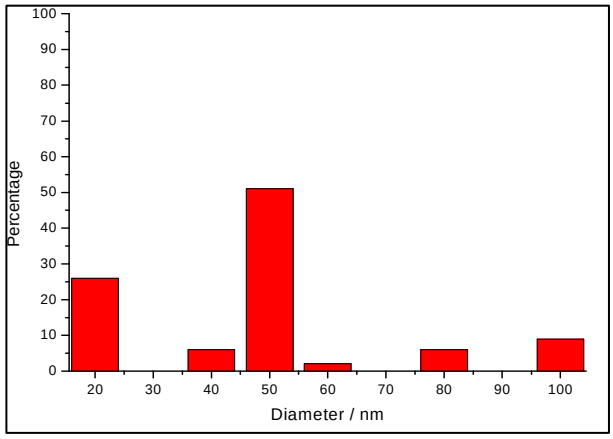

Fig. 4.2b: Average outer diameter distribution for the tubes deposited from toluene.

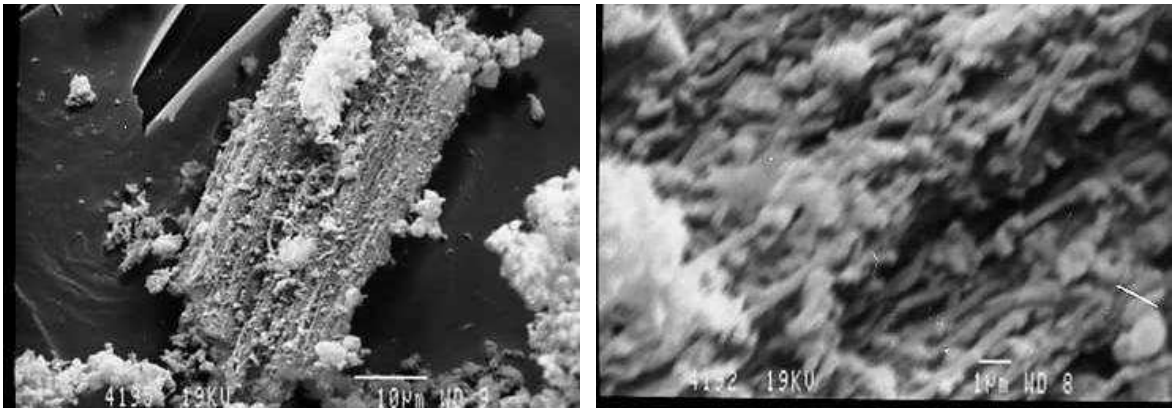

Fig.4.2c: SEM micrographs of CNTs prepared from toluene shows the different forms of carbon (tubes & amorphous matter).

4.3.2 Tertraethylorthosilicate (TEOS) as a Si source

Carbon nanotubes prepared from 5 % wt. TEOS in toluene in the presence of ferrocene are shown by the TEM images (figure 4.3a). The quality of the surface of the tubes looks rough and the interior of the tubes appear partially segmented. Figure 4.3 (b) and (c) gives more information on length dimensions and on the amount of amorphous carbon formed in the reaction. Tubes are longer (see table 4.1) and better aligned, with less amorphous carbon noted in comparison to tubes prepared from toluene in the absence of TEOS. Despite their alignment some kinks are observable from SEM images (Fig. 4.3c). The surface information provided by TEM and the kinks seen from the SEM micrographs indicate that small amounts of TEOS induces defects in the carbon graphitic lattice, leading to the distortions in the carbon nanotube walls (Fig 4.3a).

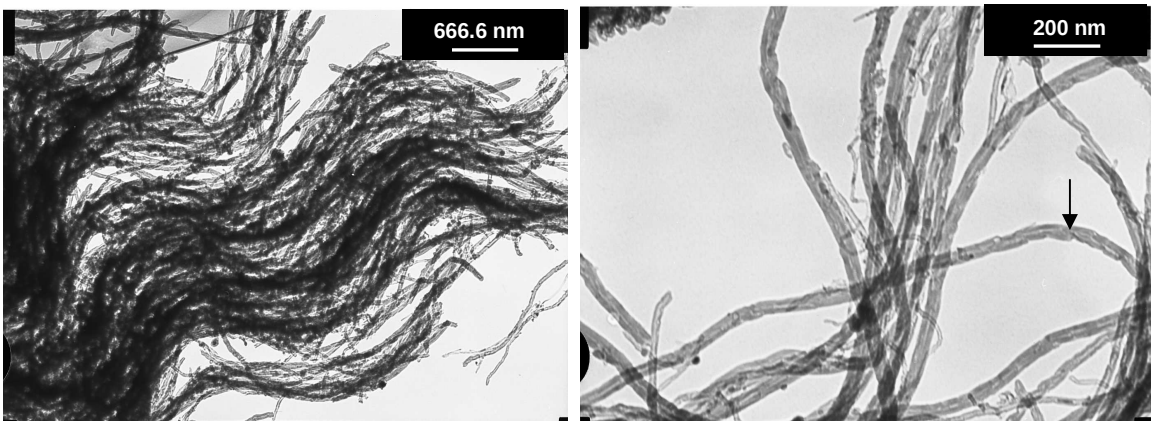

Fig. 4.3a: TEM micrographs of nanotubes prepared from a mixture of 5 wt. % TEOS in toluene. A black arrow points to one of the defects seen on the CNTs walls

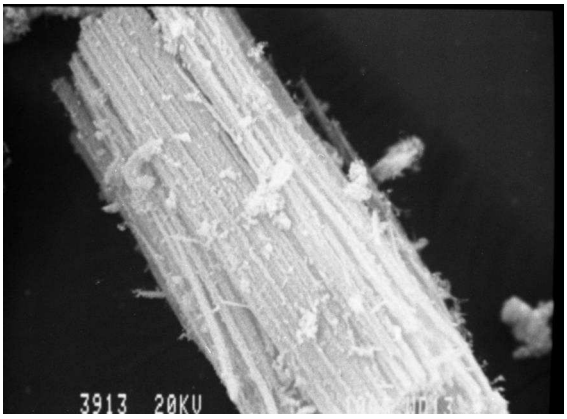

Fig. 4.3b: Tubes prepared from 5wt.% TEOS. The tubes are well aligned tubes and 300 μm in length

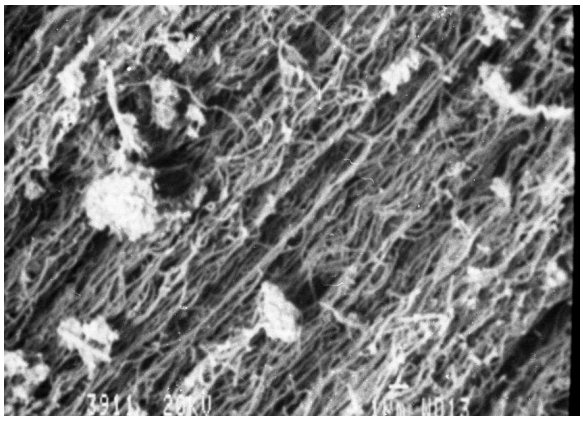

Fig. 4.3c: A closer look of the tube shows their wavy nature. Some amorphous C is also observed

TEM analysis reveals that the TEOS:toluene ratio influences the quality of the CNTs. The micrographs of tubes prepared from 10 wt. % TEOS in toluene (Fig. 4.4a) shows that tubes are smaller in diameter with the roughness on the surface still persisting. SEM analysis (Fig. 4.4b) of the same sample provides information on the CNTs length. The tubes are ~ 28 μm long (table 4.1). This is a drastic drop in length when compared to the sample prepared from 5 wt. % TEOS. It can also be seen from the SEM images that the CNTs alignment has deteriorated, which is again an indication of structural disorder in the tubes. Also from the SEM analysis there is a remarkable reduction in the amount of

amorphous carbon observed when tubes are prepared from TEOS/toluene mixture as compared to when tubes are prepared from toluene only.

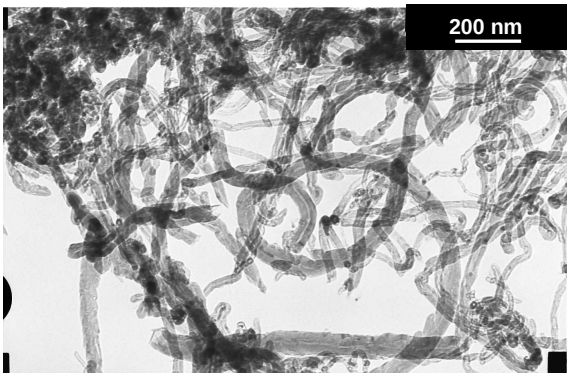

Fig. 4.4a: TEM image of TEOS 10 wt. % in toluene majority of CNTs are narrow

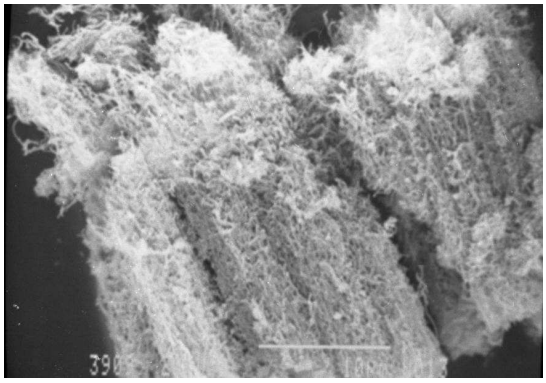

Fig. 4.4b: SEM image of TEOS 10 wt. % in toluene

It has been established from the TEM micrographs (Fig 4.4c and d) that by further increasing the amounts of TEOS to 15 wt. % and 20 wt. % in toluene the quality (diameter, length) and yield (table 4.1) of the CNTs further depreciates. It also seems that the strength of the tubes is affected as tubes appear to have broken into small fragments upon sonication during sample preparation before TEM viewing. Deterioration of the diameter implicates carbon deficiency impact on tube strength. The carbon nanotube length can be correlated with the tube growth. Hence, length deterioration indicates early termination of tube growth. Termination of tube growth is subject to carbon availability and catalyst activity. Therefore short tubes indicate either carbon deficiency, catalyst deactivation, or both, impacting on the CNT synthesis.

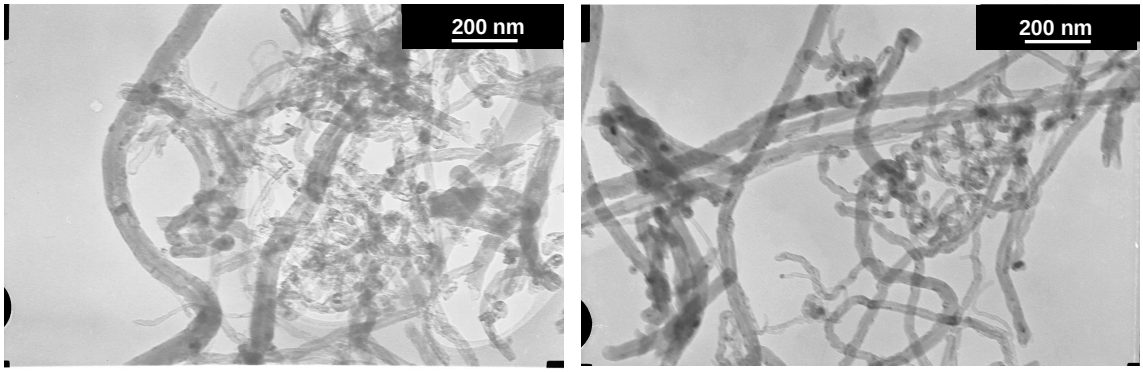

Fig. 4.4c: 15 wt. % TEOS in toluene CNTs Fig. 4.4d: 20 wt. % TEOS in toluene CNTs

Early literature studies have indicated that TEOS pyrolysis results in carbon and SiO_2 deposition. A kinetic model of TEOS decomposition, as provided by Herzler et al. [34], suggests that the carbon source during TEOS decomposition is an oxygen-containing hydrocarbon in the form of ethanol, or ethene. If ethanol is the carbon source produced in situ during TEOS decomposition then our results are consistent with the work published by Botello-Méndez et al. on "controlling the dimensions, reactivity and crystallinity of multiwalled carbon nanotubes using low ethanol concentrations" [35]. They observed improvement in length at low ethanol concentrations and a drastic drop in length at high concentrations. In their studies Hata et al. [36] suggested that the oxygen atoms play a crucial role keeping the Fe catalyst clean from carbon agglomeration for longer periods, thus resulting in longer carbon nanotubes. Oxygen atoms react with carbon atoms creating CO and CO_2 gaseous species [35]. However as additional O atoms are added (at high ethanol concentrations) reactions between Fe and O occurs leading to catalyst deactivation and hence reduced tube formation [35]. This could explain why good quality tubes are observed at low concentrations of TEOS and quality deterioration results at high concentrations of TEOS.

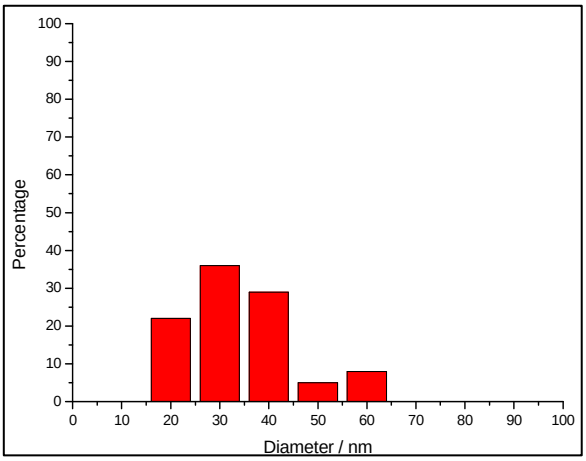

Fig. 4.5a: Mean outer diameter distribution for 5 wt. % TEOS in toluene

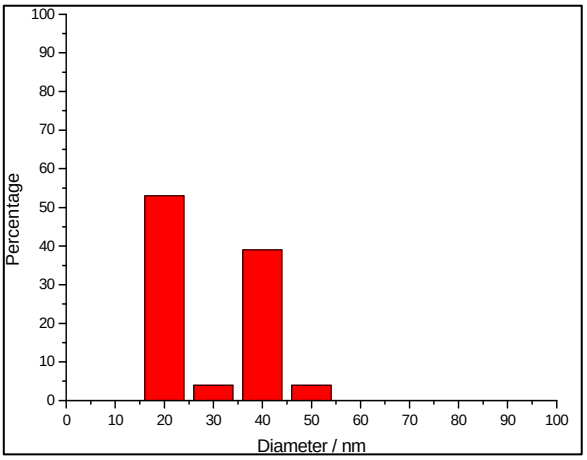

Fig. 4.5b: Mean outer diameter distribution for 10 wt. % TEOS in toluene.

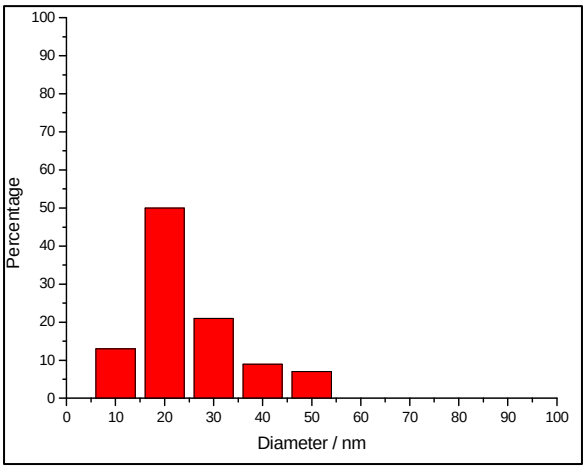

Fig. 4.5c: Mean outer diameter distribution for 15 wt. % TEOS in toluene

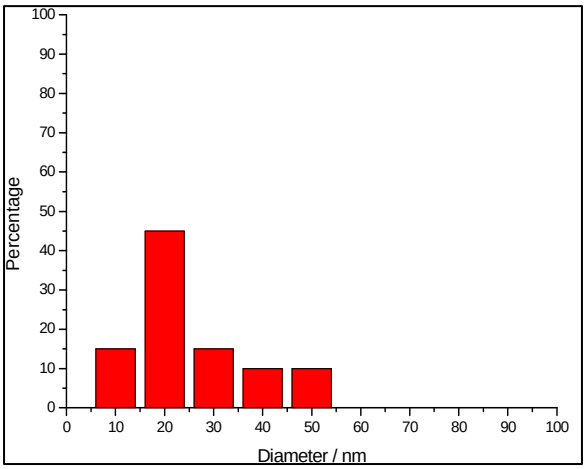

Fig. 4.5d: Mean outer diameter distribution for 20 wt. % TEOS in toluene

To further explore the effect of TEOS on Fe, TEM analysis (Fig. 4.6a) of carbon materials prepared from 30 wt. % TEOS in toluene was undertaken. A drastic change in the carbon morphology is observed from the TEM images. The carbon products now consist of a mixture of carbon spheres and CNTs, with spheres being the dominant component of this mixture. The resulting spheres have diameters ranging from 150 - 400 nm with the majority of them being ~ 200 nm (Fig. 4.6c). The appearance of carbon spheres in the presence of Fe is a clear indication of catalyst deactivation. SEM analysis (Fig. 4.6b) shows that the tubes have the appearance of short rods.

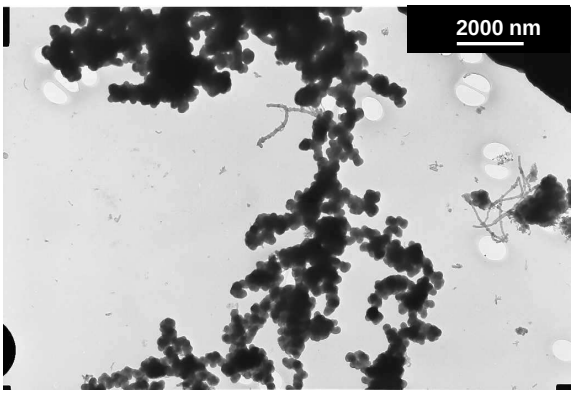

Fig. 4.6a: TEM image of 30 wt. % TEOS in toluene

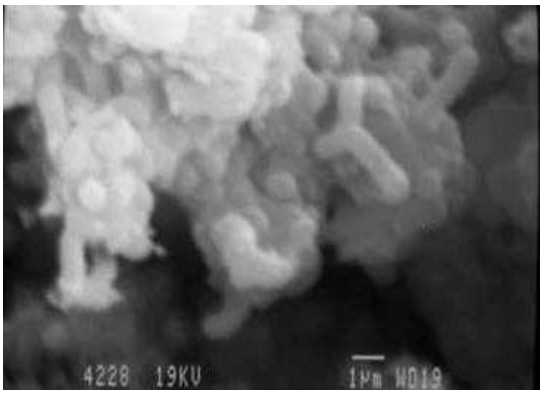

Fig. 4.6b: SEM image of 30 wt. % TEOS in toluene

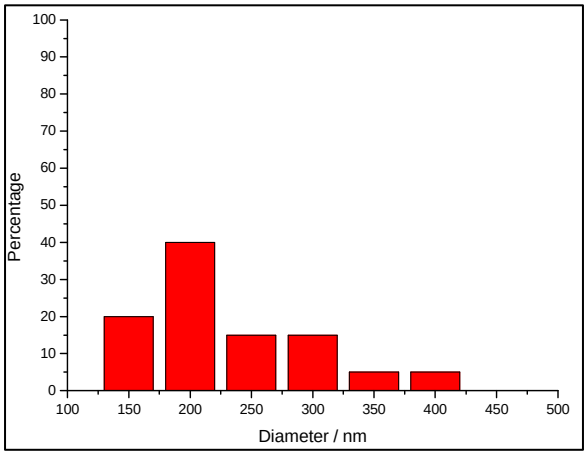

Fig. 4.6c: diameter distribution for carbon spheres prepared from 30 wt. % TEOS in toluene in the presence of the catalyst.

Raman analysis

Figure 4.7a shows the intensities of the active Raman scattering modes of the carbons, one around 1350 cm^{-1} called the D-band, denoting the degree of disorder in the carbon lattice or the extent of amorphous carbon and the other around 1580 cm^{-1} termed the G-band denoting the extent of the graphitic nature of the carbons. Figure 4.7b summarizes the I_D/I_G ratios of the products. The I_D/I_G ratios of 5 and 10 wt. % TEOS in toluene are low indicating graphitisation. The I_D/I_G ratios (Fig. 4.7b) gradually increases with

increasing amounts of TEOS, which implies that with increasing TEOS the graphitic nature and order of the products is lost. This is in agreement with what has already been observed from the TEM images, where a gradual decrease in length and diameter were noted until eventually spheres were observed.

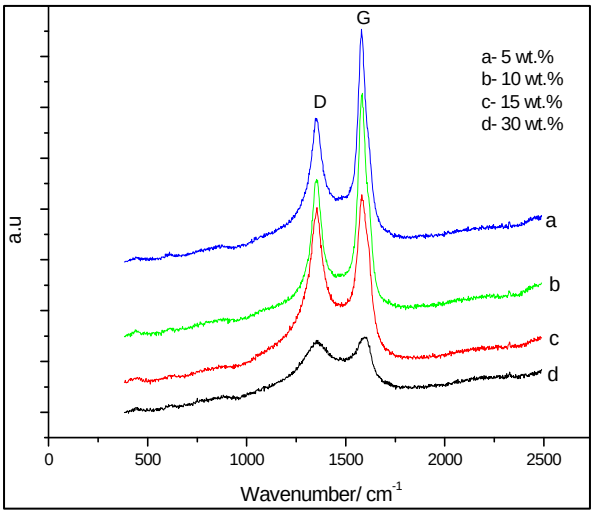

Fig. 4.7a: Active Raman scattering modes D and G- band at 1350 and 1580 cm^{-1} respectively

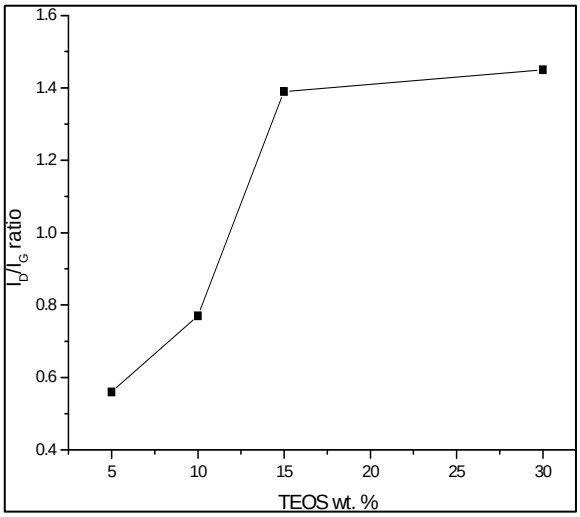

Fig. 4.7b: The I_D/I_G ratios as measure of graphitic nature

4.3.3 Non-catalytic pyrolysis of 60 % TEOS in toluene

Having established that high concentrations of TEOS deactivate the catalyst, deposition of carbon materials from high TEOS:toluene ratio was performed in the absence of the catalyst. Figure 4.8a shows that at a 60:40 wt. % ratio of TEOS:toluene, spheres were produced. These were expected in the absence of Fe. However, new features appeared not typically observed when Si is absent. The spheres appear to be encapsulated in a translucent structure. It has already been stated earlier that TEOS decomposition results in deposition of C and SiO_2. Pol et al [33] used the boiling points of carbon (4200°C) and silicon (2355 °C) to suggest that thermodynamically and kinetically carbon solidifies first on thermal decomposition of TEOS producing silicon coated carbon spheres. Based on a similar aspect we suggest that in our work carbon gets deposited before SiO_2. This would produce the core/shell structures formed with carbon wrapped in silica shells. Also a

typical Si-O bond has a bond length of ~1.49 Å with dissociation energy of 452 kJ/mol while a Si-C bond is ~1.86 Å long with dissociation energy of 360 kJ/mol. Therefore it can be assumed that during thermal pyrolysis of TEOS the strong Si-O bonds are formed at the expense of the weak Si-C bonds. The carbon spheres deposited have diameters ranging between 200 nm and 400 nm (Fig. 4.8b).

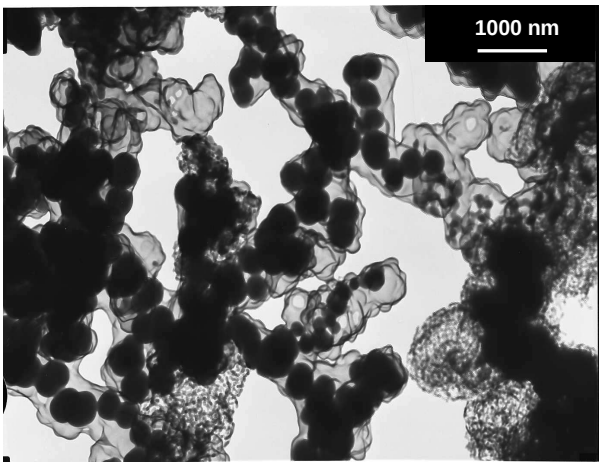

Fig. 4.8a: Carbon spheres prepared from 60 wt.% TEOS are encapsulated in silica shells

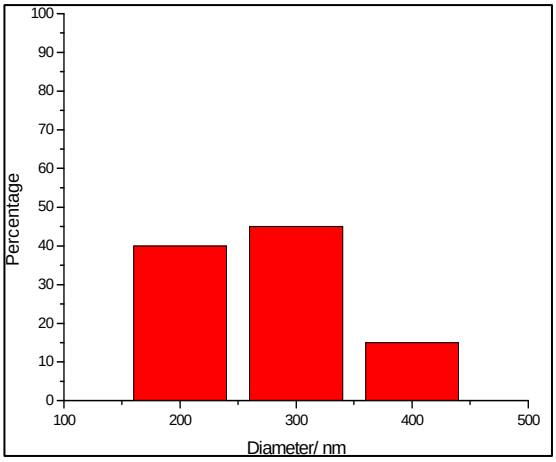

Fig. 4.8b: Spheres diameters prepared from 60 wt.% TEOS

Thermogravimetric analysis of the 60 wt. % as-synthesized sample was done in air to obtain information on the composition of the sample. The TGA profile shown in figure 4.9 reveals a mass loss of approximately 80 %, leaving 20 % residue, which in the absence of the catalyst should be silica.

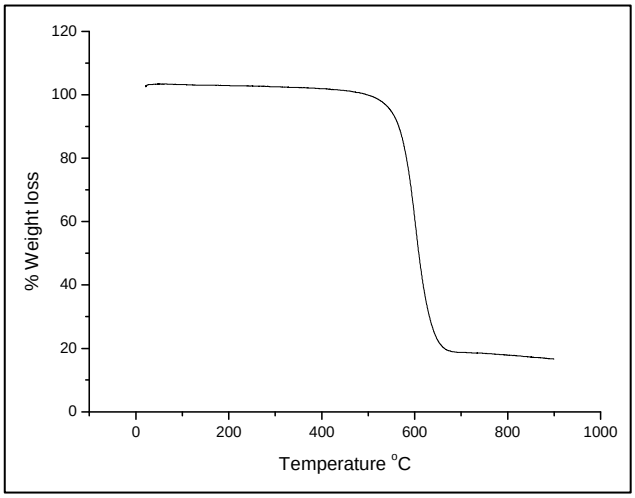

Fig. 4.9: TGA profile of 60 wt. % TEOS as-synthesized sample.

TEM analysis of the residue resulting from thermal treatment in air reveals that most of what were the carbon spheres were burned off leaving behind hollow silica shells (figure 4.10). This indicates that the silica shells are porous in nature. This is again in agreement with the findings of Pol et al. In their study, BET analysis established that products obtained from TEOS pyrolysis were porous [33].

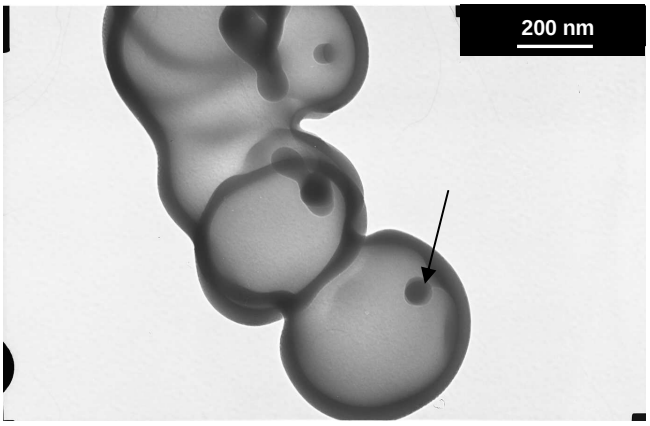

Fig. 4.10: TEM micrographs of TGA residue showing hollow silica shells with some residual carbon in amorphous form indicated by the arrow.

EDS analysis of 60%TEOS

Elemental analysis of the as-synthesized 60% TOES sample was performed by EDS. The EDS spectrum (Fig.4.11) indicates that the core/shell structures are composed of carbon, oxygen and silicon. The identification of both silicon and oxygen by EDS confirms the deposition of SiO_2. Copper is detected from the SPI Cu grid used for sample loading during analysis.

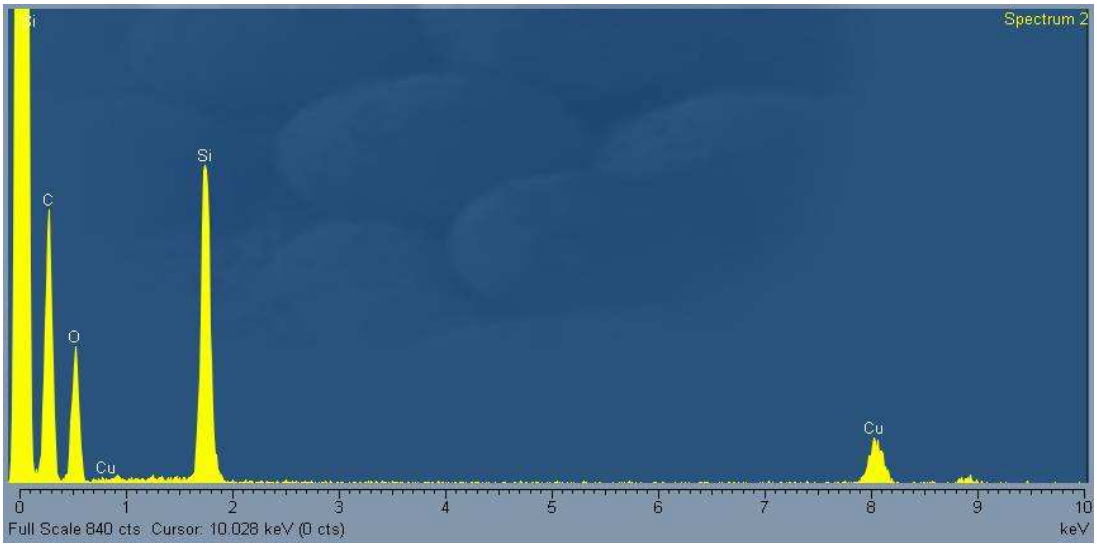

Fig. 4.11: EDS spectrum obtained from 60%TEOS.

XRD analysis

X-ray diffraction patterns of both the as-synthesized 60 wt. % TEOS sample and its TGA residue indicate that the resulting spheres contain carbon (figure 4.12). From figure 4.12a the carbon reflection peaks can be seen around 25.70° and 43.51° assigned to (002) and (101) graphitic planes respectively. However, the peak at 25.70° appears to overlap with other reflections which are difficult to identify. The expectation would be not to see the SiO_2 reflection as the instrument was calibrated using a silicon sample holder. The weak carbon signal at 20.08° seen in figure 4.12b (residue) indicates amorphous carbon which is also seen in the TEM images of the TGA residue. The observed carbon content is consistent with the loss of carbon after thermal treatment in air (in the TGA apparatus).

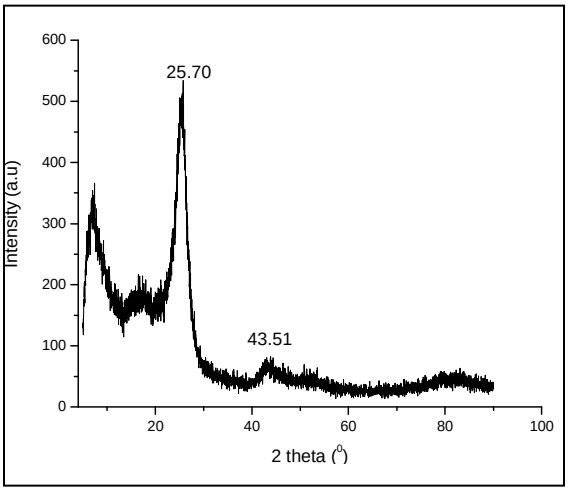

Fig. 4.12a: XRD pattern of sample produced from 60 wt.%TEOS in toluene

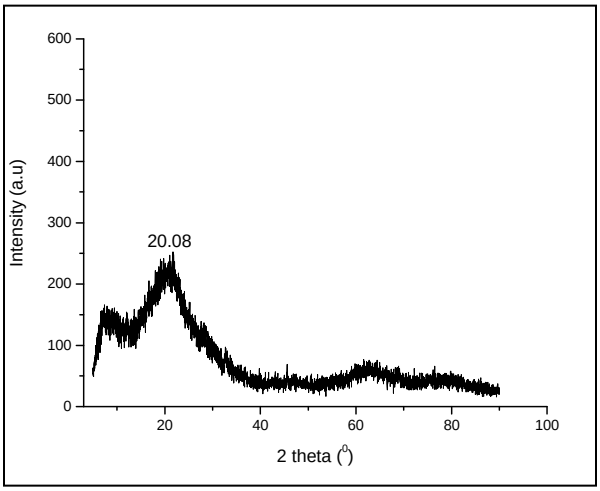

Fig. 4.12b: XRD pattern of residue

4.3.4 Thermal decomposition of TEOS

Figure 4.13 shows TEM images of carbon materials produced from pyrolysis of pure TEOS. The resulting carbon materials are imperfect spheres which closely resemble amorphous carbon. A closer look at these spheres shows bumpy uneven surfaces. The white arrows show that core/shell structures are formed, with the shell being a slightly opague rough structure while the core appears to be darker and spherical (Fig.4.13b).The shells formed are dense, thick and uneven due to SiO_2 deposition. Thermogravimetric analysis profile shows that materials prepared from pure TEOS are thermally stable in air up to temperatures as high as 600 °C after which a mass loss of approximately 40% occurs (Fig. 4.13c). The TEM image (Fig 4.13d) shows that the 60 % residue consists of carbon, carbon spheres and silica shells.

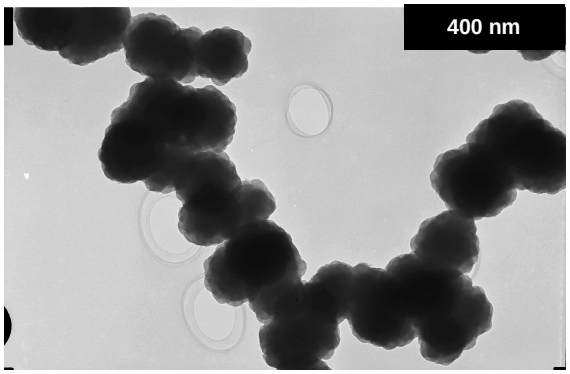

Fig. 4.13a: TEM micrographs of the irregularly shaped materials prepared from pure TEOS

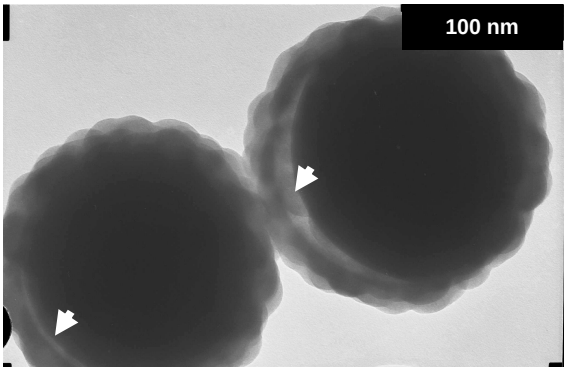

Fig. 4.13b: A closer look reveals the core/shell structures shown by arrows.

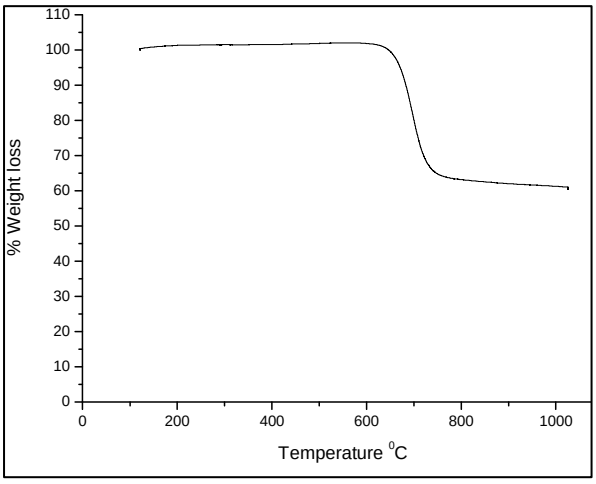

Fig. 4.13c: TGA profile of materials prepared from pure TEOS revealing 40% mass loss

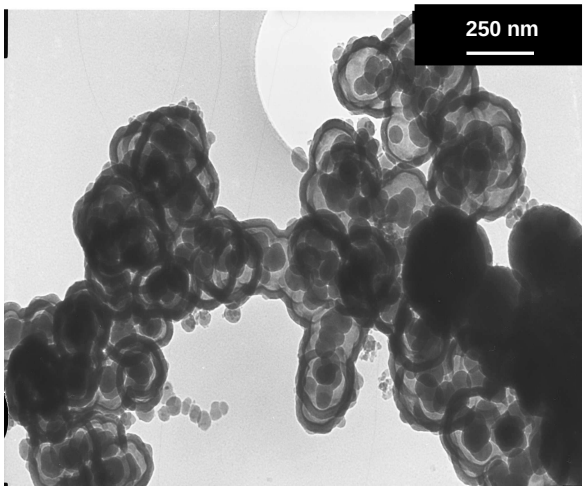

Fig. 4.13d: TEM micrograph of structures remaining after thermal analysis

IR analysis

Information on functional groups can assist in the determination of the chemical composition of the structures. The IR spectra (Fig 4.13e) provide information on functional groups available in the as-prepared materials and also from materials remaining after thermal analysis (TGA). The IR spectrum of the as-prepared materials shows the Si-O symmetric and Si-O assymmetric stretching vibrations at 798 cm^{-1} and 1069 cm^{-1} respectively. Aromatic C=C stretching vibrations are observed at 1526 cm^{-1} confirming co-deposition of carbon and silica from TEOS. The Si-O absorption peak at 1069 cm^{-1} has a shoulder at 1224 cm^{-1}, which is suspected to be due to SiC vibrations.

The Si-C bond has a modest change in dipole, and is expected to result in a weak absorption. However the model of TEOS decomposition does not indicate SiC deposition from TEOS [34]. On the other hand Sun et al. reported the synthesis of SiC from SiO and CNTs [5]. Based on this information the possibility of SiC formation during TEOS pyrolysis can not be completely ruled out. The broad weak peak seen around 1826 cm^{-1} could be due to anhydride C=O vibrations (expected at 1850 cm^{-1}), alkenyl C=C stretching vibrations (expected at 1680-1896 cm^{-1}) or aromatic C=C bending vibrations (expected at 1700 cm^{-1}). However, the intensity of this absorption is very weak and is unlikely to be associated with anhydride C=O. Therefore it is suggested that alkenyl C=C stretching and aromatic C=C bending vibrations are the contributing factors. The peak at 2101 cm^{-1} is due to an alkyne C≡C bond stretching vibrations.

After thermal analysis the peak at 2101 cm^{-1} due to an alkyne C≡C bond stretching vibrations disappeared, indicating that combustion occurred with removal of the functional group. The peak around 1826 cm^{-1} narrows and undergoes a redshift while that at 1526 cm^{-1} persists. The persistence of these two aromatic C=C vibrations after thermal analysis suggests formation of the SiC graphene sheets. All spectra show atmospheric CO_2 stretching vibrations at 2360 cm^{-1}.

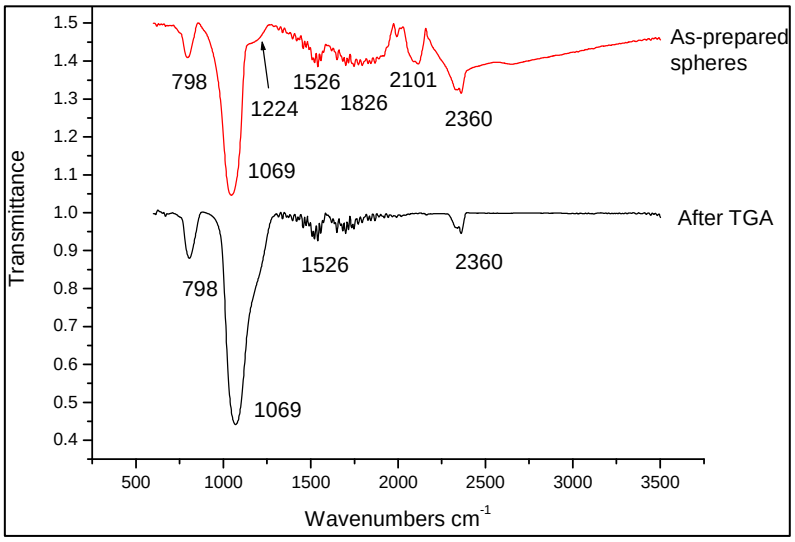

Fig. 4.13e: The IR spectra of as-prepared materials from pure TEOS and the residual materials obtained after thermal analysis

4.3.5 Thermal decomposition of triethylsilylchloride (TESCl)

Non-catalytic pyrolysis of triethylchlorosilane (TESCl) resulted in deposition of carbon spheres with a very wide diameter distribution. The same effect was observed from the pyrolysis of chlorobenzene (ClBz) (see chapter 3). The other feature common to TESCl and ClBz pyrolysis relates to the enhanced yields of the carbon materials. Both reagents are chlorinated species, so once more we see chlorine playing an important role in improving the yields of the product. TEM images (Fig. 4.14a) show abundant spheres of different sizes. The sizes are presented in the diameter distribution graph (Fig. 4.14b). Raman analysis shows the typical carbon active modes (Fig 4. 14c) associated with sp^2 and sp^3 carbon atoms

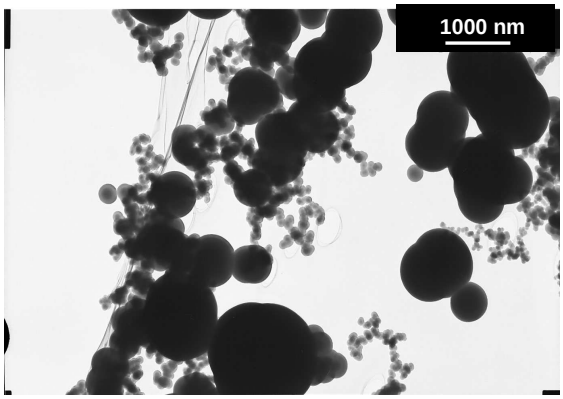

Fig. 4.14a: TEM of TESCl Spheres

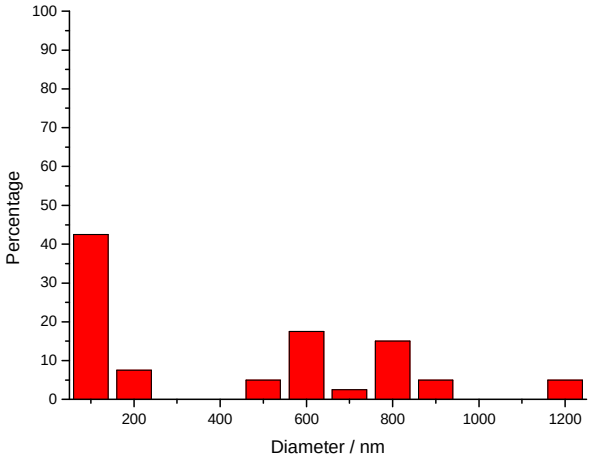

Fig. 4.14b: Diameter distribution.

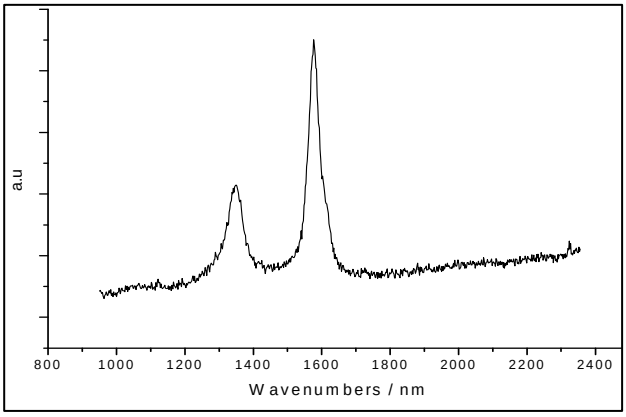

Fig. 4.14c: Raman analysis of spheres prepared from TESCl showing typical D & G-bands.

TGA studies show a mass loss of 60 % which indicates the presence of silica (Fig. 4.14d). The data do not however provide information of the form taken by the silica. To shed light on this issue TEM analysis of the TGA residue was undertaken. From TEM images (Fig. 4.14f) spheres are observed after thermal treatment in air. This suggests the possibility that these spheres are composed of silicon carbide. However the mass loss observed from TGA profile nullifies the possibility of pure SiC. Two possible explanations can be given; first is the formation of a SiC/C composite, where SiC is at the core of the sphere and carbon at the surface. However this fails to explain the formation of silica shells around the spheres upon heating the sample in air. Therefore the second possibility of silicon coated carbon spheres is proposed. The silicon coated spheres would

react with O_2 during thermal analysis to form silica. This possibility does not explain why the carbon spheres did not completely burn off during thermal treatment.

Fourier-transform infra-red spectra of spheres prepared from TESCl shows a typical atmospheric CO_2 absorbance at 2354 cm^{-1} (Fig. 4.14e). The spectrum of the as-synthesized sample shows two peaks of significance; one at 2102 cm^{-1} (alkyne C≡C vibrations) and the other around 1827 cm^{-1} (C=C vibrations). The IR spectrum of residual materials obtained after thermal analysis shows two new peaks at 802 cm^{-1} and 1066 cm^{-1} due to symmetric and asymmetric Si-O vibrations respectively. Hence, conversion of Si-Cl bonds to Si-O bonds during thermal treatment is suggested. The absence of C=C vibrations around 1827 cm^{-1} explains the mass loss seen in the TGA profile (Fig. 4.14d).

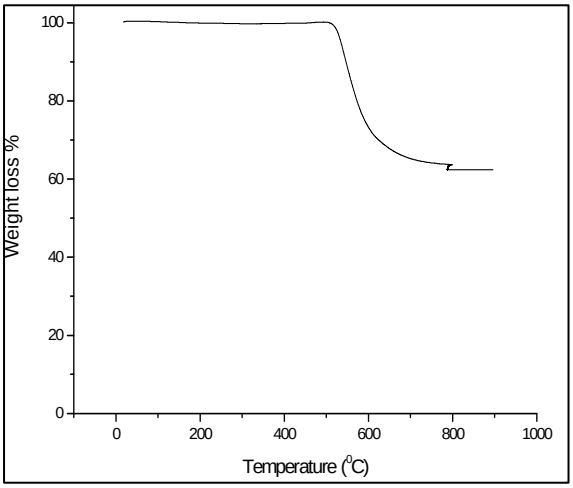

Fig. 4.14d: TGA profile of TESCl spheres performed in air

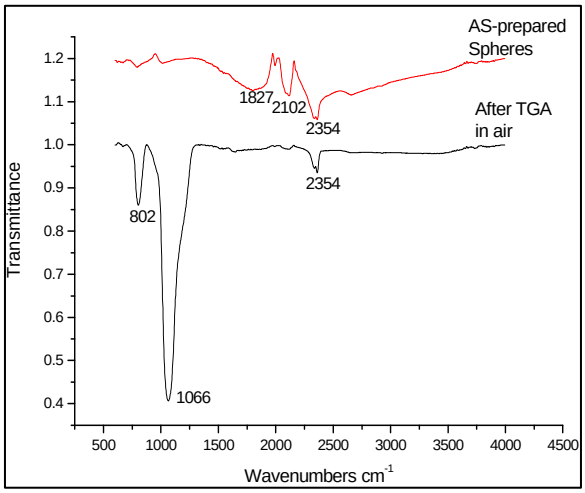

Fig. 4.14e: FT-IR spectra of the as synthesized sample and of TGA residue

TEM micrographs reveals two types of structures collected after thermal treatment: the core/shell structure in which black spheres are encapsulated in translucent silica shells (Fig. 4.14f) and structure with a golf ball surface resemblance (Fig. 4.14g). The golf ball surface appearance is believed to be a result of disproportionation and silica deposition on the surface of the carbon spheres. The information provide by TEM analysis is in agreement with the information provided by the IR spectrum. No carbon based functional groups were detected by IR spectroscopy and it can be seen from TEM micrographs that the carbon structures are covered by silica.

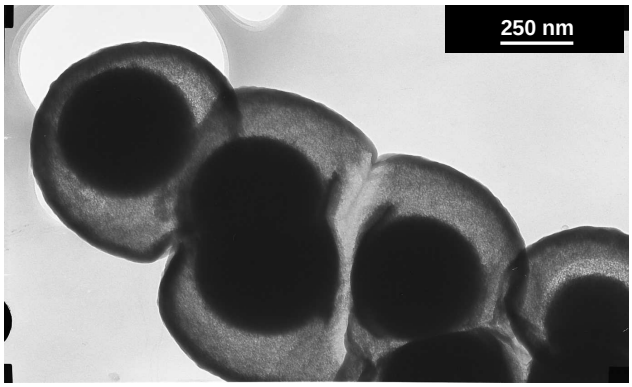

Fig. 4.14f: TEM micrograph of the core/shell (C/SiO_2) structure obtained after thermal treatment of materials prepared from TESCl**.**

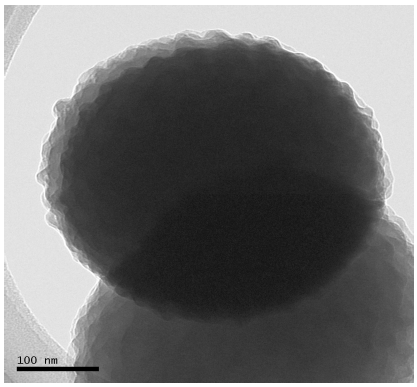

Fig. 4.14g: TEM image showing the golf-ball surface resemblance

EDS analysis

Elemental analysis by EDS of spheres prepared from triethylchlorosilane is shown in figure 4.15. EDS reveals that the spheres are composed of silicon, carbon and chlorine. Based on the result of the EDS spectrum silicon is the dominant element, this explains the observation made form the TGA profile. Copper is detected from the SPI Cu grid used to load the sample during analysis.

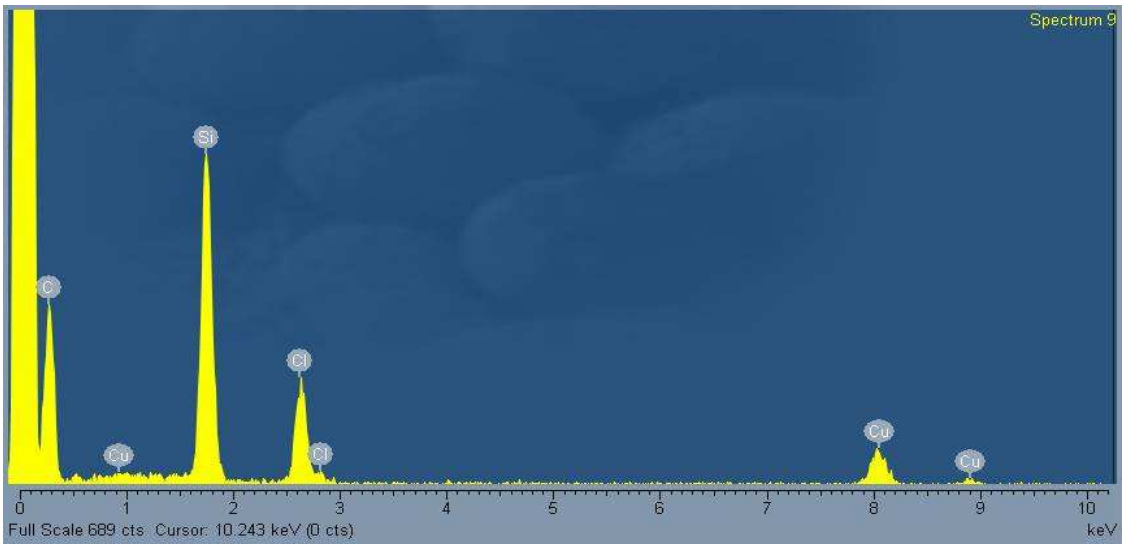

Fig. 4.15: EDS of spheres prepared from non catalytic pyrolysis of triethylchlorosilane.

4.4 Conclusions

Pyrolysis of a TEOS/toluene feed in the presence of a ferrous catalyst results in the formation of carbon nanotubes. The low concentration of TEOS (5% wt.) improves the CNT quality; i.e long tubes and less amorphous carbon are produced. On the other hand high concentrations of TEOS (10 % wt. and above) result in the formation of short tubes with increasing amorphous carbon deposition and eventually production of carbon spheres in the presence of a catalyst. Thus, small amounts of oxygenated species are constructive during the preparation of CNTs while large amounts are destructive. A low concentration of oxygenated species keeps the catalyst particles clean and active by preventing carbon agglomeration on the surface of the catalyst. However, high concentrations of oxygenated species lead to catalyst deactivation as well as carbon deficiency. TEM and IR analyses of structures produced from TEOS indicate that non-catalytic thermal decomposition of TEOS results in co-deposition of carbon and silica resulting in the formation of core/shell (C/SiO_2) structures.

Thermal pyrolysis of triethylchlorosilane in the absence of a catalyst indicates that the generation of chlorinated species results in enhanced product yields. However control of the dimensions (carbon sphere diameter) is a challenge as chlorinated species result in carbon spheres with a wide diameter distribution (100-1200 nm). EDS studies revealed an interesting new feature which according to our knowledge has not been reported previously. It shows that spheres prepared from triethylchlorosilane are composed of carbon, silicon and chlorine. We have shown in chapter 3 that chlorine generated from pyrolysis of chlorobenzene is eliminated as HCl. However in the presence of silicon, chlorine has been retained in our studies. This may be ascribed to increasing M-Cl bond strength (M = C, Si) from carbon to silicon (C – 327 kJ/mol; Si - 391 kJ/mol). However, the M-Cl bond strength does not reflect the difficulty of heterolysis; for example in spite of the high Si-Cl bond energy compounds containing these bonds are highly reactive and unstable in air. Therefore, retaining chlorine suggests that the Si-Cl bond is stabilized by attachment of carbon to silicon. Thus, silicon on these spheres is sp^3 hybridized.

4.5 References:

1. S. Iijima, *Nature* **354** (1991) 56
2. A. Mavrandonakis, G. E. Froudakis, *Nano. Lett.* **3** (2003) 1481
3. R. Saito, M. S. Dresselhaus, G. Dresselhaus, *Phys. Rev. B* **53** (1996) 2044
4. C. Pham-Huu, N. Keller, G. Ehret, M. Ledouxis, *J .Catal* **200** (2001) 400
5. X. H. Sun, C. P. Li, W. K Wong, N. B. Wong, C. S Lee, S. T Lee, B. Toe, *J. Am. Chem. Soc.* **124** (2002) 14464
6. B. K. Teo, X. H. Sun, *Chem. Rev.* **107** (2007) 1455
7. S. B. Fagan, A. J. R. da Silva, R. Mota, R. J. Baierle, A. Fazzio, *Phys. Rev. B* **61** (2000) 9994
8. R. Q. Zhang, H. L. Lee, W. K. Li, B. K. Teo, *J. Phys. Chem. B* **109** (2005) 8605
9. M. S. Pellarin, C. Ray, J. Lerme, J. L. Vialle, M. Broyer, M. Blasé, P. Keghelian, P. Mlinln, A. Perez, *Eur. Phys. J. D* **9** (1999) 49
10. H. Dai, *Surf. Sci*. **500** (2002) 218
11. S. B. Fagan, A. J. R. da Silva, R. Mota, R. J. Baierle, A. Fazzio, *Phys. Rev. B* **64** (2001) 0854131
12. S. B Fagan, A. J. R da Silva, R. Mota, A. Fazzio, *Nano. Lett.* **4** (2004) 975
13. M. Menon, E. Richter, A. Mavrandonakis, G. Froudakis, A. N. Andriotis, *Phys. Rev. B* **69** (2004) 115322
14. T. Eichner, M. Braun, K. J. Huttinger, *Carbon* **34** (1996) 1367
15. J. Gremmels, G. Geiger, M. Braun, K. J. Huttinger, *Carbon* **36** (1998) 1175
16. R. Hu, T. C. Chung, *Carbon* **35** (1997) 1101
17. X. T. Zhou, N. Wang, F. C. K. Au, H. L. Lai, H. Y. Peng, I. Bello, S. C Lee, S. T Lee, *Mater. Sci. A* **286** (2000) 119
18. Q. Cheng, L. V. Interrante, M. Lienhard, Q. Shen, Z. Wu, *J. Eur. Cer. Soc* **25** (2005) 233
19. J. Schlichting, *Powder Metal. Int.* **12** (1980) 196
20. S. Tanana, H. Komiyama, *J. Am. Ceram. Soc.* **73** (1990) 3046
21. H. Nagasawa, Y. Yamaguchi, *Appl. Surf. Sci.* **82** (1994) 405

22. Y. Ohsita, *J. Cryst. Growth* **147** (1995) 111
23. D. Cagliostro, S. Rccitiello, J. Ren, F. Zaghi, *J. Am. Ceram. Soc.* **77** (1994) 2721
24. T. M. Besmann, B. W. Sheldon, T. S. Moss, M. D. Kaster, *J. Am. Ceram. Soc.* **75** (1992) 2899
25. J. Deng, Y. Wei, W. Liu, *J. Am. Ceram. Soc.* **82** (1992)1629
26. T. Harai, *Ceram. Trans.* **34** (1993) 11
27. M. Kawase, T. Tago, M. Kurosawa, H. Utsumi, K. Hashimoto, *Chem. Eng. Sci.* **54** (1999) 3327
28. Y. Kim, J. T. Choi, J. K. Choi, K. H. Auh, *Mater. Lett.* **26** (1996) 249
29. Z. Xie, D. Tao, J. Wang, *J. Nanosci. Nanotech.* **7** (2007) 647
30. I. M. Kostjuhin, S. V. Sotichos, *Ind. Eng. Chem. Res.* **40** (2001) 2586
31. D. G. Kurth, T. Bein, *J. Phys. Chem.* **96** (1992) 6707
32. Y.-F. Shi, H. J. Quan, G. B. Zheng, H. Sano, Y. Uchiyamo, *Carbon* **411** (2002) 1645
33. V. G. Pol, S. V. Pol, Y. Gofer, J. Calderon-Moreno, A. Gedanken, *J. Mater. Chem* **14** (2004) 966
34. J. Herzler, J. A. Manoin, W. Tsang, *J. Phys. Chem. A* **101** (1997) 5500
35. A. Botello-Méndez, J. Campos-Delgado, A. Morelos-Gómez, J. M. Romo-Herrera, A. G. Rodríguez, H. Navarro, M. A. Vidal, H. Terrones, M. Terrones, *Chem. Phys. Lett.* **453** (2008) 55
36. K. Hata. D. N. Futaba, K. Mizuno, T. Namai, M. Yumara, S. Iijima, *Science* **306** (2004) 1362

Chapter 5

Conclusions

Carbon nanotubes have interesting physicochemical properties which make them attractive candidates for various applications, as discussed in chapter 1. However it is still difficult to synthesize carbon nanotubes with the characteristics required for specific applications. Therefore numerous methods of surface modification and interfacial engineering have been established and employed by various researchers to overcome the problem. Chemical modification and surface functionalization of carbon materials has been discussed in chapter 1. A more specific approach to simplifying efforts to utilize the outstanding properties of CNTs is achieved by halogenation.

Chapter 2 described the use of the injection CVD method to synthesize carbonaceous materials in the presence of a reducing gas (Ar/H_2 5%) and a hydrocarbon solvent. Carbon materials synthesized in this study were characterized by Raman spectroscopy, TEM analysis, SEM analysis, Infra-Red spectroscopy, TGA and EDS analysis. Most of these techniques have been discussed in chapter 1 (literature). An overview of issues pertaining to use of these techniques was described in chapter 2.

It has been established in this research that the percentage content of the haloarene (chlorobenzene, bromobenzene) in the feed impacts on morphology of carbonaceous materials produced during catalytic pyrolysis. It was found that catalytic pyrolysis of a feed having a high content of the haloarene produced exclusively spheres. This is an indication that high haloarene content deactivates the catalyst. A gradual change in morphology from spheres to a mixture of spheres and tubes and finally tubes was observed upon gradual reduction of the haloarene content. There are two possible explanations to this observation. In the first HCl is proposed to play a key role. It was confirmed in this study that decomposition of chlorobenzene produces hydrogen chloride gas, which at high concentrations causes surface poisoning of the catalyst. The second

possibility is that radicals generated during thermal decomposition of chlorobenzene bring about charge transfer, which results in catalyst deactivation.

The influence of the reducing gas flow rate on the morphology of the carbons prepared from catalytic pyrolysis of chlorobezene has been established in this study. At high gas flow rate ($Ar:H_2$ (400:120 ml/min)) catalytic pyrolysis of chlorobenzene produced multi-walled carbon nanotubes. The tubes had partially iron-filled cores. Etching of the tube walls was also observed. However when the flow rate was low (100 ml/min) catalytic pyrolysis of ClBz resulted in production of carbon spheres. This indicates that the residence time of the halogen species in the reaction chamber plays a crucial role in influencing the morphology of the resulting products.

Preparation of carbons from chlorinated species in the presence of the catalyst has been reported by many researchers. However, less attention has been paid to non-catalytic pyrolysis of chlorobenzene. One of the challenges that researchers have faced in the carbon nanomaterials field is up scaling of product yields. In this research we have established that non-catalytic thermal pyrolysis of halogenated species is a cost effective and energy saving process to improve the yields of carbons especially carbon spheres. In chapter 3 non-catalytic decomposition of chlorobezene produced approximately three times the yields obtained from the same volume of toluene under the same reaction conditions. We also found that the yields of products prepared from toluene can be improved by introducing chlorinated species into the toluene feed. Introducing chloroform into a toluene feed by forming a chloroform/toluene mixture of volume ratio 1:3, gave improved yields up to twice the amounts obtained using toluene only.

The impact of gas flow rate on the sizes of the prepared carbon spheres from non-halogenated carbon sources have been reported by other researchers. Their studies showed that the size decreased with increasing flow rate. In this research the effect of gas flow rate on the size of spheres prepared from non-catalytic pyrolysis of chlorobenzene was investigated. We established that the size of carbon spheres prepared from chlorobenzene is not influenced by the gas flow rate as compared to spheres prepared

from toluene. However the yields are influenced by the gas flow rate; as flow increases the yields decrease. The problem encountered was that spheres produced from ClBz have a wide diameter distribution, which is insensitive to gas flow rate. However we established that the size distribution of these spheres can be controlled by the composition of the carrier gas. When hydrogen was used as a carrier gas a narrow size distribution was obtained as compared to when argon was used.

It has been stated in the literature that one of the challenges for application of CNTs is poor dispersion due to high van der Waals interaction between the tubes. This problem is more enhanced in carbon spheres due to accretion of spheres. We have established a way to eliminated accretion without functionalizing the spheres. Non-catalytic decomposition of chlorobenzene as well as non-catalytic pyrolysis of a chloroform/toluene feed produced non-accreted spheres. EDS analysis showed that these spheres are not chlorinated. This indicates the use of chlorinated hydrocarbons as a way to eliminate carbon sphere accretion without compromising the π-network of the spheres, and thus preserving their properties.

The impact of non-carbon containing reagents such as ammonia and thiophene on non-catalytic pyrolysis of toluene and chlorobenzene was investigated. We observed that both reagents promoted production of amorphous carbon in the products prepared from toluene. However, there was no observable influence to the products prepared from chlorobenzene. This indicated that toluene has a decomposition mechanism which renders it susceptible to inhibitors such as sulphur; a mechanism different from that of chlorobenzene.

Preparation of carbon nanotubes by injection of a solvent hydrocarbon in a horizontal CVD procedure has been performed and reported by others. However, this method usually yields products with a wide distribution of diameters. One other challenge in the CNT field of research is the ability to achieve specific dimensions and homogeneity. We have established in this research that preparation of CNTs from a feed containing low concentrations of tertraethylorthosilicate (TEOS) provides a diameter distribution control

and a remarkable improvement in length as compared to CNTs prepared from toluene. It was observed that CNTs prepared from a low concentration of 5 wt. % TEOS in toluene had a narrow diameter distribution with less amorphous carbon and about six times longer tubes than prepared from toluene. However, it was found that high concentrations of TEOS in toluene are destructive. A drastic deterioration of lengths and yield was observed at high concentrations of TEOS in toluene. This is an indication that oxygen from TEOS plays a crucial role in keeping the catalyst active for longer time periods by preventing agglomeration of carbon on the catalyst surface. However, too much oxygen deactivates the catalyst.

Non-catalytic decomposition of TEOS:toluene (60:40 %) as well as TEOS alone produced core/shell structures formed from carbon/silica. It was established in this study that during non-catalytic pyrolysis of TEOS, carbon solidifies first from co-deposition of carbon and silica. Subsequent thermal treatment of the carbon/silica core/shell structures resulted in formation of hollow core silica structures, indicating the porous nature of the silica shells prepared.

Triethylchlorosilane (TESCl) was also used as a source of carbon and silicon. Thermal pyrolysis of triethylchlorosilane in the absence of a catalyst indicates that chlorinated species result in enhanced product yields, a phenomenon already observed in chapter 3. EDS analysis revealed that spheres prepared from triethylchlorosilane are composed of carbon, silicon and chlorine. Thus, chlorinated silicon/carbon composites have been prepared in this study. TGA profile of these composites indicates that 60 % residual material was obtained after thermal treatment in air. TEM analysis of the residual materials obtained after thermal treatment reveals that these composites have excellent thermal resistance. Even though pyrolysis of TESCl results in structures different from those obtained from TEOS, the stability of the Si-Cl bond in TESCl is analogous to the Si-O bond found in TEOS.

The partially iron-filled carbon nanotubes obtained in this study open a door to the possibility of forming long nanometric filaments by filling carbon nanotubes with metals.

If bimetallic catalyst systems are used in the future, nanometric filamentous alloys with remarkable properties can be prepared. Therefore, for future work catalysts other than iron should be used to investigate the impact of monohaloarenes on other metals. Also the effects of a second electron withdrawing group can be studied by examining dihaloarenes. From the thermolytic pyrolysis of silicon sources, conditions which favour formation of a Si-C bond over the Si-O or Si-Cl bond need to be established.